

**ELECTROCHEMICAL ION-IONOPHORE RECOGNITION AT MEMBRANE/WATER
INTERFACES FOR ULTRATRACE ION SENSING**

by

Benjamin Kabagambe

BS, La Roche College, 2004

MS, University of Pittsburgh, 2007

Submitted to the Graduate Faculty of
the Kenneth P. Dietrich school of Arts and Sciences in partial fulfillment
of the requirements for the degree of
Doctor of Philosophy

University of Pittsburgh

2015

UNIVERSITY OF PITTSBURGH
DIETRICH SCHOOL OF ARTS AND SCIENCES

This dissertation was presented

by

Benjamin Kabagambe

It was defended on

November 24th, 2015

and approved by

Stephen G. Weber, Professor, Department of Chemistry

Adrian C. Michael, Professor, Department of Chemistry

Minhee Yun, Associate Professor, Department of Electrical & Computer Engineering

Dissertation Advisor: Shigeru Amemiya, Associate Professor, Department of Chemistry

Copyright © by Benjamin Kabagambe

2015

**ELECTROCHEMICAL ION-IONOPHORE RECOGNITION AT
MEMBRANE/WATER INTERFACES FOR ULTRATRACE ION SENSING**

Benjamin Kabagambe, PhD

University of Pittsburgh, 2015

Electrochemical methods for trace ion analysis of organic and inorganic species with environmental and biological attention have been developed and reported during past decades. Voltammetric method is attractive not only to analyze selective ion species due to its characteristic based on ion lipophilicity, but also to lower the limit of detection by combining with stripping analysis. In my PhD work, I have developed a highly selective and sensitive electrochemical ion-ionophore recognition method that can be used to characterize fundamental transport dynamics at membrane/water interfaces. I have also demonstrated that my selective and sensitive electrochemical technique is useful for very low detection of trace ions. Specifically, cyclic voltammograms of Ag^+ , K^+ , Ca^{2+} , Ba^{2+} , and Pb^{2+} transfers facilitated by highly selective ionophores are measured and analyzed numerically using the E mechanism to obtain standard IT rate constants in the range of 10^{-2} – 10^{-3} cm/s at plasticized poly(vinyl chloride) membrane/water. We utilized ultrathin polymer membrane to maximize a current response by complete exhaustion of preconcentrated ions to detect nanomolar potassium ions using K^+ -selective valinomycin doped membrane. The selectivity of this membrane further reveals presence of NH_4^+ -valinomycin complex which is 60 times less stable than K^+ -valinomycin complex. This work also becomes the first to reveal 5nM K^+ contamination of lab nanopure water hence the need for cleaner ultrapure water to achieve a 0.6nM K^+ LOD. We further quantitatively confirm the charge-dependent

sensitivity theory by stripping voltammetry experiments of divalent ion i.e. Ca^{2+} . Specifically, the achievement of the subnanomolar LOD required two advantageous effects of higher analyte charge on sensitivity in addition to the careful prevention of the Ca^{2+} contamination of background solutions. Furthermore, we use the ionophore free double-polymer modified electrode to study lipophilicity of perfluoroalkyl surfactants. Advantageously, the high lipophilicity of perfluorooctane sulfonate allows for its stripping voltammetric detection at 50 pM in the presence of 1 mM aqueous supporting electrolytes, a $\sim 10^7$ times higher concentration. Significantly, this detection limit for perfluorooctane sulfonate is unprecedentedly low for electrochemical sensors and is lower than its minimum reporting level in drinking water set by the US Environmental Protection Agency.

TABLE OF CONTENTS

ACKNOWLEDGEMENTS	XIX
INTRODUCTION.....	1
1.0 ELECTROCHEMICAL MECHANISM OF ION-IONOPHORE RECOGNITION AT PLASTICIZED POLYMER MEMBRANE/WATER INTERFACES	3
1.1 INTRODUCTION	3
1.2 EXPERIMENTAL SECTION.....	9
1.2.1 Chemicals	9
1.2.2 Electrode Modification.....	9
1.2.3 IT Cyclic Voltammetry	10
1.3 RESULT AND DISCUSSION	12
1.3.1 Kinetic Effect on Facilitated IT at Plasticized PVC Membrane/Water Interfaces	12
1.3.2 Electrochemical Mechanism at Plasticized PVC Membrane/Water Interfaces	14
1.3.3 Assessment of the Electrochemical–Chemical Mechanism	20
1.3.4 Facilitated IT at DCE/Water Microinterfaces.....	25
1.3.5 Molecular Level Models for the E Mechanism.....	28
1.4 CONCLUSIONS	30
ACKNOWLEDGEMENTS	32
1.5 SUPPORTING INFORMATION	32

1.5.1	Characterization of PVC/PEDOT-C ₁₄ -Modified Electrodes.....	32
1.5.2	Determination of Diffusion Coefficients of Ion–Ionophore Complexes in the PVC Membrane.	33
1.5.3	Model for the EC Mechanism.	37
1.5.4	Numerical Simulation of CVs Based on the EC Mechanism at PVC Membrane/Water Interfaces.....	38
1.5.5	Potentiometric Determination of Formal Potentials of Facilitated Ca ²⁺ and Pb ²⁺ Transfers at DCE/Water Interfaces.	40
1.5.6	Numerical Simulation of Micropipet CVs Based on the EC Mechanism.	42
1.5.7	REFERENCES	45
1.6	REFERENCES	53
2.0	STRIPPING VOLTAMMETRY OF NANOMOLAR POTASSIUM AND AMMONIUM IONS USING A VALINOMYCIN-DOPED DOUBLE-POLYMER ELECTRODE	58
2.1	INTRODUCTION	58
2.2	THEORY	63
2.2.1	Model.	63
2.2.2	Equilibrium LOD.	64
2.2.3	Direct ITSV Determination of Analyte Concentration.....	65
2.3	EXPERIMENTAL SECTION.....	67
2.3.1	Chemicals	67
2.3.2	Electrode Modification.....	67

2.3.3	Electrochemical Measurement	68
2.4	RESULTS AND DISCUSSION	70
2.4.1	The CVs of K^+ and NH_4^+ Transfers at the Thin PVC Membrane Doped with Valinomycin.	70
2.4.2	Direct ITSV Determination of Potassium Ion.....	73
2.4.3	Equilibrium LODs of Potassium Ion.	78
2.4.4	Nanomolar Ammonium Contamination.....	81
2.5	CONCLUSIONS	83
2.6	SUPPORTING INFORMATION	84
2.6.1	Derivation of Eq 4 for the Preconcentration Step.	84
2.6.2	Finite Element Analysis of CVs of Facilitated K^+ and NH_4^+ Transfers.	86
2.6.3	Diffusion Problem for CV at the PVC Membrane/Water Interface. .	88
2.6.4	Finite Element Simulation by COMSOL Multiphysics.	91
2.6.5	REFERENCES	94
2.7	REFERENCES	95
3.0	SUB-NANOMOLAR DETECTION LIMIT OF STRIPPING VOLTAMMETRIC CA^{2+} SELECTIVE ELECTRODE: EFFECTS OF ANALYTE CHARGE AND SAMPLE CONTAMINATION.....	98
3.1	INTRODUCTION	98
3.2	EXPERIMENTAL SECTION.....	103
3.2.1	Chemicals.	103
3.2.2	Electrode Modification.....	104

3.2.3	Electrochemical Measurement	105
3.3	RESULTS AND DISCUSSIONS.....	106
3.3.1	Cyclic Voltammetry of Facilitated Ca ²⁺ Transfer.....	106
3.3.2	Rotating-Electrode Voltammetry.....	110
3.3.3	No Membrane Saturation with Ca ²⁺	113
3.3.4	Sub-Nanomolar Detection Limit.....	117
3.3.5	Ca ²⁺ Contamination in Commercial Ultrapure Water.....	121
3.4	CONCLUSIONS.....	124
3.5	SUPPORTING INFORMATION	125
3.5.1	Finite Element Analysis of CV of Facilitated Ca ²⁺ Transfer.....	125
3.5.2	Rotating-Electrode Setup.....	126
3.5.3	No Detectable Ca ²⁺ Contamination in Background Electrolyte Solution.	127
3.5.4	Ca ²⁺ contamination of background solutions.....	128
3.5.5	REFERENCES	131
3.6	REFERENCES	132
4.0	ION-TRANSFER VOLTAMMETRY OF PERFLUOROALKYL SULFONATES AND CARBOXYLATES: PICOMOLAR DETECTION LIMIT AND HIGH LIPOPHILICITY	135
4.1	INTRODUCTION	135
4.2	EXPERIMENTAL SECTION.....	140
4.2.1	Chemicals.....	140
4.2.2	Electrode Modification.....	141

4.2.3	Electrochemical Measurement	142
4.3	RESULTS AND DISCUSSIONS.....	143
4.3.1	Cyclic Voltammetry of Perfluoroalkyl Sulfonates.....	143
4.3.2	Lipophilicity of Perfluoroalkyl Sulfonates: Fragmental Analysis. ...	147
4.3.3	Lipophilicity and Fluophilicity of Perfluoroalkyl Sulfonates.....	149
4.3.4	Stripping Voltammetry of PFOS ⁻	150
4.3.5	Picomolar Detection Limit for PFOS ⁻	154
4.3.6	Cyclic Voltammetry of Perfluoroalkyl Carboxylates.....	157
4.3.7	Voltammetry versus Potentiometry with the <i>o</i> NPOE/PVC Membrane.	161
4.4	CONCLUSIONS.....	162
4.5	SUPPORTING INFORMATION	163
4.5.1	Finite Element Simulation.	163
4.5.2	Cyclic Voltammetry of Alkyl Sulfonates.	164
4.5.3	Background-Subtracted Stripping Voltammograms of Picomolar PFOS ⁻	166
4.5.4	Stripping Voltammetric Responses to a Contaminant Anion.	167
4.5.5	Lipophilicity of Perfluoroalkyl Carboxylates.	168
4.5.6	Oxidation of PFO ⁻ at the PVC/POT/Gold Junction.....	169
4.5.7	REFERENCES	170
4.6	REFERENCES	171

LIST OF TABLES

Table 1-1. Kinetic Parameters for the E Mechanism at PVC Membrane/Water Interfaces. 19

Table 1-2. Thermodynamic and Kinetic Parameters for the EC Mechanism at PVC Membrane/Water Interfaces..... 19

Table 1-3. Kinetic Parameters for the E Mechanism at PVC Membrane/Water Interfaces 25

Table 1-4. Thermodynamic and Kinetic Parameters for the EC Mechanism at DCE/Water Interfaces. 27

Table 1-5. Thermodynamic and Kinetic Parameters for Facilitated Ag⁺ Transfer based on the EC Mechanism at PVC Membrane/Water Interfaces. 40

Table 2-1. Parameters Employed for the Finite Element Analysis of CVs in Figure 2-2A.. 88

Table 3-1. Parameters Employed for the Finite Element Analysis of Facilitated Ca²⁺ Transfer. 126

Table 4-1. Parameters Used for Simulated CVs in Figures 4-2 and 4-6..... 164

LIST OF FIGURES

Figure 1-1. Structures of ionophores 1–4 for Ag^+ , K^+ , Ca^{2+} (and Ba^{2+}), and Pb^{2+} respectively.... 8

Figure 1-2. Background-subtracted CVs (solid lines) of facilitated IT as obtained using PVC/PEDOT- C_{14} -modified (a, d) Au or (b, c) GC electrodes in cell 1 containing (a) 20 mM ionophore **1** with 20 μM CH_3COOAg in 10 mM CH_3COOLi (pH 5.4), (b) 20 mM ionophore **2** with 20 μM KCl in 10 mM Li_2SO_4 , (c) 60 mM ionophore **3** with 10 μM CaCl_2 (left) or BaCl_2 (right) in 10 mM CH_3COOK (pH 7.1), and (d) 20 mM ionophore **4** with 20 μM PbCl_2 in 5 mM MgCl_2 (pH 4.7). The $E_i^{0'}$ value for Ca^{2+} is used in (c). Potential sweep rates are from the top to the bottom, (a, b, c) 1, 0.5, 0.2, 0.1, and 0.05 V/s, and (d) 0.2, 0.1, and 0.05 V/s. Parameters for theoretical CVs (closed circles) based on the E mechanism are listed in Table 1-1. The dotted lines in (d) were obtained using $z = 2$ and $\alpha = 0.5$ 17

Figure 1-3. Scheme of E and EC mechanisms for facilitated IT. The rate constants are assigned to each process by eqs 2, S-2, S-6, and S-7, where $k_a' = k_a L_T^n$. Facilitated cation transfers are driven around $E = E^{0'} \gg E_i^{0'}$ (see eq 5). 18

Figure 1-4. Background-subtracted micropipet CVs (solid lines) of facilitated Ag^+ transfer at DCE/water microinterfaces with 20 mM ionophore 1 in cell 2 containing 100 μM CH_3COOAg in 10 mM CH_3COOLi (pH 5.5). Parameters for the theoretical CVs (closed circles) based on the E mechanism are listed in Table 1-3. Pipet inner diameter, 4.3 μm 22

Figure 1-5. Background-subtracted micropipet CVs (solid lines) at DCE/water microinterfaces in cell 2 containing (a) 20 mM ionophore 2 with 25 μM K_2SO_4 in 10 mM MgSO_4 (pH 6.6), (b) 60 mM ionophore 3 with 30 μM $(\text{CH}_3\text{COO})_2\text{Ca}$ in 10 mM CH_3COOK (pH 7.3), and (c) 20 mM ionophore 4 with 90 μM PbCl_2 in 5 mM MgCl_2 (pH 4.7). Parameters for theoretical CVs (closed circles) based on the E mechanism are listed in Table 1-3. Pipet inner diameters, (a) 3.7, (b) 4.2, and (c) 3.7 μm . Potential sweep rates, (a) 20, (b) 5, and (c) 20 mV/s 24

Figure 1-6. Scheme of the non-linear diffusion of aqueous ions to membraneous ionophore molecules for their collision and subsequent complexation at the interface. 28

Figure 1-7. Scheme of the formation of 1:3 Ca^{2+} -ionophore **3** complexes at (a) a *o*NPOE-plasticized PVC membrane/water interface with a thicker mixed layer and (b) a sharper DCE/water interface..... 29

Figure 1-8. Background-subtracted CVs (solid lines) of simple tetrapropylammonium transfer as obtained at 0.05, 0.1, 0.2, 0.5, and 1 V/s using a PVC/PEDOT- C_{14} -modified (a) GC or (b) Au electrode without ionophore in cell 1 containing 20 μM tetrapropylammonium chloride in 10 mM Li_2SO_4 . Theoretical CVs (closed circles) are reversible..... 33

Figure 1-9. CV of 0.8 mM Ag^+ as 1:1 complexes with ionophores **1** in cell S-1 containing 0.8 mM TFAB in the PVC membrane and 1 μM CH_3COOAg in 10 mM CH_3COOLi (pH 5.4)..... 35

Figure 1-10. Plots of forward peak currents (symbols) versus membrane concentrations of ion-ionophore complexes or tetrapropylammonium (TPA^+). Solid lines represent eq S-1 (or an analogous equation for TPA^+), where non-zero intercepts are due to background currents. CVs of the facilitated transfer of each ion were obtained at 0.2 V/s using cell S-1 for ionophore **1** with 1 μM CH_3COOAg in 10 mM CH_3COOLi at pH 5.4, ionophore **2** with 1 μM KCl in 10 mM Li_2SO_4 , ionophore **3** with 1 μM CaCl_2 or BaCl_2 in 10 mM CH_3COOK at pH 7.1, and ionophore **4** with 1

μM $(\text{CH}_3\text{COO})_2\text{Pb}$ in 10 mM CH_3COOLi at pH 5.4. Cell S-1 for CVs of simple TPA^+ transfer contained TPATFAB in the PVC membrane and 1 μM TPACl in 10 mM Li_2SO_4 . A GC electrode was used for Pb^{2+} while CVs of other ions were measured using a Au electrode. 36

Figure 1-11. Background-subtracted CVs (solid lines) as shown in Figure 1-2 and theoretical CVs (circles) based on the EC mechanism with parameters listed in Table 1-2. 39

Figure 1-12. Open circuit potentials of cells (a) S-2 and (b) S-3 at different ion concentrations in the aqueous phase. 42

Figure 1-13. Background-subtracted micropipet CV (solid line) of facilitated K^+ transfer as shown in Figure 1-5a and theoretical CV (circles) based on the EC mechanism with the parameters listed in Table 1-4. 43

Figure 1-14. Background-subtracted CVs (solid lines) of facilitated Ag^+ transfer as shown in Figure 1-4 and theoretical CVs (circles) based on the EC mechanism with the parameters listed in Table 1-4. 44

Figure 2-1. Scheme of preconcentration (black arrows) and stripping (red arrows) steps in ITSV with a valinomycin-doped double-polymer electrode. 62

Figure 2-2. (A) Background-subtracted CVs and (B) their integrations for valinomycin-mediated transfers of K^+ and NH_4^+ at an *o*NPOE-plasticized PVC/PEDOT- C_{14} -modified gold electrode. Scan rate, 0.1 V/s. 72

Figure 2-3. (A) The ITSV of 50 nM K^+ at 0.1 V/s with various preconcentration times. Preconcentration potential, 0.38 V. The electrode was rotated at 4000 rpm. (B) The corresponding plot of $Q_{\text{tot}}(t_p)$ versus t_p 76

Figure 2-4. (A) The ITSV of 5.1 nM K⁺ contaminated in the laboratory-purified water at 0.1 V/s with various preconcentration times. Preconcentration potential, 0.38 V. The electrode was rotated at 4000 rpm. (B) The corresponding plot of $Q_{\text{tot}}(t_p)$ versus t_p 77

Figure 2-5. (A) The ITSV of 0–10 nM K⁺ in the ultrapure water at 0.1 V/s after 5 min preconcentration. Preconcentration potential, 0.38 V. The electrode was rotated at 4000 rpm. (b) Plot of the background-subtracted peak current versus K⁺ concentration. The solid line represents the best fit used for the determination of the LOD. The inset shows background-subtracted ITSVs. 80

Figure 2-6. The ITSV of the commercial ultrapure water at 0.1 V/s (A) before and after the addition of 100 and 200 nM NH₄⁺ and (B) with various preconcentration times. Preconcentration potential, 0.35 V and 0.27 V, respectively. The electrode was rotated at 4000 rpm. (C) Plot of $Q_{\text{tot}}(t_p)$ versus t_p as obtained from the voltammograms in part (B)..... 82

Figure 3-1. (A) CVs of 0 and 10 μM Ca²⁺ (cell 1) at a PEDOT-C₁₄-modified gold electrode spin-coated with an *o*NPOE-plasticized PVC membrane containing ETH 129. Potential sweep rate, 0.05 V/s. (B) Corresponding background-subtracted CV, simulated CV, and the integration of the background-subtracted CV. 108

Figure 3-2. (A) Background-subtracted rotating-electrode CVs of 2 μM Ca²⁺ at a PEDOT-C₁₄-modified gold electrode spin-coated with an *o*NPOE-plasticized PVC membrane containing ETH 129 (cell 2). Potential sweep rate, 0.05 V/s. (B) A plot of the corresponding limiting current versus the square root of rotation speed (radian per second). The solid line is the best fit with the Levich equation..... 112

Figure 3-3. (A) Stripping voltammograms of 10 nM Ca²⁺ in Milli-Q water (cell 2) with different preconcentration times. Potential sweep rate, 0.05 V/s. (B) Charge under the stripping

voltammograms (circles) and the best fits with eqs 7 and 9 (dotted and solid lines, respectively).
..... 115

Figure 3-4. (A) Stripping voltammograms of 0–1 nM Ca^{2+} in Milli-Q water (cell 2) after 30 minute preconcentration. Potential sweep rate, 0.05 V/s. The inset shows the corresponding background-subtracted voltammograms. (B) A plot of background-subtracted peak current versus Ca^{2+} concentration (circles) and best fit with eq 11 (solid line)..... 119

Figure 3-5. (A) Stripping voltammograms of commercial ultrapure water (cell 2) with different preconcentration times. Potential sweep rate, 0.05 V/s. (B) Charge under the stripping voltammograms (circles) as obtained by integrating current between potentials indicated by dotted lines and the best fit with eq 9 (solid line). 123

Figure 3-6. Image of electrode rotator in a Ar-filled polyethylene glove bag. The bag was accommodated in a class 100 laminar flow hood. 127

Figure 3-7. Stripping voltammograms of a background electrolyte solution prepared from Milli-Q water (cell 2) after 5 and 30 minutes preconcentration. Potential sweep rate, 0.05 V/s. The blue line represents the subtraction of the 5 minutes voltammogram from the 30 minute voltammogram.
..... 128

Figure 3-8. Stripping voltammograms of (A) three background solutions after 5 minutes preconcentration and (B) a background electrolyte solution after 5 and 30 minutes preconcentration (cell 2). In part (B), the blue line represents the subtraction of the 5 minutes voltammogram from the 30 minutes voltammogram. Potential sweep rate, 0.05 V/s..... 130

Figure 4-1. Scheme of the voltammetric transfer of PFOS^- from water into the *o*NPOE/PVC membrane coated on a POT-modified Au electrode at positive potentials. Charge transfer between

the POT film and the *o*NPOE/PVC membrane is mediated by organic electrolytes in the membrane..... 139

Figure 4-2. Background-subtracted CVs (red lines) of 20 μM perfluorooctane sulfonate, perfluorohexane sulfonate, perfluorobutane sulfonate, and octane sulfonate (from the top) in cell 1. The potential was applied to the gold electrode, swept at 0.1 V/s, and defined against the formal potential of perchlorate. Circles represent the CVs simulated by using the parameters listed in Table 4-1 (Supporting Information). Dotted lines correspond to the formal potentials of the sulfonates. 145

Figure 4-3. Plots of formal potentials versus the number of the carbon atoms of perfluoroalkyl (closed circles) and alkyl (crosses) sulfonates for the *o*NPOE/PVC membrane. The formal potentials of the perfluoroalkyl sulfonates for the fluorous membrane (open circles) were calculated from selectivity coefficients against perchlorate²⁹ by using eq 4. Solid lines are the best fits with eq 3..... 148

Figure 4-4. (A) Stripping voltammograms of 10 nM PFOS⁻ (cell 2) at different preconcentration times. The potential was applied to the gold electrode, swept at 0.1 V/s, and defined against the formal potential of perchlorate. (B) Charge under the stripping voltammograms (circles) and the best fit with eq 6 (solid line). 154

Figure 4-5. (A) Stripping voltammograms of 0–1 nM PFOS⁻ (cell 2) after 30 min preconcentration. The potential was applied to the gold electrode, swept at 0.1 V/s, and defined against the formal potential of perchlorate. (B) A plot of background-subtracted peak current versus PFOS⁻ concentration (circles) and best fit with eq 9 (solid line). 156

Figure 4-6. Background-subtracted CVs (red lines) of 20 μM perfluorooctanoate, perfluorohexanoate, perfluorobutanoate, and 10 μM tetradecanoate (from the top) in cell 1. The

potential was applied to the gold electrode, swept at 0.1 V/s, and defined against the formal potential of perchlorate. Circles represent the CVs simulated by using the parameters listed in Table 4-1 (Supporting Information). Dotted lines correspond to the formal potentials of the sulfonates with the same number of carbon atoms. 159

Figure 4-7. Background-subtracted CVs (red lines) of 20 μM dodecyl and decyl sulfonates (from the top) in cell 1. The potential was applied to the gold electrode, swept at 0.1 V/s, and defined against the formal potential of perchlorate. Dotted lines correspond to the formal potentials of the sulfonates. 165

Figure 4-8. Background-subtracted stripping voltammograms of 0.05–1 nM PFOS^- (cell 2) after 30 min preconcentration. The potential was applied to the gold electrode, swept at 0.1 V/s, and defined against the formal potential of perchlorate. The dotted line represents zero current. 166

Figure 4-9. Stripping voltammograms of 0–1 nM PFOS^- (cell 2) after 30 min preconcentration in the presence of a contaminant anion in the sample solutions. The potential was applied to the gold electrode, swept at 0.1 V/s, and defined against the formal potential of perchlorate. 167

Figure 4-10. Background-subtracted CVs (red lines) of 20 μM perfluorododecanoate and perfluorodecanoate (from the top) in cell 1. The potential was applied to the gold electrode, swept at 0.1 V/s, and defined against the formal potential of perchlorate. The dotted line corresponds to the formal potential of PFOS^- 168

Figure 4-11. CVs of a POT film with a PVC membrane/water interface non-polarized by partitioning of TBAClO_4 . The potential was applied to the gold electrode against a Ag/AgCl reference electrode in 3 M KCl . Potential sweep rate, 0.1 V/s. 170

ACKNOWLEDGEMENTS

I would like to express my sincere gratitude to my advisor, Professor Shigeru Amemiya, for the training that he has provided during my graduate program. Professor Amemiya has invested a tremendous amount of time and energy to help me develop into a professional scientist. I greatly appreciate his contributions to my success.

I want to thank Professor Adrian Michael, Professor Stephen Weber and Professor Minhee Yun for their willingness to serve on my dissertation committee. I value my interaction with each of them, which has been beneficial for my development and continued success in my scientific career. I also would like to acknowledge the present and past members of the Amemiya research group for their support and encouragement. I am thankful for their scientific contributions and friendship.

I also want to acknowledge my wife Dorothy M., and our kids Ian M., Ianna G. and Ethan B. Kabagambe for their patience during my Ph.D. Pursuit. I thank my parents and siblings in Uganda and Rwanda as well as my friends and colleagues in United States for their words of encouragement over the course of this journey. Their consistent support through challenging and successful periods during my graduate program is invaluable.

Finally I would like to thank PPG Industries for keeping me employed in their R&D as well as giving me financial support to pursue an advanced degree. I also appreciate University of Pittsburgh, Chemistry Department for giving me an opportunity to learn and develop a career in chemistry.

INTRODUCTION

In my PhD work, I have developed a highly selective and sensitive electrochemical ion-ionophore recognition method that can be used to characterize fundamental transport dynamics at membrane/water interfaces. I have also demonstrated that my selective and sensitive electrochemical technique is useful for very low detection of trace ions.

In Chapter 1, cyclic voltammograms of Ag^+ , K^+ , Ca^{2+} , Ba^{2+} , and Pb^{2+} transfers facilitated by highly selective ionophores are measured and analyzed numerically using the E mechanism to obtain standard IT rate constants in the range of 10^{-2} – 10^{-3} cm/s at both plasticized poly(vinyl chloride) membrane/water and 1,2-dichloroethane/water interfaces. My role in this study was focused on the plasticized poly (vinyl chloride) membrane/water interfaces.

In chapter 2, i utilized ultrathin polymer membrane to maximize a current response by complete exhaustion of preconcentrated ions to detect nanomolar potassium ions using K^+ -selective valinomycin doped double-polymer modified electrode. The selectivity of this membrane further reveals presence of NH_4^+ -valinomycin complex which is 60 times less stable than K^+ -valinomycin complex. This work also becomes the first to reveal 5nM K^+ contamination of lab nanopure water hence the need for cleaner ultrapure water and a cleaner to achieve a 0.6nM K^+ LOD. Moreover, an atmosbag filled with argon is utilized to prevent NH_4^+ contamination from

NH₃ in ambient air. The whole bag was accommodated in a class 100 vertical laminar flow hood to eliminate particulate K⁺ contamination from the air.

In chapter 3, i quantitatively confirm the charge-dependent sensitivity theory by stripping voltammetry experiments of divalent ion i.e. Ca²⁺. Specifically, the achievement of the subnanomolar LOD required two advantageous effects of higher analyte charge on sensitivity in addition to the careful prevention of the Ca²⁺ contamination of background solutions. Significantly, charge-dependent sensitivity is attractive for the ultrasensitive detection of multivalent ions with environmental and biomedical importance such as heavy metal ions and polyionic drugs.

In chapter 4, we use the ionophore free double-polymer membrane to study lipophilicity of perfluoroalkyl surfactants i.e. perfluoroalkyl sulfonates and carboxylates. Advantageously, the high lipophilicity of perfluorooctane sulfonate allows for its stripping voltammetric detection at 50 pM in the presence of 1 mM aqueous supporting electrolytes, a $\sim 10^7$ times higher concentration. Significantly, this detection limit for perfluorooctane sulfonate is unprecedentedly low for electrochemical sensors and is lower than its minimum reporting level in drinking water set by the US Environmental Protection Agency.

1.0 ELECTROCHEMICAL MECHANISM OF ION-IONOPHORE RECOGNITION AT PLASTICIZED POLYMER MEMBRANE/WATER INTERFACES

This work has been published as Ryoichi Ishimatsu, Anahita Izadyar, Benjamin Kabagambe, Yushin Kim, Jiyeon Kim, and Shigeru Amemiya *J. Am. Chem. Soc.* **2011**, *133*, 16300–16308. The thesis author contributed in conducting CV experiments using plasticized polymer membrane modified glassy carbon electrodes as well as Pb^{2+} ion transfer using modified gold electrode.

1.1 INTRODUCTION

Here we report on the first electrochemical study that reveals the kinetics and molecular level mechanism of heterogeneous ion–ionophore recognition at plasticized polymer membrane/water interfaces. The new kinetic data provide greater understanding of this important ion-transfer (IT) process, which determines various dynamic characteristics of the current technologies that enable highly selective ion sensing and separation. The theoretical assessment of the reliable voltammetric data confirms that the dynamics of the ionophore-facilitated IT follows the one-step electrochemical (E) mechanism controlled by ion–ionophore complexation at the very interface in contrast to the thermodynamically equivalent two-step electrochemical–chemical (EC) mechanism based on the simple transfer of an aqueous ion followed by its complexation in the

bulk membrane. Specifically, cyclic voltammograms of Ag^+ , K^+ , Ca^{2+} , Ba^{2+} , and Pb^{2+} transfers facilitated by highly selective ionophores are measured and analyzed numerically using the E mechanism to obtain standard IT rate constants in the range of 10^{-2} – 10^{-3} cm/s at both plasticized poly(vinyl chloride) membrane/water and 1,2-dichloroethane/water interfaces. We demonstrate that these strongly facilitated IT processes are too fast to be ascribed to the EC mechanism. Moreover, the little effect of the viscosity of non-aqueous media on the IT kinetics excludes the EC mechanism, where the kinetics of simple IT is viscosity-dependent. Finally we employ molecular level models for the E mechanism to propose three-dimensional ion–ionophore complexation at the two-dimensional interface as the unique kinetic requirement for the thermodynamically facilitated IT.

Current technologies for highly selective ion sensing¹ and separation² are chemically based on the recognition of an aqueous target ion by a membraneous ionophore, which thermodynamically facilitates selective ion transfer (IT) into a plasticized polymer membrane. During the past five decades, >1000 natural and synthetic ionophores have been tested as selective recognition elements of such potentiometric and optical sensors for various analyte ions.³ Especially successful are ionophores for alkaline, alkaline earth, and heavy metal ions, e.g., ionophores **1–4** (Figure 1-1), which can render plasticized polymer membranes up to 10^{10} – 10^{15} times selective for a target ion against interfering ions.^{1e} This high selectivity is ascribed to the formation of ion–ionophore complexes with unique stoichiometries, n , and large overall formation constants, β_n , in the bulk membrane. For instance, ionophores **1**, **2**, and **4** form stable 1:1 complexes with Ag^+ , K^+ , and Pb^{2+} , respectively, to yield β_1 values of $\sim 10^{10}$ – 10^{15} in plasticized poly(vinyl chloride) (PVC) membranes, where a large β_3 value of $\sim 10^{30}$ was also determined for 1:3 Ca^{2+} –ionophore **3** complexes.⁴ The strong ion–ionophore interaction overcomes an unfavorable change

in the free energy of the transfer of the hydrophilic ions into the hydrophobic membrane. Moreover, the thermodynamically facilitated IT has been assumed to be fast and instantaneously reach local equilibrium across the interface even under dynamic mass-transport conditions, thereby developing the phase boundary potential as expected from the Nernst equation.^{1b} The resulting potential is unfavorable for the transfer of an interfering ion with weaker ionophore-binding ability and/or higher hydrophilicity than the target ion to yield high thermodynamic selectivity.

The fundamental mechanism of facilitated IT is dynamic and electrochemical as demonstrated by employing voltammetry at interfaces between two immiscible electrolyte solutions (ITIES) such as water and 1,2-dichloroethane (DCE).⁵ Kinetic analysis is essential for discrimination between two thermodynamically equivalent mechanisms of IT facilitated by lipophilic ionophores, i.e., one-step electrochemical (E) mechanism and two-step electrochemical–chemical (EC) mechanism.⁶ Specifically, the EC mechanism is based on the simple transfer of an ion across the ITIES followed by its homogeneous complexation with an ionophore in the non-aqueous phase while the overall transfer process is considered as a single interfacial process in the E mechanism.⁷ The EC mechanism is inconsistent with diffusion-limited voltammograms of rapid facilitated IT as typically observed at macroscopic ITIES because the electrochemically and chemically reversible (E_rC_r) responses require that the dissociation of stable ion–ionophore complexes in the bulk phase must be faster than a diffusion limit.⁶ On the other hand, the E mechanism agrees well with not only reversible voltammograms but also kinetically limited voltammograms as obtained using microscopic⁸ and nanoscopic⁹ ITIES formed at the tip of glass pipets to achieve high mass transport conditions. The phenomenological Butler-Volmer-type kinetic model¹⁰ was employed in the E mechanism to yield large standard IT rate constants, k^0 , of

$2\text{--}10^{-2}$ cm/s and transfer coefficients, α , in a normal range of 0.4–0.6.⁸⁻⁹ Noticeably, these kinetic voltammograms have not been used to assess the EC mechanism.

Despite pioneering work by Buck and co-workers,¹¹ kinetic studies of facilitated IT at plasticized polymer membrane/water interfaces have been scarce and controversial, which seriously limits our understanding of various dynamic characteristics of the ionophore-based sensors such as response time,¹² detection limit,¹³ selectivity in mixed ion solutions¹⁴ in addition to the efficiency of ion separation across ionophore-doped polymer membranes.¹⁵ The major obstacle in the quantitative voltammetric measurement of IT kinetics at polymer membrane/water interfaces is a large Ohmic potential drop in the viscous, thick, and resistive membrane even when small current at a micrometer-sized interface is measured.¹⁶ Apparently non-reversible voltammograms of K^+ and Na^+ transfers facilitated by ionophore **2** (valinomycin) at the microinterfaces were ascribed not to the kinetic effect but to the effect of uncompensated Ohmic potential drop on reversible IT.^{16b} Controversially, earlier amperometric and impedance studies of the respective IT processes gave extremely small α ($\approx 0.05^{11b}$) and k^0 ($\approx 10^{-5}$ cm/s¹⁷) values, which indicate slow IT kinetics. Recently, we introduced a thin plasticized PVC membrane (0.7–3 μm in thickness) supported on a solid electrode to enable quantitative IT voltammetry without a significant Ohmic potential drop.¹⁸ With this new voltammetric setup, a conducting polymer film serves as the intermediate layer between the ionic PVC membrane and the electronic solid support to mediate ion-to-electron transduction, where the reduction (or oxidation) of the conducting polymer film drives the transfer of aqueous (or membraneous) cations into the opposite phase. No kinetic study, however, has been reported using such thin PVC membranes, which have been successfully applied for voltammetric/amperometric ion sensing with conducting polymers¹⁸⁻¹⁹ or redox molecules²⁰ as ion-to-electron transducers.

Here we report on the first electrochemical study that reveals the kinetics and molecular level mechanism of facilitated IT at plasticized PVC membrane/water interfaces to augment our understanding of this important charge transfer process for better ion sensing and separation. Specifically, we apply IT cyclic voltammetry (CV) at solid-supported thin PVC membranes¹⁸ to confirm the E mechanism with k^0 values of 10^{-2} – 10^{-3} cm/s and normal α values of 0.45–0.50 for Ag^+ , K^+ , Ca^{2+} , Ba^{2+} , and Pb^{2+} transfers facilitated by ionophores **1–4** using 2-nitrophenyl octyl ether (*o*NPOE) as a common plasticizer for practical ion sensing¹ and separation.² We demonstrate that these IT processes are relatively slow as E processes but are too fast to be explained by the EC mechanism, where not only ion–ionophore complexation must be faster than a diffusion limited rate⁶ but also simple IT must be much faster than the fastest simple IT reported so far. Interestingly, we also find that these facilitated IT processes with the highly viscous *o*NPOE/PVC membrane can be as fast as or even faster than those with the fluidic DCE phase. This finding also excludes the EC mechanism, where simple IT is slower with a more viscous solvent medium.²¹ Finally, the E mechanism is assessed microscopically to propose the kinetic importance of three-dimensional ion–ionophore complexation at the two-dimensional interface.

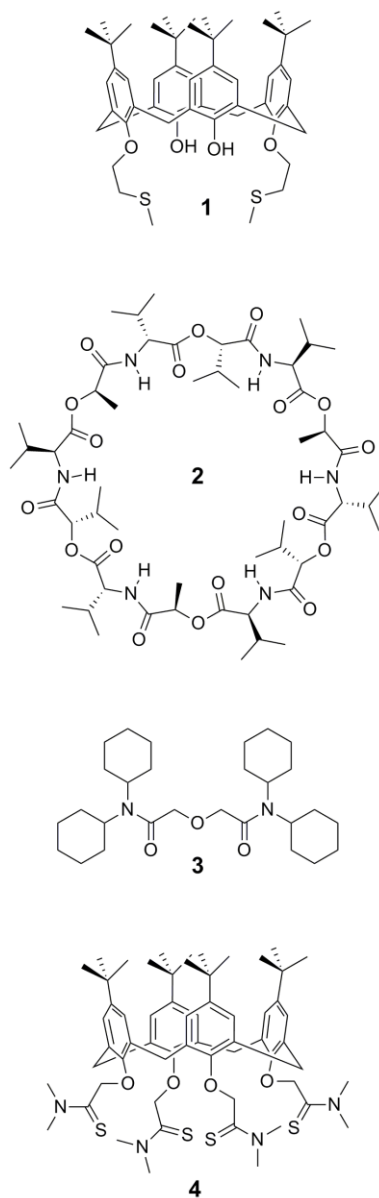


Figure 1-1. Structures of ionophores 1–4 for Ag⁺, K⁺, Ca²⁺ (and Ba²⁺), and Pb²⁺ respectively.

1.2 EXPERIMENTAL SECTION

1.2.1 Chemicals

Ionophores **1–4** (Figure 1-1), tetradodecylammonium (TDDA) bromide, tetrapropylammonium chloride, PVC (high molecular weight), and *o*NPOE were obtained from Aldrich (Milwaukee, WI). Potassium tetrakis(pentafluorophenyl)borate (TFAB) was from Boulder Scientific Company (Mead, CO). All reagents were used as received. The TFAB salt of TDDA was prepared by metathesis.^{18a} 2-*n*-Tetradecyl-2,3-dihydro-thieno[3,4-*b*][1,4]dioxine (EDOT-C₁₄) was synthesized as reported elsewhere.²² Aqueous sample solutions were prepared with 18.3 MΩ cm deionized water (Nanopure, Barnstead, Dubuque, IA).

1.2.2 Electrode Modification

A 5 mm-diameter Au or glassy carbon (GC) disk attached to a rotating disk electrode tip (Pine Research Instrumentation, Raleigh, NC) was cleaned as follows to be modified with a conducting polymer film and then with an *o*NPOE-plasticized PVC membrane. A Au or GC electrode was polished with alumina paste slurry (0.3 and 0.05 μm) on microcloth pads (Buehler, Lake Bluff, IL). A polished Au electrode was sonicated in H₂SO₄ containing 3% K₂Cr₂O₇ for 15 min and in deionized water three times for 15 min. A polished GC electrode was cleaned using a UV/ozone cleaner (UV-tip Cleaner, BioForce Nanosciences, Ames, IA) for 3 min and sonicated twice in methanol and twice in water (each for 15 min).

EDOT-C₁₄ was electropolymerized by cyclic voltammetry to coat a clean Au or GC

electrode with the polymer film (PEDOT-C₁₄). A three-electrode cell was set up with a Ag/Ag⁺ reference electrode (CH Instruments) and a Pt-wire counter electrode in the acetonitrile solution of 0.03 M TDDATFAB and 0.1 M EDOT-C₁₄. The film deposition was conducted by cycling the potential of a GC electrode 4 times between -0.50 V and 1.39 V at 0.1 V/s (or twice between -0.70 V and 1.5 V for a Au electrode) using a computer-controlled CHI 600A electrochemical workstation (CH Instruments). The modified electrode was soaked in acetonitrile for 1 min to remove the residual monomer solution and soluble fractions of the film. The potential of the modified electrode in the monomer-free acetonitrile solution of 0.03 M TDDATFAB was cycled twice between -0.7 V and 0.8 V at 0.1 V/s, and then linearly swept to 0.8 V to oxidatively dope the PEDOT-C₁₄ film with TFAB.

Finally, a PEDOT-C₁₄-modified Au or GC electrode was drop-cast with an *o*NPOE-plasticized PVC membrane from the 18 μ L THF solution prepared by dissolving 4.0 mg PVC, 16.0 mg *o*NPOE, and 2.2 mg TDDATFAB in 1 mL THF. The THF solution also contained an ionophore to give its membrane concentration as specified in legends of the corresponding figures after THF was slowly evaporated from the drop-cast solution at least for 20 minutes.

1.2.3 IT Cyclic Voltammetry

CVs of facilitated IT at plasticized PVC membrane/water and DCE/water interfaces were measured using a CHI 660B electrochemical workstation equipped with CHI 200 picoampere booster and Faraday cage (CH Instruments). All electrochemical experiments were performed at 22 ± 3 °C. Concentrations of target ion, ionophore, and supporting electrolyte in the following

electrochemical cells are given in legends of the corresponding figures. The current carried by cation transfer from the aqueous phase to the non-aqueous phase is defined to be positive.

CV with PVC/PEDOT-C₁₄-modified electrodes employed a three-electrode arrangement with a double-junction Ag/AgCl reference electrode (BASi, West Lafayette, IN) and a Pt-wire counter electrode. Electrochemical cells were as follows:

Ag | AgCl | 3 M KCl || supporting electrolyte (w) || target ion and supporting electrolyte (w)
| ionophore and 0.1 M TDDATFAB (*o*NPOE/PVC) | PEDOT-C₁₄ | Au or GC
(cell 1)

A piece of Teflon tube was put on a membrane-modified electrode to obtain a disk-shaped PVC membrane/water interface with the diameter of 1.5 mm and the interfacial area of 0.0177 cm².¹⁸

Micropipet CV employed two-electrode cells as represented by

Ag | AgCl | 3 M KCl || supporting electrolyte (w) || target ion and supporting electrolyte (w)
| ionophore and 0.1 M TDDATFAB (DCE) | Ag
(cell 2)

For Pb²⁺, a Ag/AgCl wire was used as an aqueous electrode instead. A 4–5 μm-diameter glass micropipet was prepared using a laser-based pipet puller (model P-2000, Sutter Instrument), modified with trimethylchlorosilane, and filled with a DCE solution as reported elsewhere.²³ A dual beam instrument (SMI3050SE FIB-SEM, Seiko Instruments, Chiba, Japan) was employed to

mill the tapered end of a pulled micropipet by the focused beam of high-energetic gallium ions,²⁴ thereby yielding a smoother tip for better support of the microinterface.

1.3 RESULT AND DISCUSSION

1.3.1 Kinetic Effect on Facilitated IT at Plasticized PVC Membrane/Water Interfaces

Here we demonstrate unambiguous and quantitative kinetic effect on facilitated IT at plasticized polymer membrane/water interfaces, which resolves long-standing controversy on the intrinsic rate of this practically important and fundamentally unique charge transfer process.^{1b,11,16b} The kinetic effect was observed by cyclic voltammetry at Au or GC electrodes modified with a PEDOT-C₁₄ membrane and then with an *o*NPOE-plasticized PVC membrane (cell 1). The thickness of each membrane was optimized for kinetic measurement. An Ohmic potential drop was negligible in an *o*NPOE/PVC membrane with an estimated thickness of 14 μm ,^{18a} which was chosen in this work to achieve the semi-infinite diffusion of ion-ionophore complexes in the solid-supported membrane. A PEDOT-C₁₄ film with a thickness of 0.3–0.6 μm as estimated by SEM was used as an ion-to-electron transducer with sufficient redox capacity to avoid the significant polarization of the PVC/PEDOT-C₁₄/electrode junction. These voltammetric features that are essential for reliable kinetic measurement were confirmed by reversible CVs of simple tetrapropylammonium transfer (Figure 1-8).

The kinetic effect is clearly seen as wide separations of peak potentials in CVs of

monovalent cations (Ag^+ and K^+) and divalent cations (Ba^{2+} , Ca^{2+} , and Pb^{2+}) at PVC membranes doped with ionophores **1–4** (Figure 1-2). In these CVs, potentials are defined against the formal potential of facilitated IT, $E^{0'}$, as determined below. Facilitated Ag^+ and K^+ transfers (Figure 1-2a and 2b, respectively) are nearly reversible at a potential sweep rate, ν , of 50 mV/s to give a peak separation of ~ 63 mV, which is close to $60/z$ mV as expected for the reversible transfer of a monovalent ion with a charge of $z = 1$.²⁵ At a higher sweep rate, forward and reverse peak potentials shift toward more extreme potentials. A wider peak separation of ~ 110 mV at $\nu = 1$ V/s clearly indicates quasi-reversible IT. Similarly, a peak separation for relatively fast Ba^{2+} transfer (the right CVs in Figure 1-2c) increases from a reversible limit of ~ 30 mV for $z = 2$ to a quasi-reversible value of 55 mV as ν varies from 50 mV/s to 1 V/s. On the other hand, facilitated Ca^{2+} and Pb^{2+} transfers (Figure 1-2c and 1-2d, respectively) are slow enough to be kinetically limited even at $\nu = 50$ mV/s as confirmed by the corresponding peak separations of 47 and 100 mV, respectively. The peak separations vary with ν , thereby confirming kinetic control.

Noticeably, both kinetic and thermodynamic effects are clearly seen in CVs of Ca^{2+} and Ba^{2+} transfers facilitated by ionophore **3** (Figure 1-2c). Forward and reverse waves of the Ca^{2+} transfer are broader and more widely separated from each other than those of the Ba^{2+} transfer, indicating that the former process is slower than the latter process. In addition, the transfer of more hydrophilic Ca^{2+} is observed at more positive potentials than the Ba^{2+} transfer, which gives $E^{0'} = -0.140$ V against the $E^{0'}$ value for Ca^{2+} as used in Figure 1-2c. This result indicates that ionophore **3** forms more stable complexes with Ca^{2+} than with Ba^{2+} to thermodynamically facilitate the Ca^{2+} transfer more effectively.

1.3.2 Electrochemical Mechanism at Plasticized PVC Membrane/Water Interfaces

Kinetically controlled CVs of facilitated IT at interfaces between water and the *o*NPOE-plasticized PVC membrane fit well with theoretical CVs (Figure 1-2) to validate the E mechanism, which is formulated as follows. In this mechanism, facilitated IT is considered as a heterogeneous one-step process, i.e.



where i^z is an ion with a charge of z , L is an electrically neutral ionophore, and iL_n^z is a 1: n ion-ionophore complex. In the presence of the excess amount of ionophore, facilitated IT based on the E mechanism can be defined as a first-order process (Figure 1-3)



where k_f and k_b are first-order heterogeneous rate constants for forward and reverse transfers, respectively. The rate constants are given by Butler-Volmer-type relations as^{10,26}

$$k_f = k^0 \exp[-\alpha z F (E - E^{0'}) / RT] \quad (3)$$

$$k_b = k^0 \exp[(1 - \alpha) z F (E - E^{0'}) / RT] \quad (4)$$

where E is the potential applied to the solid electrode against the reference electrode, and the formal potential, $E^{0'}$, was chosen so that $k_f = k_b$ at $E = E^{0'}$. Consequently, k^0 is independent of the membrane concentration of the excess ionophore, L_T , and the effect of the ionophore concentration on k_f and k_b as expected from the bimolecular (or multimolecular) nature of facilitated IT (eq 1) is seen in $E^{0'}$ as given by

$$E^{0'} = E_i^{0'} + \frac{RT}{zF} \ln \beta_n L_T^n \quad (5)$$

where $E_i^{0'}$ is the formal potential of simple IT. Eqs 3–5 indicates that $E^{0'}$ represents the thermodynamic effect of β_n from ion–ionophore complexation in the bulk membrane while the kinetics of ion–ionophore complexation at the interface (not in the bulk phase) determines k^0 and α .

The theoretical CVs based on the E mechanism with the Butler-Volmer-type first-order kinetics (eqs 3 and 4) was numerically obtained as reported elsewhere for simple IT^{18b} to uniquely determine k^0 , α , $E^{0'}$, and the diffusion coefficient of an aqueous ion, D_w , from kinetically controlled CVs (Table 1-1). Noticeably, negative shifts of these CVs with respect to $E^{0'}$ (Figure 1-2) result from small diffusion coefficients of ion–ionophore complexes in the viscous membrane, D_c , as quantified in recent chronoamperometric and chronopotentiometric studies.²⁷ Here we employed CV at PVC membranes doped with the complexes to determine D_c values (Table 1-1), which are required for the numerical simulation (see the Supporting Information).

The numerical analysis of CVs in Figure 1-2 gives normal α values of ~ 0.5 (Table 1-1) to confirm the one-step E mechanism based on the Butler-Volmer-type kinetics.¹⁰ Remarkably, an α value of 0.48 thus determined voltammetrically for the K^+ transfer facilitated by ionophore **2** contrasts to an extremely small value of ~ 0.05 as obtained by amperometry of the same reaction at thick PVC membranes.^{11b} This result supports higher reliability of our kinetic measurement with the thin PVC membrane that is free from a significant Ohmic potential drop. Moreover, α values of ~ 0.5 confirm the simultaneous one-step transfer of multiple charges ($z = 2$) by Ca^{2+} and Ba^{2+} as the unique feature of $IT^{8a,23,28}$ in contrast to the stepwise transfer of multiple electrons at metal electrodes. On the other hand, CVs of facilitated Pb^{2+} transfer are broader than expected with $z = 2$ and $\alpha = 0.5$ (dotted lines in Figure 1-2d) to fit better with theoretical CVs with $z = 1.1$ and $\alpha = 0.5$ (solid lines). The small charge is the effective value that represents the weak potential dependence of rates for facilitated Pb^{2+} transfer, which is ascribed to a double layer effect.^{8a,23,28} The small effective charge is not due to the transfer of Pb^{2+} -anion complexes between bulk PVC and aqueous phases. The amplitude of the observed current response is consistent with $z = 2$, which confirms that Pb^{2+} was transferred between the two phases. In fact, Cl^- was used as an aqueous supporting electrolyte to avoid significant ion pairing of Pb^{2+} in the aqueous phase²⁹ although ion pairing at or near the interface may be possible to screen the charge of Pb^{2+} , thereby causing the double layer effect.

The k^0 values thus determined for various combinations of ions and ionophores are similar to each other within a narrow range of 1×10^{-2} – 3.8×10^{-3} cm/s (Table 1-1). The fastest Ba^{2+} transfer is only ~ 3 times faster than the slowest Ca^{2+} transfer, which is consistent with wider peak separations in CVs of the latter process (Figure 1-2c). The k^0 values are lower than those reported

so far for facilitated IT at ITIES ($2\text{--}10^{-2}$ cm/s⁸⁻⁹) although similarly low k^0 values were obtained for ionophores **1–4** at DCE/water interfaces (see below). On the other hand, our k^0 values are much larger than an exceptionally small value of $\sim 10^{-5}$ cm/s as obtained by the impedance measurement of the Na⁺ transfer facilitated by ionophore **2**, which is affected by the high bulk resistance of thick PVC membranes.¹⁷

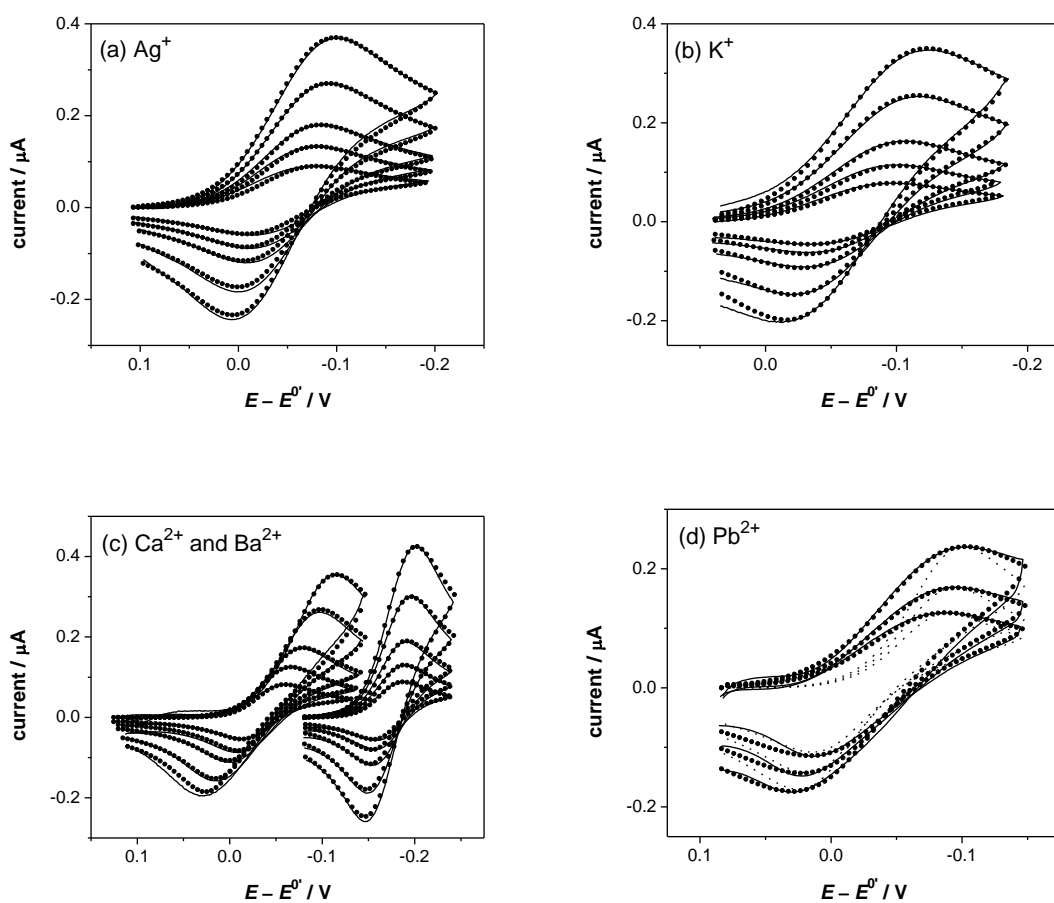


Figure 1-2. Background-subtracted CVs (solid lines) of facilitated IT as obtained using PVC/PEDOT-C₁₄-modified (a, d) Au or (b, c) GC electrodes in cell 1 containing (a) 20 mM

ionophore **1** with 20 μM CH_3COOAg in 10 mM CH_3COOLi (pH 5.4), (b) 20 mM ionophore **2** with 20 μM KCl in 10 mM Li_2SO_4 , (c) 60 mM ionophore **3** with 10 μM CaCl_2 (left) or BaCl_2 (right) in 10 mM CH_3COOK (pH 7.1), and (d) 20 mM ionophore **4** with 20 μM PbCl_2 in 5 mM MgCl_2 (pH 4.7). The $E_i^{0'}$ value for Ca^{2+} is used in (c). Potential sweep rates are from the top to the bottom, (a, b, c) 1, 0.5, 0.2, 0.1, and 0.05 V/s, and (d) 0.2, 0.1, and 0.05 V/s. Parameters for theoretical CVs (closed circles) based on the E mechanism are listed in Table 1-1. The dotted lines in (d) were obtained using $z = 2$ and $\alpha = 0.5$.

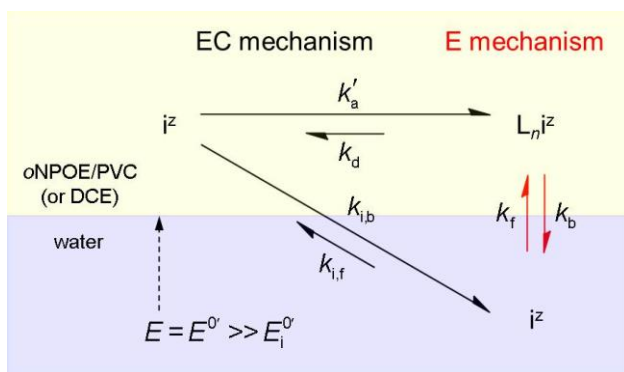


Figure 1-3. Scheme of E and EC mechanisms for facilitated IT. The rate constants are assigned to each process by eqs 2, S-2, S-6, and S-7, where $k'_a = k_a L_T^n$. Facilitated cation transfers are driven around $E = E^{0'} \gg E_i^{0'}$ (see eq 5).

Table 1-1. Kinetic Parameters for the E Mechanism at PVC Membrane/Water Interfaces.

ion/ionophore	$k^0/\text{cm s}^{-1}$	α	$D_w/\text{cm}^2 \text{s}^{-1}$	$D_c/\text{cm}^2 \text{s}^{-1}$
Ag ⁺ /1	6.2×10^{-3}	0.45	1.5×10^{-5}	4.8×10^{-8}
K ⁺ /2	9.0×10^{-3}	0.48	1.9×10^{-5}	1.0×10^{-7}
Ba ²⁺ /3	1.0×10^{-2}	0.50	1.1×10^{-5}	7.1×10^{-8}
Ca ²⁺ /3	3.8×10^{-3}	0.47	1.5×10^{-5}	5.8×10^{-8}
Pb ²⁺ /4	9.7×10^{-4}	0.50 ^a	9.1×10^{-6}	2.7×10^{-8}

^a $z = 1.1$.

Table 1-2. Thermodynamic and Kinetic Parameters for the EC Mechanism at PVC Membrane/Water Interfaces

ion/ionophore	$\beta_n (n)$	$E^{0'} - E_i^{0'}/V^a$	$k_i^0/\text{cm s}^{-1}$	α_i	$k_a/M^{-1} \text{s}^{-1}$
Ag ⁺ /1	$1.0 \times 10^{10} (1)^b$	0.49	6.0×10	0.45	$>6.8 \times 10^{17}$
K ⁺ /2	$4.3 \times 10^{11} (1)^c$	0.59	5.4×10^2	0.48	$>1.7 \times 10^{18}$
Ca ²⁺ /3	$1.6 \times 10^{29} (3)^c$	0.83	2.4×10^9	0.47	$(>1.9 \times 10^{40d})$

^a Calculated using eq 5. ^b From ref. 4b. ^c From ref. 4a. ^d With $M^{-3} \text{s}^{-3}$.

1.3.3 Assessment of the Electrochemical–Chemical Mechanism

In comparison to the E mechanism, the EC mechanism is kinetically unfavorable when ion–ionophore complexes are stable. In the EC mechanism, facilitated IT is divided into two steps, i.e., heterogeneous simple IT and homogeneous ion–ionophore complexation (eqs S-2 and S-6, respectively; see also Figure 1-3). Senda and co-workers excluded the EC mechanism for reversible facilitated IT at the ITIES, which requires that the dissociation of stable ion–ionophore complexes in the non-aqueous phase must be faster than a diffusion limit.⁶ Here we confirm the additional requirement of extremely fast simple IT for the apparently E_rC_r or E_qC_r behavior of facilitated IT, which is anticipated from the theory for EC schemes at solid electrodes.³⁰ These requirements are quantitatively evaluated by employing the EC mechanism for the numerical analysis of quasi-reversible CVs of Ag^+ , K^+ , and Ca^{2+} transfers (Figure 1-11; see Supporting Information), where β_n values are known to uniquely determine the standard rate constant for simple IT, k_i^0 , and the rate constant for ion–ionophore association, k_a , in addition to the transfer coefficient, α_i (Table 1-2).

The EC mechanism is kinetically unfavorable when strong cation–ionophore complexation causes the voltammetric wave to shift toward $E^{0'}$, which is much more positive than $E_i^{0'}$ (see eq 5). At $E = E^{0'} \gg E_i^{0'}$ (Figure 1-3), simple cation transfer from the aqueous phase into the membrane phase is dramatically slowed down as represented by kinetically unfavorable, positive overvoltages, η , of 0.5–0.8 V, which were estimated as differences between $E^{0'}$ and $E_i^{0'}$ using eq 5 with β_n values reported for Ag^+ , K^+ , and Ca^{2+} complexes of ionophores **1–3**, respectively (Table 1-2). With these η values, rate constants for the simple transfer of aqueous cations into the

membrane, $k_{i,f}$, are 10^5 – 10^9 times lower than the corresponding k_i^0 value with a normal α_i value of 0.5 (eq S-3). Subsequently, extremely large k_i^0 values of 6.0×10 – 2.4×10^9 cm/s (Table 1-2) must be employed for theoretical CVs based on the EC mechanism to fit with quasi-reversible CVs of Ag^+ , K^+ , and Ca^{2+} transfers (Figure 1-11 with potentials defined against $E_i^{0'}$). These k_i^0 values are several orders of magnitude larger than the largest value reported so far for simple IT at PVC membrane/water interfaces, i.e., 0.01 cm/s for tetraethylammonium.³¹

In addition, the numerical analysis based on the EC mechanism (Figure 1-11) require that rate constants for ion–ionophore association, k_a , for Ag^+ and K^+ complexes by far exceed a diffusion-limited value of $k_{a,d} = 1 \times 10^9 \text{ M}^{-1} \text{ s}^{-1}$ for 1:1 complexation in the bulk PVC membrane as estimated by³²

$$k_{a,d} = 4\pi N_A (D_L + D_i) d \quad (6)$$

where N_A is the Avogadro's number, d ($= 1.5 \times 10^{-7}$ cm) is the ionophore–ion separation at their collision, and D_L and D_i ($= 5 \times 10^{-7}$ cm²/s) are diffusion coefficients of free ionophore and free ion in the membrane. For a given β_n value, the rapid formation of ion–ionophore complexes corresponds to their rapid dissociation (eq S-7), which is required for yielding a current response on the reverse potential sweep (Figure 1-2) while strong ion–ionophore association drives the overall IT toward a chemically irreversible limit (Figure 1-3).

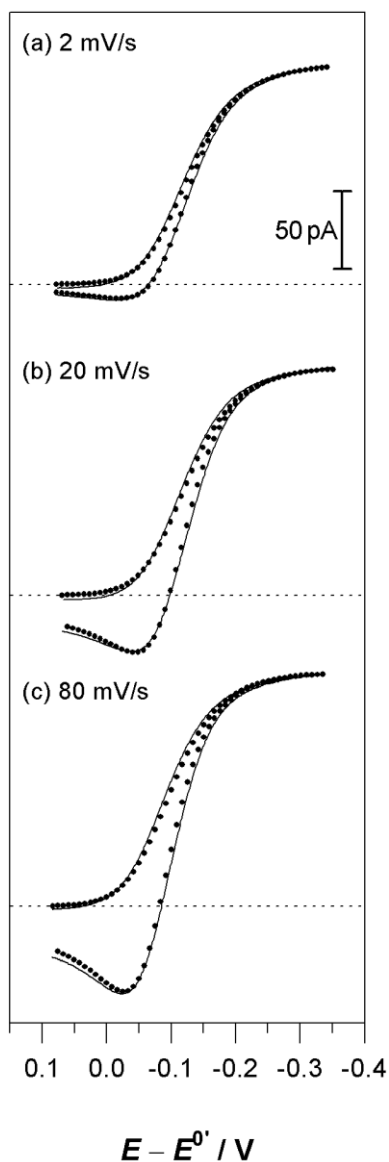
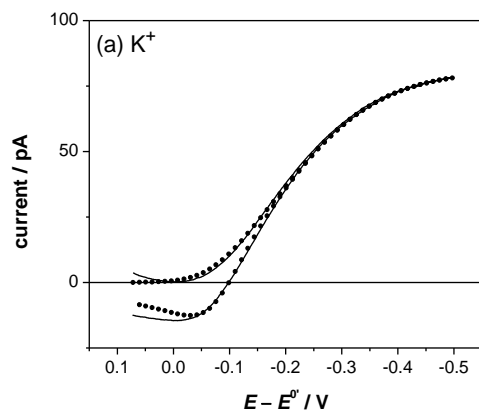


Figure 1-4. Background-subtracted micropipet CVs (solid lines) of facilitated Ag^+ transfer at DCE/water microinterfaces with 20 mM ionophore 1 in cell 2 containing $100 \mu\text{M}$ CH_3COOAg in 10 mM CH_3COOLi (pH 5.5). Parameters for the theoretical CVs (closed circles) based on the E mechanism are listed in Table 1-3. Pipet inner diameter, $4.3 \mu\text{m}$

In addition, we carried out numerical simulations using different β_n values to demonstrate that the EC mechanism can be important only when ion-ionophore complexation is weak. For

instance, quasi-reversible CVs of facilitated Ag^+ transfer (Figure 1-2a) were fitted very well with the CVs simulated using β_1 values of 10^{10} – 10^2 (data not shown), thereby yielding kinetic parameters as listed in Table 1-5. When $\beta_1 < 10^4$, k_a values are lower than the diffusion-limited value (eq 6), and relatively small k_i^0 values of <0.1 cm/s are required for the quasi-reversible responses. Therefore, k_a (or k_d) and k_i^0 must be known to assess the validity of the EC mechanism in the limit of very weak ion–ionophore complexation. The formation of a weak complex is relevant to the facilitated transfer of an interfering ion. In contrast, the EC mechanism is unambiguously excluded for the systems investigated in this work, where ionophores bind to target analytes very strongly.



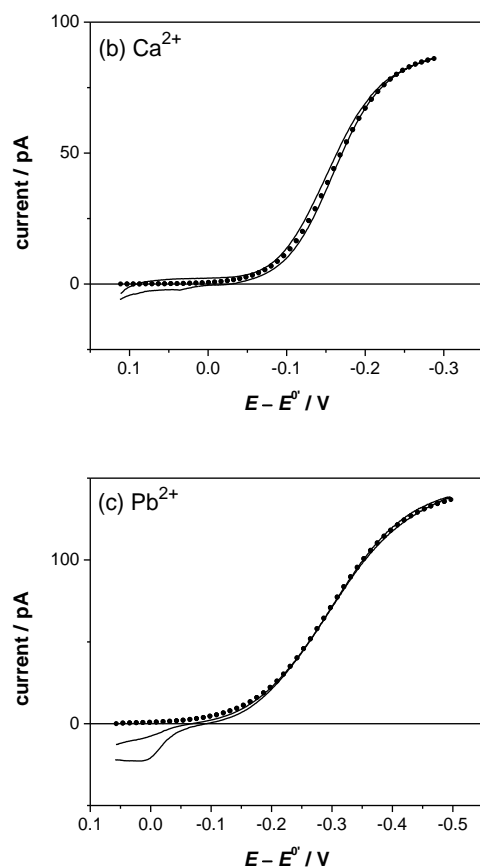


Figure 1-5. Background-subtracted micropipet CVs (solid lines) at DCE/water microinterfaces in cell 2 containing (a) 20 mM ionophore 2 with 25 μM K_2SO_4 in 10 mM MgSO_4 (pH 6.6), (b) 60 mM ionophore 3 with 30 μM $(\text{CH}_3\text{COO})_2\text{Ca}$ in 10 mM CH_3COOK (pH 7.3), and (c) 20 mM ionophore 4 with 90 μM PbCl_2 in 5 mM MgCl_2 (pH 4.7). Parameters for theoretical CVs (closed circles) based on the E mechanism are listed in Table 1-3. Pipet inner diameters, (a) 3.7, (b) 4.2, and (c) 3.7 μm . Potential sweep rates, (a) 20, (b) 5, and (c) 20 mV/s

Noticeably, 1:3^{4a} and 1:2³³ ion–ionophore **3** complexes for Ca^{2+} and Ba^{2+} , respectively, must be formed at the interface to follow the E mechanism, thereby excluding the EC mechanism.

In this case, the unlikely EC mechanism is based on the transfer of intermediate 1:2 or 1:1 ion–ionophore complexes as the E process and is followed by their complexation with additional ionophore molecule(s) in the bulk membrane as the C process. The following complexation process is highly favored thermodynamically so that the transfer of the intermediate complexes and the dissociation of the overall complexes must be unrealistically fast to be consistent with the quasi-reversible CVs.

Table 1-3. Kinetic Parameters for the E Mechanism at PVC Membrane/Water Interfaces

ion/ionophore	$k^0/\text{cm s}^{-1}$	α	$D_c/\text{cm}^2 \text{s}^{-1}$	$k_{\text{DCE}}^0 / k_{\text{PVC}}^0$	$D_{c,\text{DCE}}/D_{c,\text{PVC}}$
Ag ⁺ /1	2.6×10^{-2}	0.48	3.0×10^{-6}	4.2	63
K ⁺ /2	1.1×10^{-2}	0.33	1.1×10^{-6}	1.3	11
Ba ²⁺ /3 ^a	1.2×10^{-2}	0.45	3.7×10^{-6}	1.2	52
Ca ²⁺ /3	7.1×10^{-4}	0.39	—	0.19	—
Pb ²⁺ /4	4.4×10^{-4}	0.50 ^b	—	0.45	—

^a From ref. 8a. ^b $z = 0.85$.

1.3.4 Facilitated IT at DCE/Water Microinterfaces

We employed micropipet voltammetry to determine rates for the IT processes facilitated by ionophores **1–4** at DCE/water interfaces, which turned out to be similar to those at plasticized

PVC membrane/water interfaces. With a DCE-filled micropipet (cell 2), the forward potential sweep drives the transfer of an ion from the outer aqueous phase into the inner DCE phase. The resulting sigmoidal wave (Figures 1-4 and 1-5) confirms the non-linear diffusion of the transferring aqueous ion to the microinterface. For sufficiently fast transfers of Ag^+ (Figure 1-4), K^+ (Figure 1-5a), and Ba^{2+} (Figure 1-8 in ref. 8a), the reverse potential sweep gives a peak-shaped wave because the inner pipet wall hinders the diffusion of ion–ionophore complexes in the DCE solution. In fact, the transient reverse response varies with ν as clearly seen for quasi-reversible Ag^+ and Ba^{2+} transfers. In contrast, the reverse peak of slower Pb^{2+} transfer is small and widely separated from the forward wave to overlap with the potential window limit at $E - E^{0'} > -0.05$ V, where the background-subtracted response is distorted (Figure 1-5c). No reverse peak was observed for electrochemically irreversible Ca^{2+} transfer (Figure 1-5b).

Quasi-reversible CVs of facilitated Ag^+ , K^+ , and Ba^{2+} transfers at DCE/water microinterfaces fit well with theoretical voltammograms based on the E mechanism to give all kinetic and thermodynamic parameters in the Butler-Volmer-type model as well as D_w and D_c values (Table 1-3).^{8a} Irreversible CVs of facilitated Ca^{2+} and Pb^{2+} transfers were also numerically analyzed using the E mechanism with $E^{0'}$ values determined by potentiometry (see Supporting Information) to yield k^0 and α values (Table 1-3). The theoretical micropipet CVs of quasi-reversible and irreversible IT were simulated as reported elsewhere.^{8a} Overall, the k^0 values thus obtained at DCE/water microinterfaces are nearly as low as those at PVC membrane/water interfaces. Facilitated Ag^+ and Ba^{2+} transfers at DCE/water microinterfaces give α values of ~ 0.5 to confirm the one-step E mechanism. Smaller α values of 0.33 and 0.39 for K^+ and Ca^{2+} transfers, respectively, are ascribed to a double layer effect. A more significant double layer effect is apparent in the voltammogram of facilitated Pb^{2+} transfer, which is broader than expected for $z =$

2 and $\alpha = 0.5$ to give an effective z value of 0.85 for a normal α value of 0.5.

The EC mechanism is excluded also for facilitated IT at DCE/water microinterfaces. For any of the facilitated IT reactions examined in this work, k^0 values with DCE and *o*NPOE/PVC systems are relatively similar to each other (see $k_{\text{DCE}}^0 / k_{\text{PVC}}^0$ in Table 1-3) in contrast to very different D_c values in these media (see $D_{c,\text{DCE}}/D_{c,\text{PVC}}$), which correspond to much higher viscosity of the *o*NPOE/PVC membrane than the DEC phase (13.8 and 0.779 mPa s for pure *o*NPOE and DCE, respectively²⁶). This little viscosity effect on IT kinetics is inconsistent with the EC mechanism, where simple IT is slower with a more viscous media²¹ (e.g., $k_i^0 = 6$ cm/s with DCE³⁴ and 0.01 cm/s with *o*NPOE-plasticized PVC membrane³⁵ for tetraethylammonium transfer). In addition, the numerical analysis of quasi-reversible CVs of K^+ and Ag^+ transfers at DCE/water microinterfaces using the EC mechanism (Figures 1-13 and 1-14, respectively; see Supporting Information) shows that simple IT and the association of ion–ionophore complexes must be unrealistically fast (Table 1-4) to satisfy the apparently E_qC_r scheme. These requirements are due to strong interactions of these ions with the corresponding ionophores in the DCE phase ($\beta_1 = 2.5 \times 10^{12}$ and 6.3×10^{14} for Ag^{+36} and K^+ ,³⁷ respectively) and are also expected for strongly facilitated transfers of Ba^{2+} , Ca^{2+} , and Pb^{2+} , thereby excluding the EC mechanism.

Table 1-4. Thermodynamic and Kinetic Parameters for the EC Mechanism at DCE/Water Interfaces.

ion/ionophore	$\beta_n (n)$	$E^{0'} - E_i^{0'} / N^a$	$k_i^0 / \text{cm s}^{-1}$	α_i	$k_a / \text{M}^{-1} \text{ s}^{-1}$
$\text{Ag}^+/\mathbf{1}$	$2.5 \times 10^{12} (1)^b$	0.63	4.5×10^3	0.50	$>1.7 \times 10^{18}$

$K^+/2$	$6.3 \times 10^{14} (1)^c$	0.77	2.4×10^2	0.33	$>2.9 \times 10^{21}$
---------	----------------------------	------	-------------------	------	-----------------------

^a Calculated using eq 5. ^b From ref. 36. ^c From ref. 37.

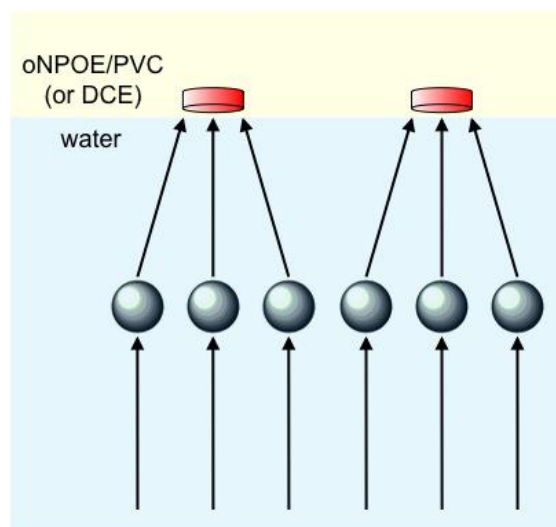


Figure 1-6. Scheme of the non-linear diffusion of aqueous ions to membraneous ionophore molecules for their collision and subsequent complexation at the interface.

1.3.5 Molecular Level Models for the E Mechanism.

We further analyzed the k^0 values for the E mechanism at the molecular level to find that the rate-determining step of bimolecular (or multimolecular) IT as facilitated by ionophores is their ion recognition at the very interface rather than the non-linear diffusion of an aqueous ion for its collision with the excess amount of ionophore at the interface (Figure 1-6). Specifically, a rate constant for the diffusion-limited collision, k , was estimated using the effective medium theory^{24,38} to yield

$$k = 4D_w r l N_A L_T \quad (7)$$

where r is the radius of the disk-like adsorber that represents an ionophore, and l is the depth of the interfacial region where the ionophore is available for collision with aqueous ions. The k^0 values at either PVC/water or DCE/water interfaces are more than three orders of magnitude lower than k values of 30–90 cm/s in eq 7 with $D_w = 1.5 \times 10^{-5}$ cm²/s, $r = 1.5$ nm, $l = 3$ nm, and $L_T = 0.02$ – 0.06 M. Similar k values were also estimated for bimolecular ET reactions at the ITIES.³⁹

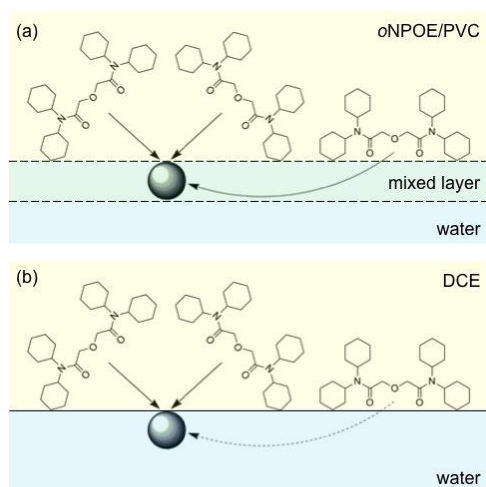


Figure 1-7. Scheme of the formation of 1:3 Ca²⁺-ionophore **3** complexes at (a) a *o*NPOE-plasticized PVC membrane/water interface with a thicker mixed layer and (b) a sharper DCE/water interface.

The unique feature of the E mechanism at the molecular level is the formation of three dimensional ion-ionophore complexes at the two-dimensional interface, which contrasts to

homogeneous ion–ionophore complexation in the EC mechanism. We speculate that this feature explains why Ca^{2+} transfer is more rapid at PVC membrane/water interfaces than at DCE/water interfaces ($k_{\text{DCE}}^0 / k_{\text{PVC}}^0 = 0.19$) while the Ba^{2+} transfer facilitated by the same ionophore is similarly fast at these interfaces ($k_{\text{DCE}}^0 / k_{\text{PVC}}^0 = 1.2$). Geometrically, a calcium ion is readily accessible to two molecules of ionophore **3** from the non-aqueous side of the interface while the third ionophore molecule must bind to the ion from its aqueous side to form three-dimensional 1:3 complexes⁴⁰ at the interface, which is required for the E mechanism as discussed above. Importantly, polar *o*NPOE molecules are dominant at the surface of an *o*NPOE-plasticized polymer membrane in contact with water⁴¹ to form a mixed layer,⁴² thereby allowing a lipophilic ionophore molecule to more easily access to the ion from its aqueous side (Figure 1-7a). In contrast, less polar DCE forms a sharper interface with a thinner mixed layer, which slows down the access of the third ionophore molecule to the ion (Figure 1-7b). The solvent-dependent accessibility of ionophore to an ion from its aqueous side is less important for the formation of 1:2 Ba^{2+} –ionophore **3** complexes³³ to yield similar k^0 values at both interfaces. Kinetically, the E mechanism is not simply the extreme case of the EC mechanism where ion–ionophore complexation occurs similarly both in the bulk solution and at the interface.

1.4 CONCLUSIONS

In this work, we revealed the electrochemical kinetics of facilitated IT at polymer membrane/water interfaces to resolve long-standing controversies on the intrinsic rate and

mechanism of this charge transfer process with practical importance and fundamental uniqueness. The kinetics observed with highly selective ionophores **1–4** is slow enough to fully assess E and EC mechanisms, which supports the former mechanism and excludes the latter. Our data also suggests that, at the molecular level, the E mechanism is controlled by three-dimensional ion–ionophore complexation at the two-dimensional interface to serve as a unique molecular-recognition system. In contrast, the three-dimensional accessibility of an ion is guaranteed for homogeneous complexation in the EC mechanism. Moreover, the theoretical assessment of the EC mechanism using kinetic voltammograms confirms that this mechanism is generally invalid when ionophore-mediated IT is both thermodynamically and kinetically facile. In fact, this is the case for most of the facilitated IT reactions reported so far, thereby augmenting the significance of this work.

The power of our double-polymer-modified electrodes for the quantitative study of IT kinetics was demonstrated in this work to make important findings for voltammetric/amperometric ion sensing by these electrodes. Interestingly, we found that the Ca^{2+} transfer facilitated by ionophore **3** is faster at PVC membrane/water interfaces than at DCE/water interfaces. This accelerating effect from a viscous medium is significant because faster transfer of a target ion is required for higher sensitivity and selectivity while a viscous non-aqueous medium is the essential component of a robust sensing device.⁴³ Moreover, the comparison of facilitated Ca^{2+} and Ba^{2+} transfers demonstrates not only the feasibility of the voltammetric detection of multiple ions using a single electrode^{18c} but also the dual ion selectivity of the voltammetric/amperometric approach as controlled both thermodynamically and kinetically. In contrast, ionophore-based potentiometric and optical sensors detect only one target ion with the highest thermodynamic selectivity as assumed in the phase boundary potential model^{1b} although this study indicates that facilitated IT

may not be rapid enough to always behave as a Nernstian process.^{11c} Finally, voltammetric and amperometric applications of the extremely selective ionophores that were developed for the potentiometric and optical sensors are highly attractive as more advanced sensing technologies.

ACKNOWLEDGEMENTS

This work was supported by a CAREER award from the National Science Foundation (CHE-0645623). We thank Prof. Toshiyuki Osakai, Department of Chemistry, Graduate School of Science, Kobe University, for valuable discussion.

1.5 SUPPORTING INFORMATION

1.5.1 Characterization of PVC/PEDOT-C₁₄-Modified Electrodes.

CVs of tetrapropylammonium transfer were obtained using a PVC/PEDOT-C₁₄-modified Au or GC electrode (cell 1) to fit well with the CVs simulated for the reversible transfer of a monovalent ion coupled with its semi-infinite diffusion in both aqueous and membrane phases (Figure 1-8). Reversible features of these CVs were maintained at $\nu = 50 \text{ mV/s} - 1 \text{ V/s}$ to be seen as a ν -independent separation of $\sim 60 \text{ mV}$ between forward and reverse peak potentials and the $\sqrt{\nu}$ -dependence of peak currents. The reversible responses confirm a negligible Ohmic potential drop and the negligible polarization of PVC/PEDOT-C₁₄/Au or GC junction.^{S-1}

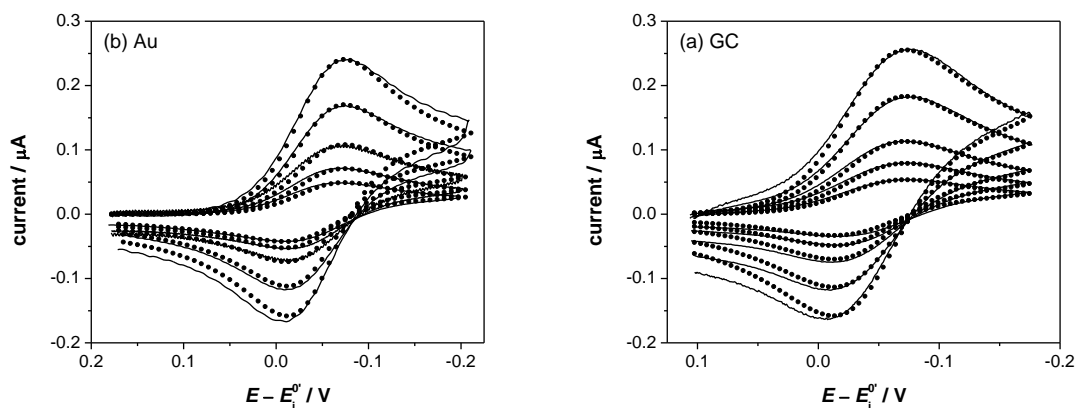


Figure 1-8. Background-subtracted CVs (solid lines) of simple tetrapropylammonium transfer as obtained at 0.05, 0.1, 0.2, 0.5, and 1 V/s using a PVC/PEDOT- C_{14} -modified (a) GC or (b) Au electrode without ionophore in cell 1 containing 20 μM tetrapropylammonium chloride in 10 mM Li_2SO_4 . Theoretical CVs (closed circles) are reversible.

1.5.2 Determination of Diffusion Coefficients of Ion–Ionophore Complexes in the PVC Membrane.

The *o*NPOE-plasticized PVC membrane was doped with ion–ionophore complexes to voltammetrically determine the diffusion coefficient of the complexes in the membrane, D_c , as listed in Table 1-1. The neutral form of poly(3-octylthiophene) (POT) was employed as an ion-to-electron transducer, which is oxidized to drive the transfer of the membraneous cation into the aqueous phase on the forward potential sweep.^{S-2} CVs were measured using the following electrochemical cell:

Ag | AgCl | 3 M KCl || supporting electrolyte (w) || target ion and supporting electrolyte (w) | ion–ionophore complex, TFAB, and 0.1 M TDDATFAB (*o*NPOE/PVC) | POT | Au or GC

(cell S-1)

where concentrations of supporting electrolyte, target ion, complex, and TFAB are given in legends of Figures 1-9 and 1-10. Before CV measurements, the PVC membrane doped with KTFAB and free ionophore was immersed for 4 hours in the aqueous solution of a target ion, which completely replaced K^+ in the membrane to form complexes with ionophores. Original membrane concentrations of ionophore and KTFAB were chosen such that there is no free ionophore in the membrane when the cation exchange is completed.

Figure 1-9 shows a CV with the PVC membrane doped with Ag^+ -ionophore **1** complexes, where the forward sweep results in a peak-shaped wave based on Ag^+ transfer from the membrane phase to the aqueous phase while the reverse wave corresponds to the back transfer of Ag^+ into the membrane phase. The forward peak current is proportional to the membrane concentration of Ag^+ -ionophore **1** complexes that are present as the counter cation of TFAB in the membrane (Figure 1-10). Similar linear relationships were also obtained for other ion-ionophore complexes. The D_c values were determined by fitting plots of peak current, i_p , versus complex concentration, $c_{c,0}$, with^{S-3}

$$i_p = 0.4463 \left(\frac{F^3}{RT} \right)^{1/2} z^{3/2} A D_c^{1/2} c_{c,0} \nu^{1/2} \quad (S-1)$$

where A is the interface area. Our D_c values are a few times larger than literature values,^{S-4} which were obtained using more viscous membranes with higher PVC content and also a more viscous plasticizer. Non-zero intercepts in Figure 1-10 are due to background currents.

To validate the aforementioned approach, the diffusion coefficient of a free ion in the ionophore-free membrane, D_i , was determined from the linear dependence of peak current on the membrane concentration of the free ion, $c_{i,0}$, using an equation as obtained by replacing D_c and $c_{c,0}$

in eq S-1 with D_i and $c_{i,0}$, respectively. A D_i value of 2.1×10^{-7} cm²/s thus determined for tetrapropylammonium in Figure 1-10 is $\sim 1/30$ of a D_w value of 5.6×10^{-6} cm²/s, which is consistent with viscosities of the two phases.^{S-5} This result confirms that little error is caused by using eq S-1 for a reversible CV to analyze the CV (e.g., Figure 1-9) that is significantly broadened by the polarization of the underlying POT film.^{S-1a}

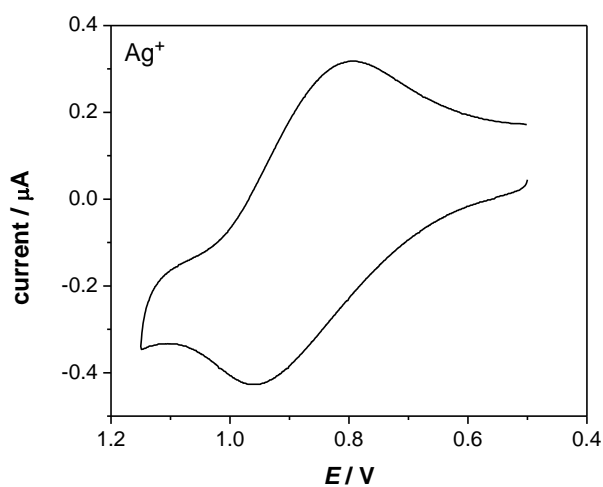


Figure 1-9. CV of 0.8 mM Ag⁺ as 1:1 complexes with ionophores **1** in cell S-1 containing 0.8 mM TFAB in the PVC membrane and 1 μM CH₃COOAg in 10 mM CH₃COOLi (pH 5.4).

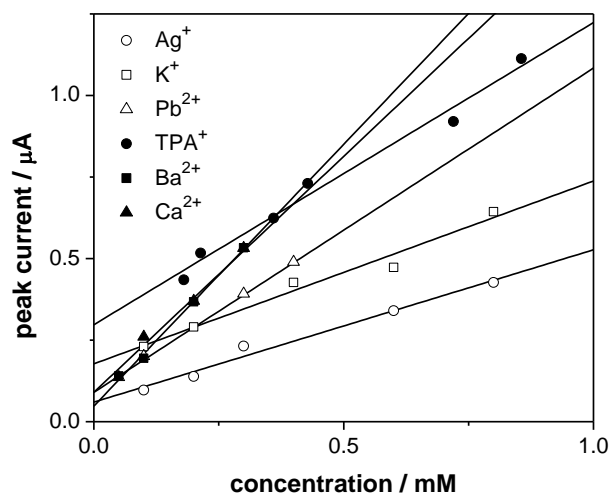


Figure 1-10. Plots of forward peak currents (symbols) versus membrane concentrations of ion–ionophore complexes or tetrapropylammonium (TPA⁺). Solid lines represent eq S-1 (or an analogous equation for TPA⁺), where non-zero intercepts are due to background currents. CVs of the facilitated transfer of each ion were obtained at 0.2 V/s using cell S-1 for ionophore **1** with 1 µM CH₃COOAg in 10 mM CH₃COOLi at pH 5.4, ionophore **2** with 1 µM KCl in 10 mM Li₂SO₄, ionophore **3** with 1 µM CaCl₂ or BaCl₂ in 10 mM CH₃COOK at pH 7.1, and ionophore **4** with 1 µM (CH₃COO)₂Pb in 10 mM CH₃COOLi at pH 5.4. Cell S-1 for CVs of simple TPA⁺ transfer contained TPATFAB in the PVC membrane and 1 µM TPAcl in 10 mM Li₂SO₄. A GC electrode was used for Pb²⁺ while CVs of other ions were measured using a Au electrode.

1.5.3 Model for the EC Mechanism.

The EC mechanism for facilitated IT is based on the combination of simple IT at the interface and homogeneous ion-ionophore complexation in the organic phase, i.e., the PVC membrane or DCE solution (Figure 1-3). Specifically, simple IT is defined as



where $k_{i,f}$ and $k_{i,b}$ are first-order heterogeneous rate constants. These rate constants are given by Butler-Volmer-type relations as^{S-6}

$$k_{i,f} = k_i^0 \exp[-\alpha_i z F (E - E_i^{0'}) / RT] \tag{S-3}$$

$$k_{i,b} = k_i^0 \exp[(1 - \alpha_i) z F (E - E_i^{0'}) / RT] \tag{S-4}$$

The rate constants are modulated by applying to the interface a triangle potential wave between the initial potential, E_i , and the switching potential, E_λ , at a constant rate, v , as given by

$$E = E_i + \frac{2(E_\lambda - E_i)}{\pi} \sin^{-1} \left\{ \sin \left[\frac{\pi v t}{2(E_\lambda - E_i)} \right] \right\} \tag{S-5}$$

Ion-ionophore complexation in the organic phase is expressed as



where k_a and k_d are association and dissociation rate constants, respectively. In the presence of the excess amount of ionophore, the homogeneous rate constants are related to each other by

$$\beta_n = \frac{L_1^n k_a}{k_d} = \frac{k'_a}{k_d} \quad (\text{S-7})$$

where k'_a is defined as an apparent first-order rate constant.

1.5.4 Numerical Simulation of CVs Based on the EC Mechanism at PVC Membrane/Water Interfaces.

A diffusion problem was solved with the EC mechanism (see Appendix I) to analyze quasi-reversible CVs of Ag^+ , K^+ , and Ca^{2+} transfers at plasticized PVC membrane/water interfaces (Figure 1-11). The numerical simulation requires β_n values in *o*NPOE/PVC membranes, which have been reported for Ag^+ , K^+ , and Ca^{2+} complexes of ionophores **1–3**, respectively (Table 1-2). $D_w/D_i = 30$ was employed in the simulation as estimated from viscosities of the two phases.^{S-5}

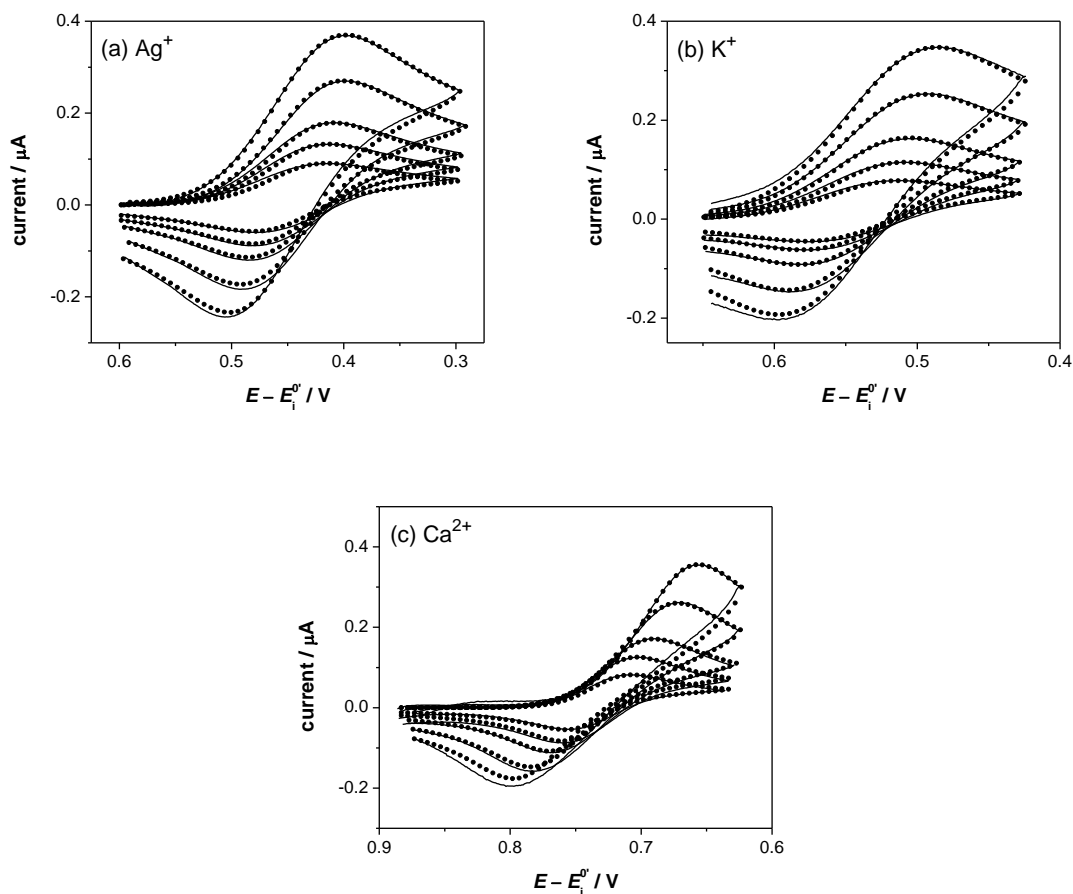


Figure 1-11. Background-subtracted CVs (solid lines) as shown in Figure 1-2 and theoretical CVs (circles) based on the EC mechanism with parameters listed in Table 1-2.

Noticeably, CVs in Figure 1-11 can be fitted well with CVs simulated using smaller β_n values, which give more reasonable k_i^0 and k_a values (e.g., Table 1-5 for Ag^+ transfer). Therefore, the EC mechanism is excluded in the limit of very strong complexation but is more significant toward the limit of very weak complexation. Eventually, negligible ion-ionophore complexation corresponds to simple IT, which can be represented by the EC mechanism.

Table 1-5. Thermodynamic and Kinetic Parameters for Facilitated Ag⁺ Transfer based on the EC Mechanism at PVC Membrane/Water Interfaces.

β_1	$E^{0'} - E_i^{0'} / N$	$k_i^0 / \text{cm s}^{-1a}$	$k_a / \text{M}^{-1} \text{s}^{-1a}$
1.0×10^8	0.373	9.0	$>2.0 \times 10^{15}$
1.0×10^6	0.254	7.9×10^{-1}	$>1.6 \times 10^{13}$
1.0×10^4	0.136	1.1×10^{-1}	$>1.6 \times 10^9$
1.0×10^3	0.077	4.5×10^{-2}	$>7.8 \times 10^6$
1.0×10^2	0.018	2.3×10^{-2}	$>3.9 \times 10^4$

^a Obtained from CVs in Figure 1-11 using the EC mechanism with $\alpha_i = 0.45$ and $L_T = 0.020$ mM. ^b Calculated using eq 5.

1.5.5 Potentiometric Determination of Formal Potentials of Facilitated Ca²⁺ and Pb²⁺ Transfers at DCE/Water Interfaces.

Irreversible micropipet CVs of facilitated Ca²⁺ and Pb²⁺ transfers (Figures 1-5b and 1-5c, respectively) were analyzed using their formal potentials as determined by potentiometry. Potentiometric measurements were performed using the following electrochemical cells with ion-ionophore complexes in the inner DCE phase

Ag | AgCl | 3M KCl || 10 mM CH₃COOK (w) || 0.5–70 μM (CH₃COO)₂Ca in 10 mM CH₃COOK (w) | 60 mM ionophore **3**, 0.05 mM 1:3 Ca²⁺-ionophore complex, 0.1 mM TFAB, and 0.1 M TDDATFAB (DCE) | Ag (cell S-2)

Ag | AgCl | 3 M KCl || 5 mM MgCl (w) || 0.5–200 μ M PbCl₂ in 5 mM MgCl (w) | 20 mM ionophore **4**, 0.05 mM 1:1 Pb²⁺–ionophore complex, 0.1 mM TFAB, and 0.1 M TDDATFAB (DCE) | Ag (cell S-3)

The DCE solutions of ion–ionophore complexes were prepared by solvent extraction, where K⁺ in the DCE solution of KTFAB and free ionophore was exchanged with a target ion in the aqueous solution. An open circuit potential was measured using a high impedance potentiometer (EMF-16, Lawson Labs Inc., Malvern, PA).

Equilibrium potentials, E_{eq} , of cells S-2 and S-3 give nearly Nernstian responses to Ca²⁺ and Pb²⁺ with slopes of 27.4 and 29.0 mV/decade, respectively (Figure 1-12) to define their formal potentials against the reference electrodes as

$$E_{\text{eq}} = E^{0'} + \frac{RT}{zF} \ln \frac{c_0}{c_{c,0}} \quad (\text{S-8})$$

Then, a formal potential was defined against the half-wave potential, $E_{1/2,d}$, of the irreversible CV of facilitated Ca²⁺ or Pb²⁺ transfer as measured using cell S-2 or S-3, respectively, where eq S-8 gives

$$E_{1/2,d} - E^{0'} = E_{1/2,d} - E_{\text{eq}} - \frac{RT}{zF} \ln \frac{c_0}{c_{c,0}} \quad (\text{S-9})$$

With aqueous Ca²⁺ and Pb²⁺ concentrations of 60 and 90 μ M, respectively, $E_{1/2,d} - E^{0'}$ values for the ions were obtained from eq S-9 and used to plot their irreversible waves with respect to $E - E^{0'}$ in Figures 1-5b and 1-5c. The numerical analysis of these CVs gives k^0 and α values (Table 1-3).

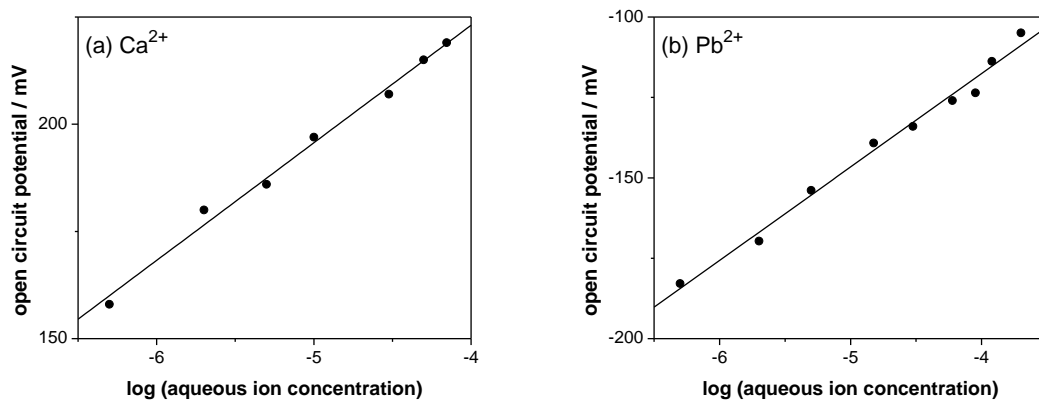


Figure 1-12. Open circuit potentials of cells (a) S-2 and (b) S-3 at different ion concentrations in the aqueous phase.

1.5.6 Numerical Simulation of Micropipet CVs Based on the EC Mechanism.

A two-dimensional diffusion problem with the EC mechanism was numerically solved^{S-7} (see also Appendix II) to analyze quasi-reversible CVs of facilitated K^+ and Ag^+ transfers at DCE/water microinterfaces (Figures 1-13 and 1-14, respectively). The simulation requires β_n values in the DCE phase, which have been reported for Ag^+ and K^+ complexes of ionophores **1** and **2**, respectively (Table 4). $D_w/D_i = 1$ was employed in the simulation as estimated from viscosities of the DCE and aqueous phases.^{S-8}

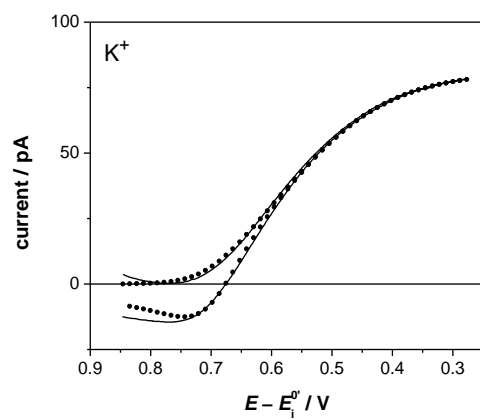


Figure 1-13. Background-subtracted micropipet CV (solid line) of facilitated K^+ transfer as shown in Figure 1-5a and theoretical CV (circles) based on the EC mechanism with the parameters listed in Table 1-4.

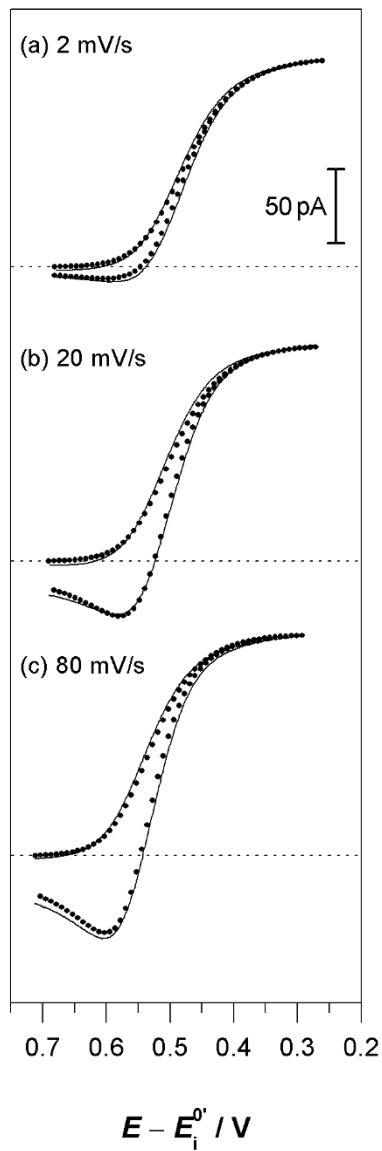


Figure 1-14. Background-subtracted CVs (solid lines) of facilitated Ag^+ transfer as shown in Figure 1-4 and theoretical CVs (circles) based on the EC mechanism with the parameters listed in Table 1-4.

1.5.7 REFERENCES

- (S-1) (a) Kim, Y.; Amemiya, S. *Anal. Chem.* **2008**, *80*, 6056. (b) Kim, Y.; Rodgers, P. J.; Ishimatsu, R.; Amemiya, S. *Anal. Chem.* **2009**, *81*, 7262.
- (S-2) Si, P. C.; Bakker, E. *Chem. Commun.* **2009**, 5260.
- (S-3) Bard, A. J.; Faulkner, L. R. *Electrochemical Methods: Fundamentals and Applications*; 2nd ed.; John Wiley & Sons: New York, 2001, p. 228.
- (S-4) (a) Bodor, S.; Zook, J. M.; Lindner, E.; Toth, K.; Gyurcsanyi, R. E. *Analyst* **2008**, *133*, 635. (b) Bodor, S.; Zook, J. M.; Lindner, E.; Toth, K.; Gyurcsanyi, R. E. *J. Solid State Electrochem.* **2009**, *13*, 171.
- (S-5) Langmaier, J.; Stejskalova, K.; Samec, Z. *J. Electroanal. Chem.* **2002**, *521*, 81.
- (S-6) (a) Samec, Z.; Homolka, D.; Marecek, V. *J. Electroanal. Chem.* **1982**, *135*, 265. (b) Samec, Z. *Pure Appl. Chem.* **2004**, *76*, 2147.
- (S-7) Rodgers, P. J.; Amemiya, S. *Anal. Chem.* **2007**, *79*, 9276.
- (S-8) Wandlowski, T.; Marecek, V.; Samec, Z. *Electrochimica Acta* **1990**, *35*, 1173.

Appendix I. A one-dimensional diffusion problem with the EC mechanism at a PVC/PEDOT-C₁₄-modified electrode is defined in a linear coordinate, x , vertical to the interfaces at $x = 0$ and also to the solid support at $x = -l_m$,^{S-1a} where the membrane thickness, l_m , is large enough to achieve the semi-infinite diffusion of species in the membrane phase ($-l_m < x < 0$). In the presence of the excess amount of ionophore, the diffusion of the free ion in the membrane phase is given by

$$\frac{\partial c_i(x,t)}{\partial t} = D_i \left[\frac{\partial^2 c_i(x,t)}{\partial x^2} \right] - k'_a c_i(x,t) + k_d c_c(x,t) \quad (-l_m < x < 0) \quad (\text{S-10})$$

where $c_i(x,t)$ and $c_c(x,t)$ are local concentrations of free ion and its ionophore complex, respectively. The diffusion of the complex in the membrane phase is described as

$$\frac{\partial c_c(x,t)}{\partial t} = D_c \left[\frac{\partial^2 c_c(x,t)}{\partial x^2} \right] + k'_a c_i(x,t) - k_d c_c(x,t) \quad (-l_m < x < 0) \quad (\text{S-11})$$

The diffusion of the target ion in the aqueous phase is expressed as

$$\frac{\partial c_w(x,t)}{\partial t} = D_w \left[\frac{\partial^2 c_w(x,t)}{\partial x^2} \right] \quad (0 < x) \quad (\text{S-12})$$

where $c_w(x,t)$ is the local concentration of the transferring ion. The boundary condition at the interface is given by

$$D_i \left[\frac{\partial c_i(x,t)}{\partial x} \right]_{x=0} = D_w \left[\frac{\partial c_w(x,t)}{\partial x} \right]_{x=0} = k_{i,f} c_w(0,t) - k_{i,b} c_i(0,t) \quad (\text{S-13})$$

Other boundary conditions are

$$D_i \left[\frac{\partial c_i(x,t)}{\partial x} \right]_{x=-l_m} = 0 \quad (\text{membrane/solid support interface}) \quad (\text{S-14})$$

$$D_c \left[\frac{\partial c_c(x,t)}{\partial x} \right]_{x=-l_m} = 0 \quad (\text{membrane/solid support interface}) \quad (\text{S-15})$$

$$\lim_{x \rightarrow \infty} c_w(x, 0) = c_0 \quad (\text{simulation limit in the aqueous phase}) \quad (\text{S-16})$$

Initial conditions are

$$c_w(x, 0) = c_0 \quad (\text{S-17})$$

$$c_i(x, 0) = 0 \quad (\text{S-18})$$

$$c_c(x, 0) = 0 \quad (\text{S-19})$$

A current response, i , is obtained from the flux of the transferring ion at the membrane/water interface as

$$i = zAFD_w \left[\frac{\partial c_w(x, t)}{\partial x} \right]_{x=0} \quad (\text{S-20})$$

The diffusion problem defined above was solved in a dimensionless form using COMSOL Multiphysics version 3.5a[®] (COMSOL, Inc., Burlington, MA). The example of the finite element simulation is attached. Dimensionless parameters are defined by

$$C_w(X, \tau) = c_w(x, t)/c_0 \quad (\text{S-21})$$

$$C_i(X, \tau) = c_i(x, t)/c_0 \quad (\text{S-22})$$

$$C_c(X, \tau) = c_c(x, t)/c_0 \quad (\text{S-23})$$

$$\tau = t\nu f \quad (\text{S-24})$$

$$X = x \sqrt{\frac{\nu f}{D_w}} \quad (\text{S-25})$$

$$L = l_m \sqrt{\frac{\nu f}{D_w}} \quad (\text{S-26})$$

where $f = F/RT$. Diffusion processes (eqs S-10–S-12) are expressed in the respective dimensionless forms as

$$\frac{\partial C_i(X, \tau)}{\partial \tau} = \gamma_i^2 \left[\frac{\partial^2 C_i(X, \tau)}{\partial X^2} \right] - K'_a C_i(X, \tau) + K_d C_c(X, \tau) \quad (\text{S-27})$$

$$\frac{\partial C_c(X, \tau)}{\partial \tau} = \gamma_c^2 \left[\frac{\partial^2 C_c(X, \tau)}{\partial X^2} \right] + K'_a C_i(X, \tau) - K_d C_c(X, \tau) \quad (\text{S-28})$$

$$\frac{\partial C_w(X, \tau)}{\partial \tau} = \left[\frac{\partial^2 C_w(X, \tau)}{\partial X^2} \right] \quad (\text{S-29})$$

with

$$K'_a = \frac{k'_a}{vf} \quad (\text{S-30})$$

$$K_d = \frac{k_d}{vf} \quad (\text{S-31})$$

$$\gamma_i = \sqrt{\frac{D_i}{D_w}} \quad (\text{S-32})$$

$$\gamma_c = \sqrt{\frac{D_c}{D_w}} \quad (\text{S-33})$$

The boundary condition at the membrane/water interface (eq S-13) is expressed using the dimensionless parameters as

$$\left[\frac{\partial C_w(X, \tau)}{\partial X} \right]_{X=0} = -\frac{A_1}{\theta^{\alpha_i}} [\gamma_i \theta C_i(0, \tau) - C_w(0, \tau)] \quad (\text{S-34})$$

$$\left[\frac{\partial C_i(X, \tau)}{\partial X} \right]_{X=0} = \theta^{1-\alpha_i} \gamma_i A_1 \left[\frac{C_w(0, \tau)}{\gamma_i \theta} - C_i(0, \tau) \right] \quad (\text{S-35})$$

with

$$A_1 = \frac{k_i^0}{\sqrt{D_w^{1-\alpha_i} D_i^{\alpha_i} fv}} \quad (\text{S-36})$$

$$\theta = \exp[zf(E - E_{1/2})] \quad (\text{S-37})$$

$$E_{1/2} = E_i^{0'} + \frac{RT}{zF} \ln \sqrt{\frac{D_i}{D_w}} \quad (\text{S-38})$$

Eqs S-34 and S-35 are equivalent to the expression of a flux boundary condition in COMSOL Multiphysics. The triangle potential wave (eq S-5) is given by

$$\theta = \theta_i^{1-(2/\pi)\sin^{-1}\{\sin[\pi z\tau/2 \ln(\theta_\lambda/\theta_i)]\}} \theta_\lambda^{(2/\pi)\sin^{-1}\{\sin[\pi z\tau/2 \ln(\theta_\lambda/\theta_i)]\}} \quad (\text{S-39})$$

with

$$\theta_i = \exp[zf(E_i - E_{1/2})] \quad (\text{S-40})$$

$$\theta_\lambda = \exp[zf(E_\lambda - E_{1/2})] \quad (\text{S-41})$$

A dimensionless current, I , is defined as

$$I = \left[\frac{\partial C_w(0, \tau)}{\partial X} \right]_{X=0} \quad (\text{S-42})$$

With eqs S-21 and S-25, eq S-42 is equivalent to

$$I = \frac{\sqrt{D_w}}{c_0 \sqrt{vf}} \left[\frac{\partial c_w(0, t)}{\partial x} \right]_{x=0} \quad (\text{S-43})$$

The comparison of eq S-43 with eq S-20 gives

$$i = (zAFc_0 \sqrt{D_w vf}) I \quad (\text{S-44})$$

Appendix II. A two-dimensional diffusion problem with the EC mechanism at a micropipet-supported DCE/water interface is defined using cylindrical coordinates, where r and z are the coordinates in directions parallel and normal to the disk-shaped interface with the radius, a , respectively.^{S-7} In the presence of the excess amount of ionophore, the diffusion of ions in free and complex forms in the inner DCE solution is expressed as

$$\frac{\partial c_i(r, z, t)}{\partial t} = D_i \left[\frac{\partial^2 c_i(r, z, t)}{\partial r^2} + \frac{1}{r} \frac{\partial c_i(r, z, t)}{\partial r} + \frac{\partial^2 c_i(r, z, t)}{\partial z^2} \right] - k'_a c_i(r, z, t) + k_d c_c(r, z, t) \quad (\text{S-45})$$

$$\frac{\partial c_c(r, z, t)}{\partial t} = D_c \left[\frac{\partial^2 c_c(r, z, t)}{\partial r^2} + \frac{1}{r} \frac{\partial c_c(r, z, t)}{\partial r} + \frac{\partial^2 c_c(r, z, t)}{\partial z^2} \right] + k'_a c_i(r, z, t) - k_d c_c(r, z, t) \quad (\text{S-46})$$

where $c_i(r, z, t)$ and $c_c(r, z, t)$ are local concentrations of the free ion and its ionophore complex, respectively. The diffusion of the ion in the outer aqueous phase is described as

$$\frac{\partial c_w(r, z, t)}{\partial t} = D_w \left[\frac{\partial^2 c_w(r, z, t)}{\partial r^2} + \frac{1}{r} \frac{\partial c_w(r, z, t)}{\partial r} + \frac{\partial^2 c_w(r, z, t)}{\partial z^2} \right] \quad (\text{S-47})$$

where $c_w(r, z, t)$ is the local concentration of the transferring ion. The boundary condition at the DCE/water interface is given by

$$D_i \left[\frac{\partial c_i(r, z, t)}{\partial z} \right]_{z=0} = D_w \left[\frac{\partial c_w(r, z, t)}{\partial z} \right]_{z=0} = k_{i,t} c_w(r, 0, t) - k_{i,b} c_i(r, 0, t) \quad (\text{S-48})$$

A current response, i , is obtained from the flux of the transferring ion at the DCE/water solution interface as

$$i = 2\pi z_1 F D_w \int_0^a r \left[\frac{\partial c_w(r, 0, t)}{\partial z} \right] dr \quad (\text{S-49})$$

where z_i is used as the ionic charge to avoid conflict with the variable for the z coordinate.

The diffusion problem was solved in a dimensionless form using COMSOL Multiphysics version 3.5a[®]. Dimensionless parameters are given by

$$R = r/a \quad (S-50)$$

$$Z = z/a \quad (S-51)$$

$$C_i(R,Z,\tau) = c_i(r,z,t)/c_0 \quad (S-52)$$

$$C_c(R,Z,\tau) = c_c(r,z,t)/c_0 \quad (S-53)$$

$$C_w(R,Z,\tau) = c_w(r,z,t)/c_0 \quad (S-54)$$

$$\tau = \frac{4D_w t}{a^2} \quad (S-55)$$

$$\sigma = \frac{a^2}{4D_w} \frac{Fv}{RT} \quad (S-56)$$

Diffusion processes coupled with ion–ionophore complexation (eqs S-45 and S-46) are expressed in the respective dimensionless forms as

$$\frac{\partial C_i(R,Z,\tau)}{\partial \tau} = 0.25\gamma_i^2 \left[\frac{\partial^2 C_i(R,Z,\tau)}{\partial R^2} + \frac{1}{R} \frac{\partial C_i(R,Z,\tau)}{\partial R} + \frac{\partial^2 C_i(R,Z,\tau)}{\partial Z^2} \right] - K'_a C_i(R,Z,\tau) + K_d C_c(R,Z,\tau) \quad (S-57)$$

$$\frac{\partial C_c(R,Z,\tau)}{\partial \tau} = 0.25\gamma_c^2 \left[\frac{\partial^2 C_c(R,Z,\tau)}{\partial R^2} + \frac{1}{R} \frac{\partial C_c(R,Z,\tau)}{\partial R} + \frac{\partial^2 C_c(R,Z,\tau)}{\partial Z^2} \right] + K'_a C_i(R,Z,\tau) - K_d C_c(R,Z,\tau) \quad (S-58)$$

with

$$K'_a = \frac{k'_a a^2}{4D_w} \quad (S-59)$$

$$K_d = \frac{k_d a^2}{4D_w} \quad (\text{S-60})$$

Ion diffusion in the aqueous phase (eq S-47) corresponds to

$$\frac{\partial C_w(R, Z, \tau)}{\partial \tau} = 0.25 \left[\frac{\partial^2 C_w(R, Z, \tau)}{\partial R^2} + \frac{1}{R} \frac{\partial C_w(R, Z, \tau)}{\partial R} + \frac{\partial^2 C_w(R, Z, \tau)}{\partial Z^2} \right] \quad (\text{S-61})$$

The boundary condition at the DCE/water interface (eq S-48) is expressed using dimensionless parameters as

$$0.25 \left[\frac{\partial C_i(R, Z, \tau)}{\partial Z} \right]_{z=0} = 0.25 \lambda_i \theta^{(1-\alpha_i)} \left[\frac{C_w(R, 0, \tau)}{\theta \gamma_i^2} - C_i(R, 0, \tau) \right] \quad (\text{S-62})$$

$$0.25 \left[\frac{\partial C_w(R, Z, \tau)}{\partial Z} \right]_{z=0} = -\frac{0.25 \lambda_i}{\theta^{\alpha_i}} [\theta \gamma_i^2 C_i(R, 0, \tau) - C_w(R, 0, \tau)] \quad (\text{S-63})$$

with

$$\lambda_i = \frac{k_i^0 a}{D_w^{1-\alpha_i} D_i^{\alpha_i}} \quad (\text{S-64})$$

$$E_{1/2} = E_i^{0'} + \frac{RT}{z_i F} \ln \frac{D_i}{D_w} \quad (\text{S-65})$$

The triangle potential wave (eq S-5) is given by

$$\theta = \theta_i^{1-(2/\pi)\sin^{-1}\{\sin[\pi z_i \sigma \tau / 2 \ln(\theta_\lambda / \theta_i)]\}} \theta_\lambda^{(2/\pi)\sin^{-1}\{\sin[\pi z_i \sigma \tau / 2 \ln(\theta_\lambda / \theta_i)]\}} \quad (\text{S-66})$$

Eqs S-62 and S-63 are equivalent to the expression of a flux boundary condition in COMSOL Multiphysics. Other boundary conditions and initial condition are also given using dimensionless parameters (see the attached example). The simulation gives a dimensionless current normalized with respect to a limiting current at an inlaid disk-shaped interface as

$$I = \frac{i}{i_{\text{lim}}} = \frac{\pi}{2} \int_0^1 R \left[\frac{\partial C_w(R, 0, \tau)}{\partial Z} \right] dR \quad (\text{S-67})$$

with

$$i_{\text{lim}} = 4z_i F D_w c_0 a \quad (\text{S-68})$$

1.6 REFERENCES

- (1) (a) Meyerhoff, M. E.; Opdycke, W. N. *Adv. Clin. Chem.* **1986**, *25*, 1. (b) Bakker, E.; Bühlmann, P.; Pretsch, E. *Chem. Rev.* **1997**, *97*, 3083. (c) Buck, R. P.; Lindner, E. *Acc. Chem. Res.* **1998**, *31*, 257. (d) Buck, S. M.; Koo, Y. E. L.; Park, E.; Xu, H.; Philbert, M. A.; Brasuel, M. A.; Kopelman, R. *Curr. Opin. Chem. Biol.* **2004**, *8*, 540. (e) Bakker, E.; Pretsch, E. *Angew. Chem. Int. Ed.* **2007**, *46*, 5660. (f) Amemiya, S. In *Handbook of Electrochemistry*; Zoski, C. G., Ed.; Elsevier: New York, 2007, p 261.
- (2) Nghiem, L. D.; Mornane, P.; Potter, I. D.; Perera, J. M.; Cattrall, R. W.; Kolev, S. D. *J. Memb. Sci.* **2006**, *281*, 7.
- (3) (a) Bühlmann, P.; Pretsch, E.; Bakker, E. *Chem. Rev.* **1998**, *98*, 1593. (b) Umezawa, Y.; Bühlmann, P.; Umezawa, K.; Tohda, K.; Amemiya, S. *Pure Appl. Chem.* **2000**, *72*, 1851. (c) Umezawa, Y.; Umezawa, K.; Bühlmann, P.; Hamada, N.; Aoki, H.; Nakanishi, J.; Sato, M.; Xiao, K. P.; Nishimura, Y. *Pure Appl. Chem.* **2002**, *74*, 923. (d) Umezawa, Y.; Bühlmann, P.; Umezawa, K.; Hamada, N. *Pure Appl. Chem.* **2002**, *74*, 995.
- (4) (a) Qin, Y.; Mi, Y.; Bakker, E. *Anal. Chim. Acta* **2000**, *421*, 207. (b) Szigeti, Z.; Malon, A.; Vigassy, T.; Csokai, V.; Grun, A.; Wygladacz, K.; Ye, N.; Xu, C.; Chebny, V. J.; Bitter, I.; Rathore, R.; Bakker, E.; Pretsch, E. *Anal. Chim. Acta* **2006**, *572*, 1.

- (5) (a) Vanysek, P.; Ramirez, L. B. *J. Chil. Chem. Soc.* **2008**, *53*, 1455. (b) Girault, H. H. In *Electroanalytical Chemistry*; Bard, A. J., Zoski, C. G., Eds.; Taylor & Francis: Boca Raton, 2010; Vol. 23, p 1. (c) Liu, S. J.; Li, Q.; Shao, Y. H. *Chem. Soc. Rev.* **2011**, *40*, 2236.
- (6) Kakutani, T.; Nishiwaki, Y.; Osakai, T.; Senda, M. *Bull. Chem. Soc. Jpn.* **1986**, *59*, 781.
- (7) E and EC mechanisms are also known as "transfer by interfacial complexation (TIC)" and "ion transfer followed by complexation in the organic phase (TOC)," respectively; see Shao, Y.; Osborne, M. D.; Girault, H. H. *J. Electroanal. Chem.* **1991**, *318*, 101.
- (8) (a) Rodgers, P. J.; Amemiya, S. *Anal. Chem.* **2007**, *79*, 9276. (b) Cui, R.; Li, Q.; Gross, D. E.; Meng, X.; Li, B.; Marquez, M.; Yang, R.; Sessler, J. L.; Shao, Y. *J. Am. Chem. Soc.* **2008**, *130*, 14364.
- (9) (a) Shao, Y.; Mirkin, M. V. *J. Am. Chem. Soc.* **1997**, *119*, 8103. (b) Yuan, Y.; Shao, Y. H. *J. Phys. Chem. B* **2002**, *106*, 7809. (c) Cai, C. X.; Tong, Y. H.; Mirkin, M. V. *J. Phys. Chem. B* **2004**, *108*, 17872.
- (10) Samec, Z.; Homolka, D.; Marecek, V. *J. Electroanal. Chem.* **1982**, *135*, 265.
- (11) (a) Buck, R. P. In *Ion-Transfer Kinetics: Principles and Applications*; Sandifer, J. R., Ed.; VCH: New York, 1995, p 19. (b) Sandifer, J. R.; Iglehart, M. L.; Buck, R. P. *Anal. Chem.* **1989**, *61*, 1624. (c) Buck, R. P. *Anal. Chem.* **1968**, *40*, 1439.
- (12) Senda, M. *J. Electroanal. Chem.* **1994**, *378*, 215.
- (13) (a) Bakker, E.; Willer, M.; Pretsch, E. *Anal. Chim. Acta* **1993**, *282*, 265. (b) Sokalski, T.; Ceresa, A.; Zwickl, T.; Pretsch, E. *J. Am. Chem. Soc.* **1997**, *119*, 11347.
- (14) Bakker, E.; Pretsch, E.; Bühlmann, P. *Anal. Chem.* **2000**, *72*, 1127.
- (15) Kolev, S. D.; Argiropoulos, G.; Cattrall, R. W.; Hamilton, I. C.; Paimin, R. *J. Membr. Sci.* **1997**, *137*, 261.

- (16) (a) Lee, H. J.; Beattie, P. D.; Seddon, B. J.; Osborne, M. D.; Girault, H. H. *J. Electroanal. Chem.* **1997**, *440*, 73. (b) Lee, H. J.; Beriet, C.; Girault, H. H. *J. Electroanal. Chem.* **1998**, *453*, 211.
- (17) Armstrong, R. D. *J. Electroanal. Chem.* **1988**, *245*, 113.
- (18) (a) Guo, J.; Amemiya, S. *Anal. Chem.* **2006**, *78*, 6893. (b) Kim, Y.; Amemiya, S. *Anal. Chem.* **2008**, *80*, 6056. (c) Kim, Y.; Rodgers, P. J.; Ishimatsu, R.; Amemiya, S. *Anal. Chem.* **2009**, *81*, 7262.
- (19) (a) Si, P. C.; Bakker, E. *Chem. Commun.* **2009**, 5260. (b) Yoshida, Y.; Yamaguchi, S.; Maeda, K. *Anal. Sci.* **2010**, *26*, 137.
- (20) Zhang, J.; Harris, A. R.; Cattrall, R. W.; Bond, A. M. *Anal. Chem.* **2010**, *82*, 1624.
- (21) (a) Kakiuchi, T. *J. Electroanal. Chem.* **1992**, *322*, 55. (b) Samec, Z.; Langmaier, J.; Trojanek, A. *J. Electroanal. Chem.* **1997**, *426*, 37. (c) Marcus, R. A. *J. Chem. Phys.* **2000**, *113*, 1618.
- (22) Breiby, D. W.; Samuelsen, E. J.; Groenendaal, L.; Struth, B. *J. Polym. Sci., Part B: Polym. Phys.* **2003**, *41*, 945.
- (23) Amemiya, S.; Yang, X.; Wazenegger, T. L. *J. Am. Chem. Soc.* **2003**, *125*, 11832.
- (24) Ishimatsu, R.; Kim, J.; Jing, P.; Striemer, C. C.; Fang, D. Z.; Fauchet, P. M.; McGrath, J. L.; Amemiya, S. *Anal. Chem.* **2010**, 7127.
- (25) Bard, A. J.; Faulkner, L. R. *Electrochemical Methods: Fundamentals and Applications*; 2nd ed.; John Wiley & Sons: New York, 2001, p.243.
- (26) Samec, Z. *Pure Appl. Chem.* **2004**, *76*, 2147.

- (27) (a) Bodor, S.; Zook, J. M.; Lindner, E.; Toth, K.; Gyurcsanyi, R. E. *Analyst* **2008**, *133*, 635.
(b) Bodor, S.; Zook, J. M.; Lindner, E.; Toth, K.; Gyurcsanyi, R. E. *J. Solid State Electrochem.* **2009**, *13*, 171.
- (28) (a) Yuan, Y.; Amemiya, S. *Anal. Chem.* **2004**, *76*, 6877. (b) Yuan, Y.; Wang, L.; Amemiya, S. *Anal. Chem.* **2004**, *76*, 5570.
- (29) Ceresa, A.; Bakker, E.; Hattendorf, B.; Günther, D.; Pretsch, E. *Anal. Chem.* **2001**, *73*, 343.
- (30) Bard, A. J.; Faulkner, L. R. *Electrochemical Methods: Fundamentals and Applications*; 2nd ed.; John Wiley & Sons: New York, 2001, p. 499.
- (31) Langmaier, J.; Stejskalova, K.; Samec, Z. *J. Electroanal. Chem.* **2002**, *521*, 81.
- (32) Houston, P. L. *Chemical Kinetics and Reaction Dynamics* Dover Publications, Inc.: New York, 2001.
- (33) Wang, E.; Yu, Z.; Xu, C.; Qi, D. *Anal. Sci.* **1993**, *9*, 405.
- (34) Wang, Y.; Velmurugan, J.; Mirkin, M. V.; Rodgers, P. J.; Kim, J.; Amemiya, S. *Anal. Chem.* **2010**, *82*, 77.
- (35) Langmaier, J.; Stejskalova, K.; Samec, Z. *J. Electroanal. Chem.* **2002**, *521*, 81.
- (36) Dwyer, P.; Cunnane, V. J. *J. Electroanal. Chem.* **2005**, *581*, 16.
- (37) Osborne, M. D.; Girault, H. H. *Electroanalysis* **1995**, *7*, 425
- (38) (a) Berg, H. C. *Random Walks in Biology*; Princeton University Press: Princeton, NJ, 1993, p. 17. (b) Kim, E.; Xiong, H.; Striemer, C. C.; Fang, D. Z.; Fauchet, P. M.; McGrath, J. L.; Amemiya, S. *J. Am. Chem. Soc.* **2008**, *130*, 4230 and references cited therein.
- (39) (a) Osakai, T.; Hotta, H.; Sugihara, T.; Nakatani, K. *J. Electroanal. Chem.* **2004**, *571*, 201.
(b) Osakai, T.; Okamoto, M.; Sugihara, T.; Nakatani, K. *J. Electroanal. Chem.* **2009**, *628*, 27.

- (40) (a) Neupert-Laves, K.; Dobler, M. *J. Crystallogr. Spectrosc. Res.* **1982**, *12*, 287. (b) Schefer, U.; Ammann, D.; Pretsch, E.; Oesch, U.; Simon, W. *Anal. Chem.* **1986**, *58*, 2282.
- (41) Clarke, M. L.; Wang, J.; Chen, Z. *Anal. Chem.* **2003**, *75*, 3275.
- (42) Jorge, M.; Natalia, M.; Cordeiro, D. S. *J. Phys. Chem. B* **2008**, *112*, 2415.
- (43) Amemiya, S.; Kim, Y.; Ishimatsu, R.; Kabagambe, B. *Anal. Bioanal. Chem.* **2011**, 399, 571.

2.0 STRIPPING VOLTAMMETRY OF NANOMOLAR POTASSIUM AND AMMONIUM IONS USING A VALINOMYCIN-DOPED DOUBLE-POLYMER ELECTRODE

This work has been published as Benjamin Kabagambe, Anahita Izadyar, and Shigeru Amemiya, *Anal. Chem.*, **2012**, *84*, 7979–7986. The thesis author contributed in conducting experiments and data analysis.

2.1 INTRODUCTION

Here, we report on the first application of an ionophore-doped double-polymer electrode for ion-transfer stripping voltammetry (ITSV) to explore the nanomolar limit of detection (LOD) and multiple-ion detectability. We developed a theoretical model for ITSV at a thin ionophore-doped membrane on the solid supporting electrode to demonstrate that its LOD is controlled by the equilibrium preconcentration of an aqueous analyte ion as an ionophore complex into the thin polymer membrane and is lowered by the formation of a more stable ion–ionophore complex. The theoretical predictions were confirmed using valinomycin as a K^+ -selective ionophore, which forms a ~60 times more stable complex with K^+ than with NH_4^+ as confirmed by cyclic voltammetry. A LOD of 0.6 nM K^+ was achieved by ITSV using commercial ultrapure water as a K^+ -free media, where NH_4^+ contamination at a higher concentration was also detected by ITSV.

The dependence of the ITSV response on the preconcentration time was monitored under the rotating electrode configuration and analyzed theoretically to directly determine ~ 100 nM NH_4^+ and ~ 5 nM K^+ contaminations in commercial ultrapure water and laboratory-purified water, respectively, without the background ITSV measurement of an analyte-free blank solution.

Ion-transfer stripping voltammetry (ITSV) at the interface between two immiscible electrolyte solutions (ITIES)¹ is a powerful electroanalytical method that enables the trace analysis of various ions that have environmental^{2,3} and biomedical^{4,5} importance. In comparison to traditional redox-based stripping voltammetry,⁶ the ITSV technique has complementary principles and more versatile applicability because target ions do not need to be reduced or oxidized. Moreover, the ITSV of reducible heavy metal ions at the ITIES² is attractive as a replacement of traditional anodic stripping voltammetry based on their amalgamation at a mercury electrode.⁷ In ITSV, aqueous analyte ions are potentiostatically transferred across the ITIES to be accumulated at higher concentrations in the water-immiscible organic phase. Subsequently, a largely enhanced voltammetric response is obtained by stripping the preconcentrated ions from the organic phase into the aqueous phase.

The range of analytes detectable by ITSV has been widened by employing different types of ion-transfer reactions at the ITIES.⁸ The simple transfers of relatively lipophilic ions such as acetylcholine,^{9,10} vitamin B1,¹¹ various protonated amines,¹² tetraalkylammoniums,¹³⁻¹⁵ anionic surfactants,^{15,16} and β -blocker propranolol,^{17,18} have allowed for their preconcentration into the hydrophobic organic phase by controlling the phase boundary potential across the ITIES. In addition, ionophores were doped in the organic phase to facilitate the accumulative transfers of highly hydrophilic ions such as heavy metal ions,^{2,19-21} alkaline earth metal ions,²² and oligopeptides.²³ Moreover, macromolecular ions such as anticoagulant/antithrombotic heparin,⁴

lysozyme,²⁴ and digested proteins²⁵ were adsorbed at the ITIES as ion pairs with organic counterions during the preconcentration step to obtain ITSV responses based on analyte desorption from the interface. ITSV is also useful for the detection of neutral surfactants, which form electrically charged complexes with aqueous metal ions to be preconcentrated associatively and stripped dissociatively.^{16,26,27}

Recently, we developed novel double-polymer-modified electrodes to lower the limit of detection (LOD) of ITSV to low nanomolar^{3,28,29} and subnanomolar³⁰ levels. Remarkably, the LODs of 0.2–0.5 nM perchlorate³ and 90 pM hexafluoroarsenate³⁰ based on their simple transfers at double-polymer electrodes were comparable to the LODs of these environmental contaminants for highly sensitive analytical methods such as inductively coupled plasma mass spectrometry (ICP-MS). To achieve such low LODs, a plasticized poly(vinyl chloride) (PVC) membrane with a micrometer thickness was supported on a solid electrode to serve as a robust and thin organic phase. The solid-supported membrane was rotated to accelerate the mass transport of aqueous analyte ions to the membrane surface during the preconcentration step. The preconcentrated analyte ions were exhaustively stripped from the thin membrane to maximize the resultant voltammetric response. Alternatively, adsorptive ITSV was employed for the detection of nanomolar heparin, which was hardly extracted into the non-polar membrane.²⁸ Importantly, the ion transfer during the preconcentration and stripping steps was coupled with the electrolysis of an intermediate conducting-polymer film between the PVC membrane and the solid electrode to voltammetrically mediate ion-to-electron transduction.²⁸

Here, we report on the first ITSV application of an ionophore-based double-polymer electrode that enables the detection of nanomolar potassium ion by adding a K⁺-selective ionophore, valinomycin,³¹ to the PVC membrane coated on the solid-supported film of tetradecyl-

substituted poly(3,4-ethylenedioxythiophene) (PEDOT-C₁₄) (Figure 2-1). A valinomycin-doped PVC/PEDOT-C₁₄-modified electrode was recently characterized by cyclic voltammetry (CV) to show the electrochemical mechanism of facilitated K⁺ transfer.³² In this work, we employed thinner PVC and PEDOT- C₁₄ membranes for the ITSV application to achieve a LOD of 0.6 nM K⁺. This LOD is lower than a LOD of 5 nM K⁺ for potentiometric ion-selective electrodes based on valinomycin³³ and is close to the LODs of 0.1–0.2 nM K⁺ for ICP-MS³⁴ as required for monitoring the K⁺ contamination in the ultrapure water used in the electronics and semiconductor industries.³⁵ We also demonstrate theoretically and experimentally that the LOD based on the dynamic ITSV response is dictated by the equilibrium preconcentration of an analyte ion into the thin membrane as facilitated by an ionophore.

In addition, we applied the valinomycin-doped double-polymer electrode to explore the multiple-ion detectability of ITSV,^{2,30} which resolves K⁺ and NH₄⁺ responses at different potentials because of the stronger binding of valinomycin to K⁺ than to NH₄⁺,³⁶ as shown by CV. We found that the LOD of K⁺ for ITSV was compromised by NH₄⁺ contamination at a much higher concentration in the commercial ultrapure water, which was free from K⁺ contamination as confirmed by ITSV. Advantageously, we determined ~100 nM NH₄⁺ and ~5 nM K⁺ in commercial ultrapure water and laboratory-purified water, respectively, by monitoring the dependence of the ITSV response on the preconcentration time under the rotating electrode configuration without the background ITSV measurement of an analyte-free blank solution.³

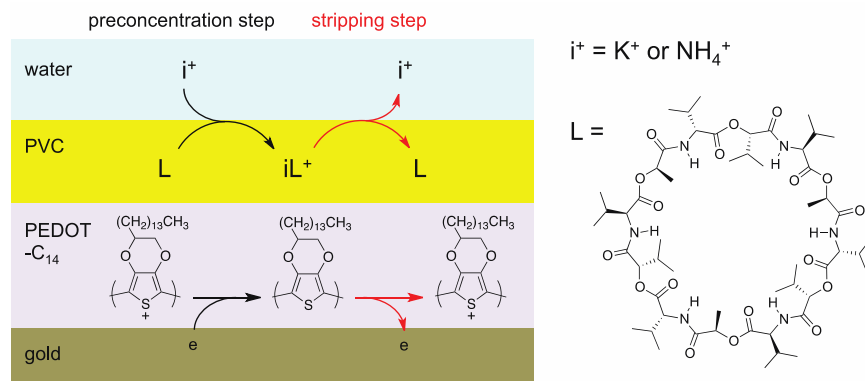


Figure 2-1. Scheme of pre-concentration (black arrows) and stripping (red arrows) steps in ITSV with a valinomycin-doped double-polymer electrode.

Moreover, pre-concentration of cationic analytes into the membrane phase requires reduction of an intermediate conducting-polymer layer while a POT film is not readily reduced or stable in an oxidized form, which is discharged to a reduced form under an open circuit condition.¹⁹

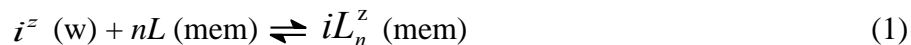
In this paper, we achieve subnanomolar LODs for both cationic and anionic analytes by ion-transfer stripping voltammetry with solid-supported thin polymeric membranes. These lower LODs represent the first experimental confirmation of a theoretical prediction that a more lipophilic analyte ion gives a lower LOD for stripping voltammetry with a solid-supported thin polymeric membrane.¹⁸ Importantly, lipophilicity of either a cation or an anion is generally quantified by a pre-concentration factor, Y ,¹⁸ (also known as the apparent ion partition coefficient²¹) to dictate an LOD as demonstrated in proof-of-concept experiments. A subnanomolar LOD of 80 nM tetrapropylammonium (TPA) is compared with a LOD of less lipophilic tetraethylammonium (TEA). Importantly, the voltammetric detection of cationic analytes is enabled by newly introducing an oxidatively doped poly(3,4-ethylenedioxythiophene) (PEDOT) film, which is

reduced to preconcentrate cations in the PVC membrane (Figure 1b). This conducting polymer has a very high stability in the oxidized form and undergoes a facile redox reaction.^{22,23} A practical significance of the theoretical prediction is demonstrated for trace analysis of a lipophilic inorganic anion, hexafluoroarsenate, which is known as an arsenical biocide^{24,25} and was recently found in waste water.^{26,27} An LOD of 90 nM hexafluoroarsenate as obtained with a PVC/POT-modified Au electrode is lower than that of less lipophilic perchlorate and compared to a LOD of hexafluoroarsenate by inductively coupled plasma mass spectrometry with anionexchange chromatography. Finally, the voltammetric anion- and cation-selective electrodes are characterized by electrochemical impedance spectroscopy (EIS). While both PVC/POT- and PVC/PEDOT-modified electrodes have been used for ion-selective potentiometry,²⁸ the solid-supported PVC membranes for iontransfer stripping voltammetry must be not only thinner for exhaustive ion stripping¹⁸ but also more conductive for avoiding a significant Ohmic potential drop in the membranes,¹⁹ which is confirmed by EIS.

2.2 THEORY

2.2.1 Model.

We developed a model for ITSV at an ionophore-based double-polymer electrode (Figure 2-1) to assess the effect of ion-ionophore complexation on the preconcentration and stripping steps. The respective steps correspond to the forward and reverse directions of the facilitated ion transfer as defined by



where i^z is an aqueous analyte ion with charge z , L is a free ionophore, and iL_n^z is a 1: n ion-ionophore complex.

Our model is based on the following assumptions. A free analyte ion in the membrane phase was neglected because the total concentration of the ionophore, L_T , was in excess and because the overall formation constant, β_n , of 1: n ion-ionophore complexes in the membrane was large enough ($\beta_1 = 4.3 \times 10^{11}$ for the K^+ -valinomycin complex³⁷). The membrane was thin enough to achieve the uniform distribution of a membranous species by its diffusion during the preconcentration step. The mass transfer of an aqueous species between the aqueous phase and the rotating membrane-modified electrode was always maintained at steady states. The facilitated ion transfer at the membrane/water interface was reversible under the hydrodynamic condition.

2.2.2 Equilibrium LOD.

The LOD of ITSV at an ionophore-doped double-polymer electrode is eventually limited by the equilibrium preconcentration of an aqueous analyte ion as an ionophore complex into the membrane. The resulting equilibrium membrane concentration of the complex, c_{PVC} , is the highest achievable at a preconcentration potential, E_p , as applied between the aqueous and membrane phases and is related to the sample concentration of an analyte ion, c_w , by a preconcentration factor, Y ,³ based on the Nernst equation as

$$Y = \frac{c_{\text{PVC}}}{c_w} = b_n L_T^n \exp \left[-\frac{zF(E_p - E_i^{0'})}{RT} \right] \quad (2)$$

where $E_i^{0'}$ is the formal potential of the simple transfer of an analyte ion without an ionophore, which serves as a measure of ion lipophilicity.³⁸ Eq 2 indicates that a stronger ionophore-binding capability (i.e., larger β_n) corresponds to a larger Y and, subsequently, a higher c_{PVC} corresponds to a lower LOD. In addition, a lower LOD can be obtained for a more lipophilic analyte ion (i.e., a cation with more positive $E_i^{0'}$) or simply by applying more favorable E_p (i.e., more negative for a cation) as indicated by the exponential term of Eq 2, which is equivalent to the preconcentration factor of an ionophore-free system.³⁰

2.2.3 Direct ITSV Determination of Analyte Concentration.

The analyte concentration in the sample solution can be directly determined by monitoring the dependence of the ITSV response on the preconcentration time under the rotating electrode configuration without a separate measurement of the background ITSV response.³ This feature is essential for the quantification of a contaminant in a blank solution³ and is applied in this work for the analysis of K^+ and NH_4^+ contaminations in laboratory-purified water and commercial ultrapure water, respectively (see the Results and Discussion section).

Essentially, the ITSV-based approach without the need for a blank measurement is based on the determination of an analyte concentration from the limiting current at the rotating double-membrane electrode, which is given by the Levich equation as³⁹

$$i_1 = 0.62zFAD_w^{2/3}\omega^{1/2}\nu^{-1/6}c_w \quad (3)$$

where A is an effective area of the PVC membrane/water interface, D_w is a diffusion coefficient of the ion in the aqueous phase, ω is the angular frequency of the electrode rotation, and ν is the kinematic viscosity. A limiting current with a nanomolar analyte concentration is too low in comparison to a background current (mainly charging current) to be directly measured by voltammetry. In contrast, the low limiting current is integrated over the preconcentration time, t_p , in ITSV to give an easily measurable t_p -dependent response, which also includes a t_p -independent background response.

Specifically, a limiting current is determined from the total charge under a stripping voltammogram, $Q_{\text{tot}}(t_p)$, which is the sum of the charge owing to the stripping of the preconcentrated analyte ion, $Q_i(t_p)$, and the charge owing to background processes during the voltammetric stripping step, Q_{bg} , as given by (see Supporting Information)

$$Q_{\text{total}}(t_p) = Q_{\text{eq}} \left[1 - \exp\left(-\frac{i_1}{Q_{\text{eq}}} t_p\right) \right] + Q_{\text{bg}} \quad (4)$$

with

$$Q_{\text{eq}} = zFAlc_{\text{PVC}} \quad (5)$$

where $Q_i(t_p)$ represents the first term of the left-hand side of eq 4, Q_{eq} is an equilibrium value of $Q_i(t_p)$, i.e., $Q_i(\infty)$, and l is the effective membrane thickness. A plot of $Q_{tot}(t_p)$ versus t_p is fitted with eq 4 to determine i_l in addition to Q_{eq} and Q_{bg} .

2.3 EXPERIMENTAL SECTION

2.3.1 Chemicals

Valinomycin, tetradodecylammonium (TDDA) bromide, tetrapropylammonium chloride, PVC (high molecular weight), and 2-nitrophenyl octyl ether (*o*NPOE) were obtained from Aldrich (Milwaukee, WI). Sulfuric acid (BDH Aristar Ultra, WVR International, West Chester, PA) and hydrochloric acid (Trace Select Ultra, Aldrich) with high purities were used as aqueous supporting electrolytes. Potassium tetrakis(pentafluorophenyl)borate (TFAB) was from Boulder Scientific Company (Mead, CO). All reagents were used as received. All aqueous sample solutions were prepared using a commercial ultrapure water (Trace Select Ultra, Aldrich) with the exception of the ITSV determination of the K^+ contamination in laboratory-purified water with a resistivity of 18.2 M Ω ·cm (Nanopure, Barnstead, Dubuque, IA).

2.3.2 Electrode Modification.

A 5 mm-diameter gold disk attached to a rotating disk electrode tip (Pine Research Instrumentation, Raleigh, NC) was modified with an oxidatively doped PEDOT-C₁₄ membrane and then with an *o*NPOE-plasticized PVC membrane (Figure 2-1). A PEDOT-C₁₄ membrane was

electrodeposited on a clean gold electrode using a three-electrode cell with a Pt wire (0.25 mm diameter, 99.9 %, Alfa Aesar, Ward Hill, MA) as a quasi-reference electrode and a graphite rod (99 %, Alfa Aesar) as a counter electrode in 1.5 mL of the acetonitrile solution of 0.03 M TDDATFAB²⁸ and 0.01 M 2-*n*-tetradecyl-2,3-dihydro-thieno[3,4-*b*][1,4]dioxine (EDOT-C₁₄).⁴⁰ A thin PEDOT-C₁₄ membrane in the reduced form resulted from one cycle of the potential of the gold electrode between -0.85 V and 1.40 V at 0.1 V/s. We chose a switching potential of 1.40 V where the current based on the oxidation of EDOT-C₁₄ reached 0.6 mA. The PEDOT-C₁₄ film was cleaned in the monomer-free acetonitrile solution of 0.03 M TDDATFAB by twice cycling the electrode potential between -0.85 V and 0.8 V at 0.1 V/s, and was oxidatively doped with TFAB by linearly sweeping the potential to 0.8 V. The peak current based on the oxidation of the PEDOT-C₁₄ film with an optimum thickness was 50 μ A. Then, a thin *o*NPOE-plasticized PVC membrane was spin-coated on the PEDOT-C₁₄-modified electrode from the THF solution as prepared by dissolving 1.48 mg valinomycin, 4.0 mg PVC, 16.0 mg *o*NPOE, and 2.2 mg TDDATFAB in 1 mL THF. A 10 μ L THF solution of the membrane cocktail was injected onto the surface of the electrode in a spin-coating device (model SCS-G3-8, Cookson Electronics, Providence, RI), which was immediately followed by electrode rotation at 1500 rpm for 1 minute. The spin-coated electrode was dried in air for 30 min.

2.3.3 Electrochemical Measurement.

An electrochemical workstation (CHI 660B, CH Instruments, Austin, TX) was used for voltammetric measurements with valinomycin-doped PVC/PEDOT-C₁₄-modified electrodes. A Pt-wire counter electrode was employed in the following three-electrode cell

Ag | AgCl | x M K₂SO₄ in 0.5 mM H₂SO₄ and 0.1 mM HCl (aq) | PVC membrane | PEDOT-C₁₄ | Au

(cell 1)

The concentrations of K₂SO₄ are given in the Results and Discussion section. The current carried by a positive charge from the aqueous phase to the PVC membrane was defined to be positive. All electrochemical experiments were performed at 22 ± 3 °C. For CV, a piece of Teflon tube²⁸ was put on a PVC/PEDOT-C₁₄-modified gold electrode to form a disk-shaped PVC membrane/water interface with a diameter of 1.5 mm.

ITSV measurements were performed as follows. A modified electrode without the Teflon tube was rotated using a modulated speed rotator (Pine Research Instrumentation) while a potentiostatic preconcentration step was followed by linear sweep stripping voltammetry. No pulse voltammetric approach was attempted. Preconcentrated analyte ions were exhaustively stripped from the thin membrane (see the Results and Discussion section) and convectively transported from the rotating membrane surface to the bulk aqueous solution, thereby quickly recovering the initial conditions required for the successive preconcentration step. Practically, a preconcentration step was initiated 2 minutes after the end of the previous stripping step to change the sample concentration of an analyte ion.

Importantly, the contamination of a sample solution with NH₄⁺ from NH₃ in the ambient air was avoided by placing the electrochemical cell and electrode rotator in a glove bag (AtmosBag, Aldrich) filled with argon gas. Moreover, the whole bag was accommodated in a class 100 vertical laminar flow hood (model AC632LFC, AirClean Systems, Raleigh, NC) to protect it

from K^+ -contaminated particles in the ambient air. Nevertheless, an as-prepared electrode was contaminated with K^+ and was cleaned in the K^+ -free ultrapure water solution of supporting electrolytes in cell 1 until no K^+ was detected by ITSV. All volumetric flasks and beakers were made of polytetrafluoroethylene and were immersed in the laboratory-purified water solution of 0.5 mM H_2SO_4 during their storage in the hood.

2.4 RESULTS AND DISCUSSION

2.4.1 The CVs of K^+ and NH_4^+ Transfers at the Thin PVC Membrane Doped with Valinomycin.

Figure 2-2A shows the CVs of the K^+ and NH_4^+ transfers facilitated by valinomycin at the thin PVC membrane supported on the PEDOT- C_{14} -modified gold electrode. The facilitated transfers of the aqueous ions as valinomycin complexes into the PVC membrane were driven by the forward sweep of the electrode potential in the cathodic direction, which was coupled with the reduction of the oxidatively doped PEDOT- C_{14} film (Figure 2-1). The reverse potential sweep resulted in the stripping of the transferred ions from the membrane, which requires the reoxidation of the PEDOT- C_{14} film in the reduced form. All experimental CVs fit well with the theoretical CVs simulated by the finite element method using the kinetic and transport parameters as reported elsewhere³² (see Supporting Information). An ionophore-free PVC/PEDOT- C_{14} -modified

electrode gave no voltammetric response to K^+ or NH_4^+ , which are too hydrophilic to be transferred as free ions into the hydrophobic PVC membrane.

Importantly, the CVs of the facilitated K^+ and NH_4^+ transfers confirm the exhaustive stripping of transferred ions from the thin PVC membrane, which is required for maximizing the sensitivity of ITSV. The thin layer effect is seen in both CVs, where the reverse peak currents of $\sim 0.20 \mu A$ are higher than the forward peak currents of $\sim 0.14 \mu A$. Quantitatively, the finite element analysis demonstrates that the reverse peak currents agree with the exhaustive stripping of an ion from a $\sim 3.7 \mu m$ -thick membrane and that the forward peak currents are controlled by the semi-infinite diffusion of an aqueous ion with a diffusion coefficient, D_w , of $1.9 \times 10^{-5} \text{ cm}^2/\text{s}$.³² Moreover, the exhaustive stripping of K^+ and NH_4^+ from the thin membrane is indicated by the quick decay of the reverse peaks to zero current at the positive side of the peak potentials in contrast to the forward peaks with diffusional tails (Figure 2-2A). Finally, the integration of the CVs (Figure 2-2B) verifies that the total charge under the CVs returned to nearly zero by the end of a potential cycle because all ions transferred into the membrane phase were transferred back to the aqueous phase.

Another important feature of the CVs in Figure 2-2A is that the facilitated K^+ transfer is thermodynamically more favorable than the facilitated NH_4^+ transfer, which forms the basis of the ITSV detection of K^+ and NH_4^+ using a single electrode. Specifically, the forward and reverse peak potentials for the K^+ transfer are $\sim 125 \text{ mV}$ more positive than those for the NH_4^+ transfer. The finite element analysis shows that this offset potential corresponds to a ~ 60 times larger formation constant, β_1 , for the K^+ -valinomycin complex than for the NH_4^+ complex when the same hydrophilicity is assumed for both ions (see Supporting Information). This result is in agreement with the formation of a ~ 50 times more stable complex of valinomycin with K^+ than with NH_4^+ in

1,2-dichloroethane as determined by ion-transfer CV.³⁶ Moreover, our result confirms the formation of a stable NH_4^+ -valinomycin complex with a large β_1 value of 7.2×10^9 in the *o*NPOE-plasticized PVC membrane, where a β_1 value of 4.3×10^{11} was determined for a more stable K^+ -valinomycin complex by potentiometry.³⁷

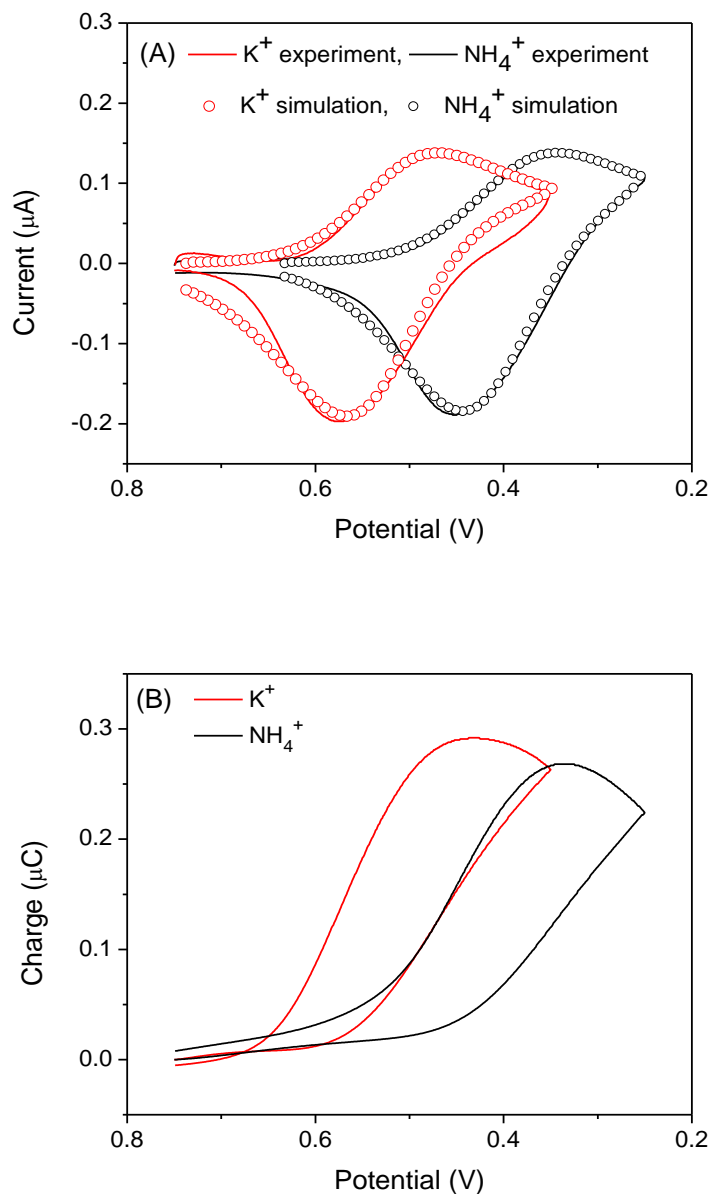


Figure 2-2. (A) Background-subtracted CVs and (B) their integrations for valinomycin-mediated

transfers of K^+ and NH_4^+ at an *o*NPOE-plasticized PVC/PEDOT- C_{14} -modified gold electrode. Scan rate, 0.1 V/s.

2.4.2 Direct ITSV Determination of Potassium Ion.

The dependence of the ITSV response to K^+ on the preconcentration time was studied to confirm the corresponding theory (eq 4), which predicts that an unknown concentration of an analyte ion can be determined directly by ITSV under the rotating electrode configuration without the measurement of a background response to an analyte-free blank solution. Although this advantageous feature of ITSV is demonstrated for the quantification of the K^+ contamination in the laboratory purified water, this direct ITSV method requires the measurement of smaller non-equilibrium responses at shorter preconcentration times, which compromises the LOD in comparison to the calibration method based on equilibrium preconcentration (see below).

For the validation of the theory, 50 nM K^+ was added to the commercial ultrapure water, which was originally free from K^+ as confirmed by ITSV (data not shown). The peak-shaped K^+ responses at ~ 0.54 V varied with the preconcentration time up to 3 minutes and then saturated (Figure 2-3A). This saturation indicates the equilibrium preconcentration of K^+ into the thin membrane as predicted by the Nernst equation (eq 2). In contrast, smaller ITSV responses to NH_4^+ as a contaminant in the ultrapure water were observed at ~ 0.42 V as expected from the CV and were independent of the preconcentration time, t_p , thereby making a small contribution to the t_p -independent background current. This result indicates that 30 s of preconcentration time was long enough to saturate the thin membrane with a less stable NH_4^+ -valinomycin complex at a lower equilibrium concentration in comparison with K^+ as predicted by eq 2.

Each stripping voltammogram of 50 nM K^+ spiked in the ultrapure water was integrated to obtain a total charge, $Q_{tot}(t_p)$, as a function of t_p , which fits well with eq 4 to yield $i_l = 19.9$ nA, $Q_{eq} = 1.39$ μ C, and $Q_{bg} = 0.79$ μ C (Figure 2-3B). This diffusion-limited current, i_l , corresponds to a K^+ concentration of 54 nM in the Levich equation (eq 3) with $A = 0.196$ cm^2 , $D_w = 1.9 \times 10^{-5}$ cm^2/s , $\omega = 419$ rad/s (i.e., 4000 rpm), and $\nu = 1.0 \times 10^{-2}$ cm^2/s . This K^+ concentration is in agreement with the concentration of K^+ spiked in the ultrapure water, thereby confirming the reliability of the ITSV approach. Noticeably, this limiting current is too small in comparison to a background response to be directly measured voltammetrically. In fact, the significant background ITSV response mainly based on the voltammetric charging current was integrated to yield the Q_{bg} value, which is almost a half of the Q_{eq} value based on the diffusion-limited ion preconcentration for 5 minutes.

Remarkably, we observed easily detectable ITSV responses to 50 nM K^+ (Figure 2-3A), which was preconcentrated as a valinomycin complex up to an equilibrium concentration, c_{PVC} , of 0.20 mM as estimated from the Q_{eq} value using eq 5 with $l = 3.7$ μ m. The submillimolar equilibrium concentration of the complex with respect to the nanomolar concentration of aqueous K^+ reflects a large preconcentration factor, Y , of 3.7×10^3 in eq 2. This high preconcentration efficiency occurs because of the large β_1 value of 4.3×10^{11} for the stable K^+ complexes of valinomycin³⁷ and is significantly suppressed because of the extreme hydrophilicity of K^+ with a very negative $E_{K^+}^{0c}$ value of $E_p - 0.38$ V as obtained using eq 2 with the Y and β_1 values.

We measured the t_p -dependence of the ITSV response to K^+ contaminated in the laboratory-purified water (Figure 2-4A) to determine its concentration. The resulting $Q_{tot}(t_p)-t_p$ plot fits well with eq 4 (Figure 2-4B) to yield an i_l value of 1.88 nA in addition to Q_{eq} and Q_{bg}

values. This small limiting current corresponds to a low K^+ concentration of 5.1 nM in eq 3. The trace K^+ contamination originates from the laboratory-purified water because no ITSV response to K^+ was observed when the blank solution of 0.5 mM H_2SO_4 and 0.1 mM HCl was prepared using the commercial ultrapure water (data not shown). In fact, the low nanomolar K^+ contamination is hard to eliminate from purified water⁴¹ and is undetectable as a change in its resistivity (i.e., 18.2 $M\Omega\cdot cm$), which is limited by 0.1 μM H_3O^+ and OH^- with high mobility.⁴² Moreover, small ITSV peaks at ~ 0.42 V (Figure 2-4A) indicate the contamination of the laboratory-purified water with NH_4^+ , which can originate from NH_3 in the ambient air.

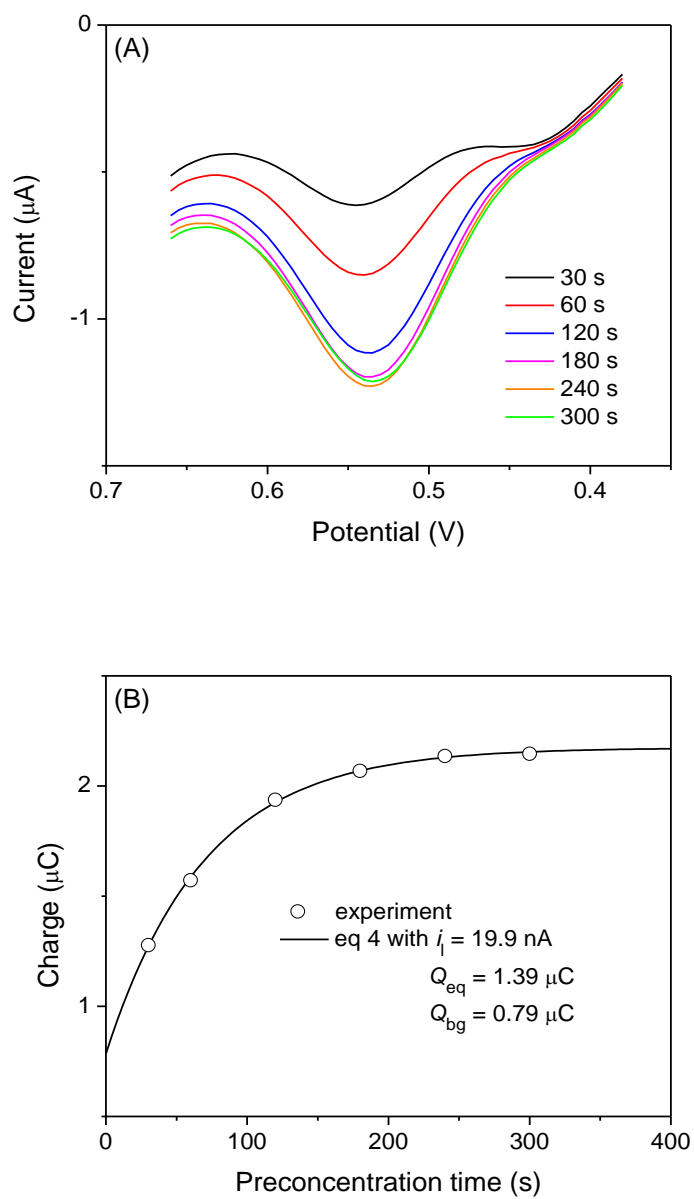


Figure 2-3. (A) The ITSV of 50 nM K⁺ at 0.1 V/s with various pre-concentration times. Preconcentration potential, 0.38 V. The electrode was rotated at 4000 rpm. (B) The corresponding plot of $Q_{\text{tot}}(t_p)$ versus t_p .

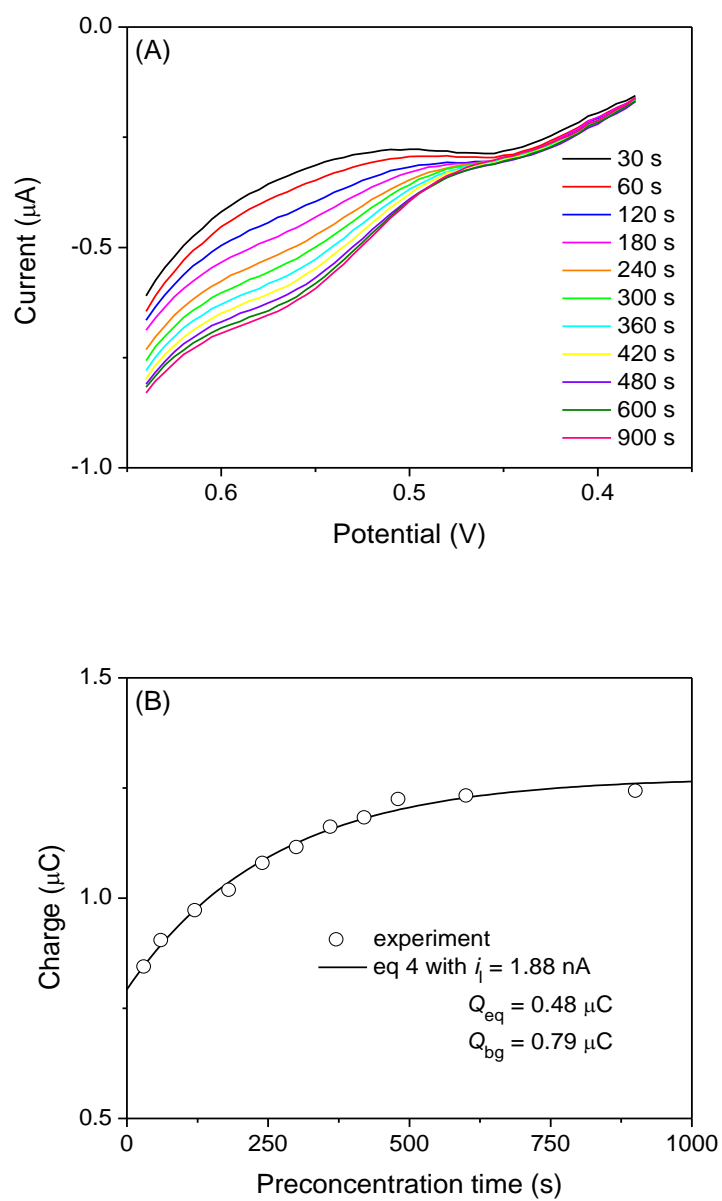


Figure 2-4. (A) The ITSV of 5.1 nM K^+ contaminated in the laboratory-purified water at 0.1 V/s with various preconcentration times. Preconcentration potential, 0.38 V . The electrode was rotated at 4000 rpm . (B) The corresponding plot of $Q_{\text{tot}}(t_p)$ versus t_p .

2.4.3 Equilibrium LODs of Potassium Ion.

The LOD of K^+ for ITSV at the valinomycin-doped PVC/PEDOT- C_{14} -modified electrode was determined using a preconcentration time of 5 minutes, which resulted in the equilibrium preconcentration of K^+ to maximize the resultant stripping response. The ITSV response varied with K^+ concentrations in the range of 1–10 nM (Figure 2-5A) to yield a linear plot of the background-subtracted peak current versus the K^+ concentration (Figure 2-5B). This calibration plot gives a LOD of 0.6 nM K^+ (confidence level of 95%) based on the IUPAC's upper limit approach.⁴³ This LOD value is approximately one order of magnitude lower than the LODs of 5 nM K^+ for potentiometric valinomycin-based electrodes with an inert inner solution.³³ A higher LOD of 100 nM K^+ was reported for potentiometry with solid-contact valinomycin-based electrodes.⁴⁴ These results apparently indicate the superior sensitivity of the ITSV approach employed in this work, where the use of K^+ -free ultrapure water also contributed to lowering the LODs. Thus, another advantage of the ITSV approach for trace ion analysis is the ability to detect an analyte contamination in the blank solution, which is not recognizable by potentiometry. In contrast, the lower LODs of 0.1–0.2 nM were reported for ICP-MS. In this case, high resolution was required for detecting K with an exact mass of 38.9637 in the presence of interfering molecular ions (e.g., ^{38}ArH with an exact mass of 38.971).³⁴

A LOD of 0.6 nM K^+ for ITSV at the valinomycin-doped double-polymer electrode is limited by the background current and the presence of trace NH_4^+ contamination in the ultrapure water. A peak current response of 20 nA to 1 nM K^+ is >10 times smaller than the background current at the peak potential (Figure 2-5A). This background current response mainly includes the charging current as well as the tail of an ITSV response to NH_4^+ , which slightly overlaps with the

K^+ response (Figure 2-2A). Therefore, a LOD of K^+ in the presence of NH_4^+ in the sample solution cannot be improved by the application of a more negative preconcentration potential, which results in higher equilibrium concentrations of both K^+ and NH_4^+ complexes in the membrane (eq 2). In fact, we optimized the preconcentration potential for K^+ such that a LOD of 0.6 nM K^+ was obtained in the presence of ~160 times excess NH_4^+ in the ultrapure water (see below). A more negative preconcentration potential would lower the LOD of K^+ in the water sample that is not only originally free from NH_4^+ but also protected from NH_3 in the ambient air as achieved in this study by employing argon atmosphere. We observed a gradual increase in the ITSV response to NH_4^+ when the sample solution was exposed to ambient air (data not shown).

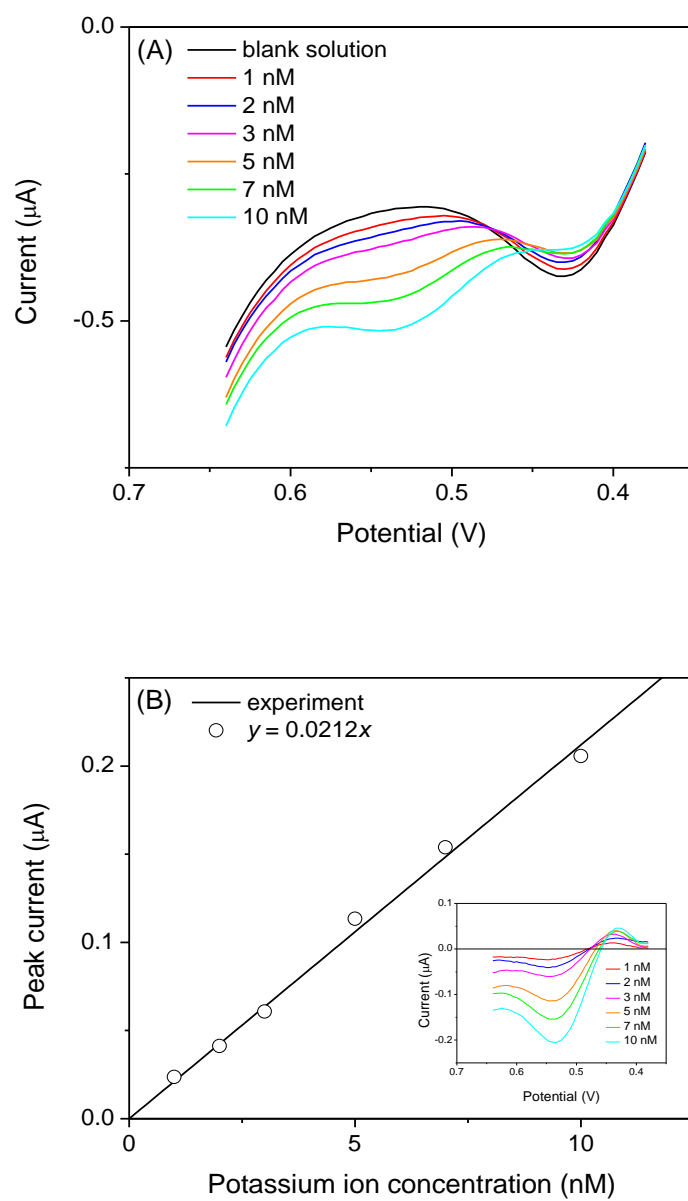


Figure 2-5. (A) The ITSV of 0–10 nM K^+ in the ultrapure water at 0.1 V/s after 5 min preconcentration. Preconcentration potential, 0.38 V. The electrode was rotated at 4000 rpm. (b) Plot of the background-subtracted peak current versus K^+ concentration. The solid line represents the best fit used for the determination of the LOD. The inset shows background-subtracted ITSVs.

2.4.4 Nanomolar Ammonium Contamination.

We determined a nanomolar concentration of NH_4^+ contaminated in the commercial ultrapure water by ITSV. First, we assigned the ITSV response at ~ 0.4 V to NH_4^+ , because the peak current varied with the addition of standard NH_4^+ solutions (Figure 2-6A). The original NH_4^+ concentration in the ultrapure water, however, can not be determined by this standard addition method, which requires the measurement of a background response to a NH_4^+ -free blank solution. Therefore, we measured the dependence of the ITSV response to NH_4^+ on the preconcentration time. In comparison to the ITSV of K^+ , a more negative preconcentration potential was applied to enhance the ITSV response to NH_4^+ (see eq 2), which grew with the preconcentration time up to 3 minutes and then saturated (Figure 2-6B). The total charge under each voltammogram, $Q_{\text{tot}}(t_p)$, is plotted against the preconcentration time, t_p , in Figure 2-6C. This plot fitted very well with eq 4 to yield $i_l = 35.6$ nA, $Q_{\text{eq}} = 2.57$ μC , and $Q_{\text{bg}} = 0.87$ μC . In eq 3 with $D_w = 1.9 \times 10^{-5}$ cm^2/s , this i_l value corresponds to 97 nM NH_4^+ in the ultrapure water. Moreover, an equilibrium concentration of 0.37 mM NH_4^+ -valinomycin complexes was obtained from the Q_{eq} value using eq 5 with $l = 3.7$ μm , thereby yielding a large preconcentration factor, Y , of 3.8×10^3 for NH_4^+ . This Y value is comparable to the Y value obtained for a more stable K^+ -valinomycin complex at a less negative potential. Since the sensitivity of ITSV is dictated by the preconcentration factor, a LOD for NH_4^+ is predicted to be similar to a LOD of 0.6 nM for K^+ . The confirmation of this theoretical prediction, however, requires NH_4^+ -free water, which is beyond the scope of this work. Noticeably, a relatively modest LOD of 25 nM NH_4^+ was obtained for potentiometric NH_4^+ -selective electrodes based on nonactin.³³ This LOD may be limited by the contamination of the laboratory-purified water with NH_4^+ , which is not recognizable by potentiometry.

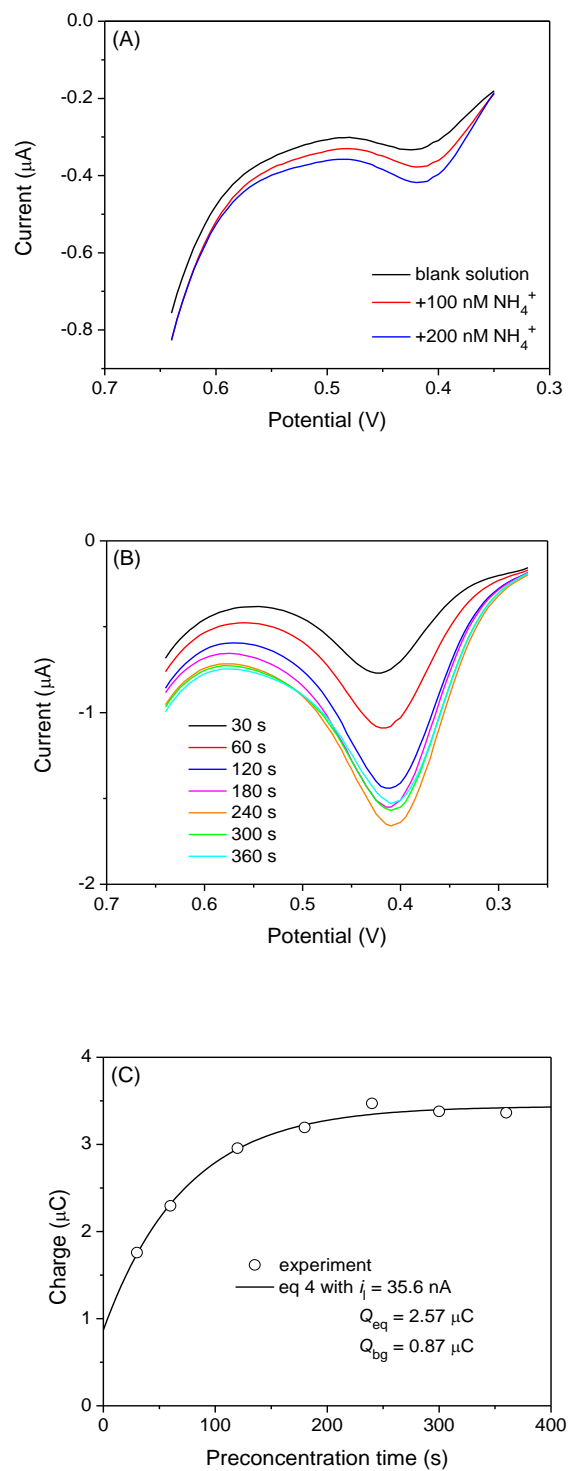


Figure 2-6. The ITSV of the commercial ultrapure water at 0.1 V/s (A) before and after the

addition of 100 and 200 nM NH_4^+ and (B) with various preconcentration times. Preconcentration potential, 0.35 V and 0.27 V, respectively. The electrode was rotated at 4000 rpm. (C) Plot of $Q_{\text{tot}}(t_p)$ versus t_p as obtained from the voltammograms in part (B).

2.5 CONCLUSIONS

This work is the first to demonstrate the unique features and analytical applications of ITSV at an ionophore-doped double-polymer electrode. A highly K^+ -selective ionophore, valinomycin, was successfully employed to explore not only the high sensitivity of ITSV for achieving a LOD of 0.6 nM K^+ but also its multiple-ion detectability based on resolved voltammetric responses to K^+ and NH_4^+ in their mixed solutions. In addition, the power of the ITSV approach was demonstrated by determining the unknown nanomolar concentrations of K^+ and NH_4^+ contaminations in purified water without the background measurement of a contaminant-free blank solution. In contrast, traditional potentiometric electrodes and optodes based on ionophore-doped membranes give a mixed response to analyte and interfering ions^{31,45} and, subsequently, are unable to recognize trace analyte contamination in a blank solution, which compromises their LODs for hardly removable or easily contaminable ions such as K^+ and NH_4^+ . The double-polymer electrode is thus a promising platform for the ITSV application of the various ionophores, which have been developed for the potentiometric and optical ion sensors.^{46,47}

ACKNOWLEDGEMENTS

This work was supported by a CAREER award from the National Science Foundation (CHE-0645623).

2.6 SUPPORTING INFORMATION

2.6.1 Derivation of Eq 4 for the Preconcentration Step.

The preconcentration of an analyte ion into the thin membrane phase can be modeled as follows to derive eq 4. The concentration of the transferred ion at the aqueous side of the rotating PVC membrane surface, $c_w(0,t)$, is related to the current response limited by the steady-state mass transfer of the aqueous ion, $i(t)$, as

$$i(t) = 0.62zFAD_w^{2/3}\omega^{1/2}\nu^{-1/6}[c_w - c_w(0, t)] \quad (\text{S-1})$$

A combination of eq 3 with S-1 results in

$$c_w(0, t) = c_w \frac{i_1 - i(t)}{i_1} \quad (\text{S-2})$$

On the other hand, the membrane concentration of an ion-ionophore complex, $c_{PVC}(t)$, is given by integrating the current as

$$c_{PVC}(t) = \frac{\int_0^t i(t) dt}{zFAI} \quad (S-3)$$

Since the reversible facilitated transfer of the analyte ion is assumed, the resulting Nernst equation gives

$$Y = \frac{c_{PVC}(t)}{c_w(0, t)} \quad (S-4)$$

A combination of eq S-4 with eqs S-2 and S-3 gives

$$Y = \frac{i_1 \int_0^t i(t) dt}{zFAI c_w [i_1 - i(t)]} \quad (S-5)$$

Using eq 5, eq S-5 can be simplified to

$$\frac{\int_0^t i(t) dt}{Q_{eq}} = \frac{i_1 - i(t)}{i_1} \quad (S-6)$$

Eq S-6 can be solved for $i(t)$ analytically using the Laplace transformation^{S-1} with an initial condition of $i(0) = i_1$, which implies that the current decays to i_1 immediately after the potential step at $t = 0$. Finally, eq 5 is obtained by integrating $i(t)$ from $t = 0$ to $t = t_p$.

2.6.2 Finite Element Analysis of CVs of Facilitated K^+ and NH_4^+ Transfers.

Experimental CVs in Figure 2-2A were fitted with CVs simulated using the finite element method as detailed in the following two sections. Transport and kinetic parameters for valinomycin-facilitated K^+ transfer as reported elsewhere² were used for the finite element simulation (Table 2-1). To obtain the best fits, we assumed that the potential applied to the gold electrode, E_{app} , was distributed to the PVC membrane/water interface to drive facilitated ion transfer and also to the PVC/PEDOT-C₁₄/gold junction to mediate ion-to-electron transduction, thereby yielding³

$$E_{app} = D_{PVC}^{Au} f + D_w^m f - E_{ref} \quad (S-7)$$

where $\Delta_{PVC}^{Au} \phi$ is the potential drop at the PVC/ PEDOT-C₁₄/gold junction, $D_w^m f$ is the phase boundary potential at the PVC membrane/sample solution interface, and E_{ref} is the reference electrode potential. Also, we assumed that $D_w^m f$ and $D_{PVC}^{Au} f$ varied linearly with E_{app} during a potential sweep to yield

$$D_w^m f - D_w^m f_i^{0'} = (E_{\text{app}} - E_{\text{app},i}^{0'}) \frac{\partial D_w^m f}{\partial E_{\text{app}}} \quad (\text{S-8})$$

where $\Delta_w^{\text{PVC}} \phi_i^{0'}$ is the formal ion-transfer potential at the PVC membrane/water interface, and $E_{\text{app},i}^{0'}$ is the applied potential at $D_w^m f = D_w^m f_i^{0'}$. Table 2-1 lists $D_w^m f_i^{0'}$, $\partial D_w^m f / \partial E_{\text{app}}$, and the effective membrane thickness, l , used as fitting parameters.

For facilitated ion transfer, the formal potential is defined as

$$D_w^m f_i^{0'} = E_i^{0'} + \frac{RT}{zF} \ln b_n L_T \quad (\text{S-9})$$

Subsequently, the difference in $D_w^m f_i^{0'}$ values for K^+ and NH_4^+ with valinomycin is given by eq S-9 as

$$D_w^m f_{\text{K}^+}^{0'} - D_w^m f_{\text{NH}_4^+}^{0'} = (E_{\text{K}^+}^{0'} - E_{\text{NH}_4^+}^{0'}) + \frac{RT}{F} \ln \frac{b_1(\text{K}^+)}{b_1(\text{NH}_4^+)} \quad (\text{S-10})$$

The finite element analysis gives $D_w^m f_{\text{K}^+}^{0'} - D_w^m f_{\text{NH}_4^+}^{0'} = 0.105 \text{ V}$ (see Table 2-1), which corresponds to $b_1(\text{K}^+) / b_1(\text{NH}_4^+) = 60$ in eq S-10 with $E_{\text{K}^+}^{0c} = E_{\text{NH}_4^+}^{0c}$ based on the assumption of the same lipophilicity for K^+ and NH_4^+ .

Table 2-1. Parameters Employed for the Finite Element Analysis of CVs in Figure 2-2A.

	K ⁺	NH ₄ ⁺
D_w (cm ² /s) ^a	1.9×10^{-5b}	1.9×10^{-5c}
D_m (cm ² /s) ^a	1.0×10^{-7b}	1.0×10^{-7c}
k^0 (cm/s) ^a	9.0×10^{-3b}	9.0×10^{-3c}
α ^a	0.48 ^b	0.48 ^c
$D_w^m f_i^{\theta'}$ (V)	0.365	0.260
$\partial D_w^m f / \partial E_{app}$	0.70	0.65
l (μm)	4.0	3.4

^a Defined in the following section. ^b From ref. S-2. ^c The same value as K⁺ transfer was assumed.

2.6.3 Diffusion Problem for CV at the PVC Membrane/Water Interface.

The theoretical CVs in Figure 2-2A were obtained by solving the following diffusion problem. The diffusion of an analyte ion in the aqueous phase is expressed as

$$\frac{\partial c_w(x,t)}{\partial t} = D_w \left[\frac{\partial^2 c_w(x,t)}{\partial x^2} \right] \quad (0 < x) \quad (\text{S-11})$$

where $c_w(x,t)$ is the local concentration of the transferring ion in the aqueous phase. The diffusion of the ion in the membrane phase is expressed as

$$\frac{\partial c_m(x,t)}{\partial t} = D_m \left[\frac{\partial^2 c_m(x,t)}{\partial x^2} \right] \quad (-l < x < 0) \quad (\text{S-12})$$

where $c_m(x,t)$ is the local concentration of the ion in the membrane phase.

The boundary condition at the PVC membrane/water interface ($x = 0$) is given by

$$D_m \left[\frac{\partial c_m(x,t)}{\partial x} \right]_{x=0} = D_w \left[\frac{\partial c_w(x,t)}{\partial x} \right]_{x=0} = k_f c_w(0,t) - k_b c_m(0,t) \quad (\text{S-13})$$

where k_f and k_b are the first-order heterogeneous rate constants for the forward and reverse transfers as given by Butler-Volmer-type relations as^{S-2}

$$k_f = k^0 \exp[-a\alpha f(D_w^m f - D_w^m f_i^{\theta'})] \quad (\text{S-14})$$

$$k_b = k^0 \exp[(1-a)\alpha f(D_w^m f - D_w^m f_i^{\theta'})] \quad (\text{S-15})$$

where k^0 is the standard rate constant, α is the transfer coefficient. In cyclic voltammetry, the phase boundary potential, $D_w^m f$, is swept linearly at a constant rate, v , from the initial potential, $\Delta_w^m \phi_i$, and

the sweep direction is reversed at the switching potential, $\Delta_w^m \phi_\lambda$, maintaining the potential sweep rate. This triangle potential wave is expressed as

$$\Delta_w^m \phi = \Delta_w^m \phi_1 + \frac{2(\Delta_w^m \phi_\lambda - \Delta_w^m \phi_1)}{\pi} \sin^{-1} \left\{ \sin \left[\frac{\pi vt}{2(\Delta_w^m \phi_\lambda - \Delta_w^m \phi_1)} \right] \right\} \quad (\text{S-16})$$

Other boundary conditions are given by

$$D_m \left[\frac{\partial c_m(x,t)}{\partial x} \right]_{x=-l} = 0 \quad (\text{membrane/solid support interface}) \quad (\text{S-17})$$

$$\lim_{x \rightarrow \infty} c_w(x,0) = c_0 \quad (\text{simulation limit in the aqueous phase}) \quad (\text{S-18})$$

Initial conditions are given by

$$c_w(x,0) = c_0 \quad (\text{S-19})$$

$$c_m(x,0) = 0 \quad (\text{S-20})$$

The current response based on the ion transfer, i , is obtained from the flux of the transferring ion at the PVC membrane/sample solution interface as

$$i = zAFD_w \left[\frac{\eta c_w(x, t)}{\eta x} \right]_{x=0} \quad (\text{S-21})$$

2.6.4 Finite Element Simulation by COMSOL Multiphysics.

The diffusion problem defined above was solved in a dimensionless form using COMSOL Multiphysics version 3.5a[®] (COMSOL, Inc., Burlington, MA). An example of the finite element simulation is attached. Dimensionless parameters are defined by

$$C_w(X, \tau) = c_w(x, t)/c_0 \quad (\text{S-22})$$

$$C_m(X, \tau) = c_m(x, t)/c_0 \quad (\text{S-23})$$

$$\tau = t\nu f \quad (\text{S-24})$$

$$X = x \sqrt{\frac{\nu f}{D_w}} \quad (\text{S-25})$$

$$L = l \sqrt{\frac{\nu f}{D_w}} \quad (\text{S-26})$$

Diffusion processes (eqs S-11 and S-12) are expressed in the respective dimensionless forms as

$$\frac{\partial C_w(X, t)}{\partial t} = \left[\frac{\partial^2 C_w(X, t)}{\partial X^2} \right] \quad (\text{S-27})$$

$$\frac{\partial C_m(X, t)}{\partial t} = g^2 \left[\frac{\partial^2 C_m(X, t)}{\partial X^2} \right] \quad (\text{S-28})$$

with

$$g = \sqrt{\frac{D_m}{D_w}} \quad (\text{S-29})$$

The boundary condition at the PVC membrane/water interface (eq S-13) is expressed using the dimensionless parameters as

$$\left[\frac{\partial C_w(X, t)}{\partial X} \right]_{X=0} = -\frac{L}{q_{1/2}^a} [gq_{1/2} C_m(0, t) - C_w(0, t)] \quad (\text{S-30})$$

$$\left[\frac{\partial C_m(X, t)}{\partial X} \right]_{X=0} = q_{1/2}^{1-a} g L \left[\frac{C_w(0, t)}{gq_{1/2}} - C_m(0, t) \right] \quad (\text{S-31})$$

with

$$L = \frac{k^0}{\sqrt{D_w^{1-a} D_m^a f v}} \quad (\text{S-32})$$

$$q_{1/2} = \exp\left[z_i f(D_w^m f - D_w^m f_{1/2})\right] \quad (\text{S-33})$$

$$D_w^m f_{1/2} = D_w^m f_i^{\theta'} + \frac{RT}{z_i F} \ln \sqrt{\frac{D_m}{D_w}} \quad (\text{S-34})$$

The triangle potential wave (eq S-16) is given by

$$q_{1/2} = q_i^{1-(2/\rho)\sin^{-1}\{\sin[\rho z_i t/2 \ln(q_i/q_{1/2})]\}} q_{1/2}^{(2/\rho)\sin^{-1}\{\sin[\rho z_i t/2 \ln(q_i/q_{1/2})]\}} \quad (\text{S-35})$$

with

$$q_i = \exp\left[z_i f(D_w^m f_i - D_w^m f_{1/2})\right] \quad (\text{S-36})$$

$$q_{1/2} = \exp\left[z_i f(D_w^m f_{1/2} - D_w^m f_i)\right] \quad (\text{S-37})$$

$$t_1 = f(D_w^m f_{1/2} - D_w^m f_i) \quad (\text{S-38})$$

where θ_i is the initial and final potentials in the dimensionless form, θ_λ is the dimensionless switching potential, and τ_λ is the dimensionless switching time. The current is normalized with respect to the peak current on the forward scan, i_{pa} , thereby yielding

$$I = \frac{i}{i_{pa}} = \frac{[\partial C_w(0, \tau) / \partial X]}{[\partial C_w(0, \tau) / \partial X]_{pa}} \quad (\text{S-39})$$

where $[\partial C_w(0, \tau) / \partial X]_{pa}$ is the interfacial gradient of the dimensionless concentration at the anodic peak potential.

2.6.5 REFERENCES

- (S-1) Bard, A. J.; Faulkner, L. R. *Electrochemical Methods: Fundamentals and Applications*; 2nd ed.; John Wiley & Sons: New York, 2001.
- (S-2) Ishimatsu, R.; Izadyar, A.; Kabagambe, B.; Kim, Y.; Kim, J.; Amemiya, S. *J. Am. Chem. Soc.* **2011**, *133*, 16300.
- (S-3) Kim, Y.; Amemiya, S. *Anal. Chem.* **2008**, *80*, 6056.

2.7 REFERENCES

- (1) Samec, Z.; Samcová, E.; Girault, H. H. *Talanta* **2004**, *63*, 21.
- (2) Senda, M.; Katano, H.; Kubota, Y. *Collect. Czech. Chem. Commun.* **2001**, *66*, 445.
- (3) Kim, Y.; Amemiya, S. *Anal. Chem.* **2008**, *80*, 6056.
- (4) Guo, J.; Yuan, Y.; Amemiya, S. *Anal. Chem.* **2005**, *77*, 5711.
- (5) Amemiya, S.; Kim, Y.; Ishimatsu, R.; Kabagambe, B. *Anal. Bioanal. Chem.* **2011**, 399, 571.
- (6) Wang, J. *Stripping Analysis: Principles, Instrumentation, and Applications*; VCH: Deerfield Beach, FL, 1985.
- (7) Economou, A.; Fielden, P. R. *Analyst* **2003**, *128*, 205.
- (8) Girault, H. H. Electrochemistry at Liquid/Liquid Interfaces. In *Electroanalytical Chemistry*; Bard, A. J., Zoski, C. G., Eds.; Taylor & Francis: Boca Raton, 2010; Vol. 23, p 1.
- (9) Marecek, V.; Samec, Z. *Anal. Lett.* **1981**, *14*, 1241.
- (10) Ohkouchi, T.; Kakutani, T.; Osakai, T.; Senda, M. *Anal. Sci.* **1991**, *7*, 371.
- (11) Huang, B.; Yu, B. Z.; Li, P. B.; Jiang, M. A.; Bi, Y. S.; Wu, S. F. *Anal. Chim. Acta* **1995**, *312*, 329.
- (12) Homolka, D.; Marecek, V.; Samec, Z.; Base, K.; Wendt, H. *J. Electroanal. Chem.* **1984**, *163*, 159.
- (13) Marecek, V.; Samec, Z. *Anal. Chim. Acta* **1982**, *141*, 65.
- (14) Strutwolf, J.; Scanlon, M. D.; Arrigan, D. W. M. *J. Electroanal. Chem.* **2010**, *641*, 7.
- (15) Ohtani, T.; Nishi, N.; Kakiuchi, T. *J. Electroanal. Chem.* **2011**, *656*, 102.

- (16) Katano, H.; Senda, M. *J. Electroanal. Chem.* **2001**, *496*, 103.
- (17) Collins, C. J.; Arrigan, D. W. M. *Anal. Chem.* **2009**, *81*, 2344.
- (18) Collins, C. J.; Lyons, C.; Strutwolf, J.; Arrigan, D. W. M. *Talanta* **2010**, *80*, 1993.
- (19) Katano, H.; Senda, M. *Anal. Sci.* **1998**, *14*, 63.
- (20) Sherburn, A.; Arrigan, D. W. M.; Dryfe, R. A. W.; Boag, N. M. *Electroanalysis* **2004**, *16*, 1227.
- (21) Lee, H. J.; Lagger, G.; Pereira, C. M.; Silva, A. F.; Girault, H. H. *Talanta* **2009**, *78*, 66.
- (22) Marecek, V.; Samec, Z. *Anal. Chim. Acta* **1983**, *151*, 265.
- (23) Scanlon, M. D.; Herzog, G.; Arrigan, D. W. M. *Anal. Chem.* **2008**, *80*, 5743.
- (24) Alvarez de Eulate, E.; Arrigan, D. W. M. *Anal. Chem.* **2012**, *84*, 2505.
- (25) Herzog, G.; Roger, A.; Sheehan, D.; Arrigan, D. W. M. *Anal. Chem.* **2010**, *82*, 258.
- (26) Senda, M.; Katano, H.; Yamada, M. *J. Electroanal. Chem.* **1999**, *468*, 34.
- (27) Katano, H.; Senda, M. *Anal. Sci.* **2001**, *17*, i337.
- (28) Guo, J.; Amemiya, S. *Anal. Chem.* **2006**, *78*, 6893.
- (29) Izadyar, A.; Kim, Y.; Muscatello, M. M. W.; Amemiya, S. *J. Chem. Edu.* **2012**, ASAP, <http://pubs.acs.org/doi/abs/10.1021/ed200749m>.
- (30) Kim, Y.; Rodgers, P. J.; Ishimatsu, R.; Amemiya, S. *Anal. Chem.* **2009**, *81*, 7262.
- (31) Bakker, E.; Bühlmann, P.; Pretsch, E. *Chem. Rev.* **1997**, *97*, 3083.
- (32) Ishimatsu, R.; Izadyar, A.; Kabagambe, B.; Kim, Y.; Kim, J.; Amemiya, S. *J. Am. Chem. Soc.* **2011**, *133*, 16300.
- (33) Qin, W.; Zwickl, T.; Pretsch, E. *Anal. Chem.* **2000**, *72*, 3236.
- (34) Ferrero, E. J.; Posey, D. J. *Anal. At. Spectrom.* **2002**, *17*, 1194.
- (35) *Standard Guide for Ultra-Pure Water Used in the Electronics and Semiconductor*

- Industries*; D5127-07; ASTM International: West Conshohocken, PA.
- (36) Osborne, M. D.; Girault, H. H. *Electroanalysis* **1995**, *7*, 425.
- (37) Qin, Y.; Mi, Y.; Bakker, E. *Anal. Chim. Acta* **2000**, *421*, 207.
- (38) Jing, P.; Rodgers, P. J.; Amemiya, S. *J. Am. Chem. Soc.* **2009**, *131*, 2290.
- (39) Bard, A. J.; Faulkner, L. R. *Electrochemical Methods: Fundamentals and Applications*; 2nd ed.; John Wiley & Sons: New York, 2001, p 339.
- (40) Breiby, D. W.; Samuelsen, E. J.; Groenendaal, L.; Struth, B. *J. Polym. Sci., Part B: Polym. Phys.* **2003**, *41*, 945.
- (41) Kano, I.; Castillo, E.; Darbouret, D.; Mabic, S. *J. Chromatogr. A* **2004**, *1039*, 27.
- (42) Francis, M. J. *J. Phys. Chem. C* **2008**, *112*, 14563.
- (43) Mocak, J.; Bond, A. M.; Mitchell, S.; Scollary, G. *Pure Appl. Chem.* **1997**, *69*, 297.
- (44) Chumbimuni-Torres, K. Y.; Rubinova, N.; Radu, A.; Kubota, L. T.; Bakker, E. *Anal. Chem.* **2006**, *78*, 1318.
- (45) Amemiya, S. Potentiometric Ion-Selective Electrodes. In *Handbook of Electrochemistry*; Zoski, C. G., Ed.; Elsevier: New York, 2007, p 261.
- (46) Bühlmann, P.; Pretsch, E.; Bakker, E. *Chem. Rev.* **1998**, *98*, 1593.
- (47) Umezawa, Y.; Bühlmann, P.; Umezawa, K.; Tohda, K.; Amemiya, S. *Pure Appl. Chem.* **2000**, *72*, 1851.
- .

3.0 SUB-NANOMOLAR DETECTION LIMIT OF STRIPPING VOLTAMMETRIC Ca²⁺ SELECTIVE ELECTRODE: EFFECTS OF ANALYTE CHARGE AND SAMPLE CONTAMINATION

This work has been published as Benjamin Kabagambe, Mohammed B. Garada, Ryoichi Ishimatsu, and Shigeru Amemiya, *Anal. Chem.* **2014**, *86*, 7939–7946. The thesis author contributed in conducting experiments and analyzing data.

3.1 INTRODUCTION

Ultrasensitive ion-selective electrode measurements based on stripping voltammetry are an emerging sensor technology with low- and sub-nanomolar detection limits. Here, we report on stripping voltammetry of down to 0.1 nM Ca²⁺ by using a thin-polymer-coated electrode and demonstrate the advantageous effects of the divalent charge on sensitivity. A simple theory predicts that the maximum concentration of an analyte ion preconcentrated in the thin membrane depends exponentially on the charge and that the current response based on exhaustive ion stripping from the thin membrane is proportional to the square of the charge. The theoretical predictions are quantitatively confirmed by using a thin ionophore-doped polymer membrane spin-coated on a conducting-polymer-modified electrode. The potentiostatic transfer of hydrophilic Ca²⁺ from an aqueous sample into the hydrophobic double-polymer membrane is facilitated by an

ionophore with high Ca^{2+} affinity and selectivity. The resultant concentration of the Ca^{2+} -ionophore complex in the $\sim 1 \mu\text{m}$ -thick membrane can be at least 5×10^6 times higher than the aqueous Ca^{2+} concentration. The stripping voltammetric current response to the divalent ion is enhanced to achieve a sub-nanomolar detection limit under the condition where a low-nanomolar detection limit is expected for a monovalent ion. Significantly, charge-dependent sensitivity is attractive for the ultrasensitive detection of multivalent ions with environmental and biomedical importance such as heavy metal ions and polyionic drugs. Importantly, this stripping voltammetric approach enables the absolute determination of sub-nanomolar Ca^{2+} contamination in ultrapure water containing 10 mM supporting electrolytes, i.e., an eight orders of magnitude higher background concentration.

In the past 15 years, ion-selective electrodes (ISEs) were transformed into an ultrasensitive analytical method for trace ion analysis with nanomolar and picomolar detection limits. In principle, ultrasensitive ISEs can be potentiometric,^{1,2} amperometric,³ or voltammetric.⁴ Among them, potentiometric approaches have been most extensively developed⁵ since the finding that their micromolar detection limits were compromised by the contamination of the membrane/sample interface with the analyte ions transported from the inner filling solution.⁶ To suppress the transmembrane flux of an analyte ion and, subsequently, lower detection limits, an analyte ion was buffered at a low concentration in the inner solution containing EDTA⁶ or ion-exchange resins.⁷ In addition, transmembrane ion diffusion was slowed down by using a more viscous poly(vinyl chloride) (PVC) membrane with less plasticizers⁸ or a plasticized PVC membrane supported by a porous monolithic column⁹ or incorporating hydrophobic microparticles.¹⁰ Alternatively, hydrodynamic¹¹ and galvanostatic¹² approaches were proposed to actively remove analyte ions from the aqueous side of the membrane/sample interface. Eventually,

the inner solution was eliminated by coating an ion-selective membrane on the solid electrode modified with a conducting polymer film as an intermediate layer for ion-to-electron transduction.^{13,14} By contrast, the contamination of sample solutions with analyte or interfering ions was not adequately considered or noticed in the recent studies of ultrasensitive potentiometric ISEs.

Recently, we developed the ultrasensitive ISEs based on stripping voltammetry as a powerful alternative to the potentiometric counterpart.¹⁶ Among several advantages, the high sensitivity of this emerging approach was demonstrated by enabling the detection of relatively hydrophobic monovalent ions at nanomolar^{17,18} and sub-nanomolar¹⁹ levels. In the stripping voltammetric mode, an analyte ion was potentiostatically transferred from the aqueous sample solution into the thin PVC membrane supported by a conducting-polymer-modified electrode. Importantly, the transferred analyte ions were confined within and exhaustively stripped from the thin membrane to enhance the resultant voltammetric current response. This thin-layer effect lowered detection limits by 1–2 orders of magnitude in comparison to those of ion-transfer stripping voltammetry with thick membranes.^{4,20} The lowered detection limits, however, were still compromised by the saturation of the thin membrane with preconcentrated analyte ions. Membrane saturation was quantitatively explained by the Nernst equation as a preconcentration factor, Y ,¹⁷

$$Y = \frac{c_m}{c_w} = \exp \left[- \frac{zF(D_w^m f - D_w^m f_i^{\theta'})}{RT} \right] \quad (1)$$

where c_m and c_w are the equilibrium membrane and aqueous concentrations of an analyte ion,

respectively, z is the charge of the analyte ion, $D_w^m f$ is the phase boundary potential across the membrane/sample interface during preconcentration, and $D_w^m f_i^{\theta'}$ is the formal potential of the simple transfer of the analyte ion across the interface.

The thin double-polymer membrane of stripping voltammetric ISEs was also doped with ionophores to enable the detection of low-nanomolar hydrophilic ions such as heparins²¹ and potassium ion.²² While heparin was adsorbed at the membrane/water interface,²¹ K^+ was potentiostatically transferred into the thin PVC membrane doped with a K^+ -selective ionophore, valinomycin.²² The membrane, however, was quickly saturated with K^+ complexes despite the presence of excess valinomycin to obtain a low-nanomolar detection limit. In this case, an equilibrium membrane concentration of the complex, c_m , was also given by the Nernst equation (eq 1) with a formal potential for ionophore-facilitated ion transfer, $D_w^m f_{iL}^{\theta'}$, which is defined as

$$D_w^m f_{iL}^{\theta'} = D_w^m f_i^{\theta'} + \frac{RT}{zF} \ln b_n L_T \quad (2)$$

where β_n is the overall formation constant of a 1: n ion–ionophore complex, and L_T is the total ionophore concentration.²² The quick membrane saturation was due to a low preconcentration factor of 4×10^3 for a $D_w^m f - D_w^m f_{KL}^{\theta'}$ value of -0.21 V. The preconcentration potential, $D_w^m f$, was limited by interference with airborne ammonium ion contaminating the background electrolyte solution of ultrapure water. Advantageously, contamination levels of ~ 100 nM NH_4^+ and ~ 5 nM K^+ were directly determined by using the stripping voltammetric ISE based on valinomycin. Importantly, these background NH_4^+ and K^+ concentrations are similar to the detection limits of

ultrasensitive ISEs based on potentiometry,⁷ which is incapable of identifying the contaminants.

Herein, we report on the sub-nanomolar detection limit of a stripping voltammetric Ca²⁺-selective electrode based on a thin ionophore-doped membrane. Specifically, the achievement of the extremely low detection limit requires two advantageous effects of higher analyte charge on sensitivity in addition to the careful prevention of the Ca²⁺ contamination of background solutions. As the first advantage, the exponential dependence of preconcentration factor on analyte charge is predicted by eq 1 and is confirmed experimentally to yield an extremely large preconcentration factor of 5×10^6 for Ca²⁺ with a $D_w^m f - D_w^m f_{CaL}^{0'}$ value of -0.20 V, thereby enabling the preconcentration of Ca²⁺ for 1 hour without membrane saturation. By contrast, an $\sim 10^3$ times smaller preconcentration factor was obtained for K⁺ with a similar $D_w^m f - D_w^m f_{KL}^{0'}$ value (see above).²² Second, a peak current response, i_p , based on exhaustive analyte stripping from the thin membrane varies with the square of analyte charge as given by²³

$$i_p = \frac{z^2 F^2 \nu V_m c_m(t_p)}{4RT} \quad (3)$$

where ν is potential sweep rate during stripping process, V_m is membrane volume, and $c_m(t_p)$ is the membrane ion concentration at preconcentration time of t_p . Together, Ca²⁺ concentrations down to 0.1 nM are detected by stripping voltammetry with the thin ionophore-doped membrane coated on a conducting-polymer-modified electrode. Importantly, we identify and remove the sources of the Ca²⁺ contamination of background solutions to demonstrate the sub-nanomolar detection limit. In fact, the stripping voltammetric approach enables us to directly determine low- and sub-nanomolar

Ca²⁺ contaminations in ultrapure water.

3.2 EXPERIMENTAL SECTION

3.2.1 Chemicals.

Calcium ionophore II (ETH 129; *N,N,N',N'*- tetracyclohexyl-3-oxapentanediamide), tetradodecylammonium (TDDA) bromide, PVC (high molecular weight), and 2-nitrophenyl octyl ether (*o*NPOE) were obtained from Aldrich (Milwaukee, WI). Potassium tetrakis(pentafluorophenyl)borate (TFAB) was from Boulder Scientific Company (Mead, CO). Acetic acid (Trace Select, Aldrich), tetramethylammonium (TMA) hydroxide (Trace Select Ultra, Aldrich), and hydrochloric acid ($\geq 30\%$, Trace Select, Aldrich) were used as high purity supporting electrolytes. All reagents were used as received. All aqueous sample solutions were prepared using commercial ultrapure water (Trace Select Ultra, Aldrich) or laboratory-purified water (18.2 M Ω ·cm and TOC 3 ppb) from a Milli-Q Advantage A10 system equipped with Q-Gard T2 Pak and Quantum TIX Cartridge (EMD Millipore Corporation, Billerica, MA). The Milli-Q system was fed with the building deionized water that was pretreated with the ultrapure (D0809) and organic removal (D0813) cartridges of a Barnstead B-Pure system (Thermo Scientific, Marietta, OH) to yield a resistivity of ~ 0.5 M Ω cm. The ultrapure water was directly collected from the Milli-Q system without a porous membrane filter and immediately used to prevent the introduction of inorganic contaminants.²⁴ The dispenser of the Milli-Q system was placed in a class 100 vertical

laminar flow hood (model AC632LFC, AirClean Systems, Raleigh, NC) to prevent the airborne contamination of Milli-Q water for the preparation of contamination-free solutions. The solutions were prepared in the Ar-filled polyethylene bag (AtmosBag, Aldrich) in the laminar flow hood (Figure 3-6) by using polypropylene volumetric flasks (VITLAB GmbH, Grossostheim, Germany) and were filled in polytetrafluoroethylene beakers (VITLAB GmbH) for electrochemical measurement (see below). During storage, the flasks were filled with Milli-Q water and the beakers were immersed in Milli-Q water filled in polypropylene wide-mouth jars (Thermo Scientific).

3.2.2 Electrode Modification.

A cleaned 5 mm-diameter gold disk was attached to a rotating disk electrode tip (Pine Research Instrumentation, Raleigh, NC) and modified with an oxidatively doped film of tetradecyl-substituted poly(3,4-ethylenedioxythiophene) (PEDOT-C₁₄) and then with an *o*NPOE-plasticized PVC membrane as reported elsewhere.²² To minimize Ca²⁺ contamination, a bare gold disk was cleaned in piranha solution (a 1:1 mixture of 30% H₂O₂ and 95.0–98.0% H₂SO₄) for 15 minutes and in Milli-Q water for 15 minutes (3 times), and dried in air for 5 minutes. Caution: piranha solution reacts violently with organics and should be handled with extreme care. A thin *o*NPOE-plasticized PVC membrane was spin-coated from the THF solution of membrane components (0.61 mg ETH 129, 4.0 mg PVC, 16.0 mg *o*NPOE, and 2.2 mg TDDATFAB in 1 mL THF) by using a spin-coating device (model SCS-G3-8, Cookson Electronics, Providence, RI).

3.2.3 Electrochemical Measurement.

An electrochemical workstation (CHI 900A or CHI 600A, CH Instruments, Austin, TX) was used for voltammetric measurements. A Pt-wire counter electrode was employed in the following three-electrode cell

Ag | AgCl | 3 M KCl | 10 mM CH₃COOK | x M (CH₃COO)₂Ca in 10 mM CH₃COOK |
PVC membrane | PEDOT-C₁₄ | Au

(cell 1)

Ag | AgCl | y M (CH₃COO)₂Ca in 10 mM CH₃COOTMA and 0.1 mM HCl | PVC
membrane | PEDOT-C₁₄ | Au

(cell 2)

The concentrations of (CH₃COO)₂Ca are given in the Results and Discussion section. The current carried by a positive charge from the aqueous phase to the PVC membrane was defined to be positive. All electrochemical experiments were performed at 22 ± 3 °C.

Additional setups and procedures were used for different voltammetric measurements as follows. For cyclic voltammetry, a piece of Teflon tube²¹ was put on a PVC/PEDOT-C₁₄-modified gold electrode to form a disk-shaped PVC membrane/water interface with a diameter of 1.5 mm. For rotating-electrode cyclic voltammetry and stripping voltammetry, the electrochemical cell and a modulated speed rotator (Pine Research Instrumentation) were placed in the polyethylene glove bag. The bag was accommodated in the class 100 vertical laminar flow hood (Figure 3-6) to

prevent the contamination of a sample solution with airborne Ca^{2+} . The glove bag was cleaned under vacuum by using a diaphragm vacuum pump (DOL-701-AA, Allegheny Fluid Power, Sewickley, PA) and filled with Ar. Low-humidity brushes (Pine Research Instrumentation) were used to obtain good electrical connection to the rotating shaft of the electrode rotator in the Ar atmosphere, which was humidified by placing a polypropylene wide-mouth jar filled with Milli-Q water placed in the bag. An as-prepared electrode was contaminated with Ca^{2+} and was cleaned in the background Milli-Q water solution of supporting electrolytes (cell 2) by repeating stripping voltammetric measurements until no Ca^{2+} peak was detected.

3.3 RESULTS AND DISCUSSIONS

3.3.1 Cyclic Voltammetry of Facilitated Ca^{2+} Transfer.

We employed cyclic voltammetry (CV) to characterize the Ca^{2+} transfer facilitated by ETH 129 at a PVC/PEDOT- C_{14} -modified gold electrode. ETH 129 has been used as a highly Ca^{2+} -selective ionophore for potentiometric ISEs²⁵ and is known to form a very stable 1:3 complex¹⁵ with a large β_3 value of 1.6×10^{29} in the *o*NPOE/PVC membrane.²⁶ In fact, extremely hydrophilic Ca^{2+} was transferred into the hydrophobic *o*NPOE/PVC membrane doped with ETH 129 at negative potentials on the forward sweep of CV (Figure 3-1A). In contrast to our previous voltammetric study,²⁷ a much thinner PVC/PEDOT- C_{14} membrane was used in this study to exhaustively strip Ca^{2+} from the membrane. This thin-layer effect was confirmed experimentally,

where the reverse peak current based on the stripping of membranous Ca^{2+} was higher than the forward peak current based on the transfer of aqueous Ca^{2+} into the membrane. The exhaustive stripping also resulted in the quick decay of the reverse peak current without a diffusional tail. Noticeably, the forward and reverse transfers of Ca^{2+} are coupled with the reduction and oxidation of the PEDOT- C_{14} film on the underlying gold electrode, respectively.²⁷ The exhaustive stripping of Ca^{2+} is required to recover the initially oxidized state of the PEDOT- C_{14} film upon the completion of the reverse potential sweep of CV or in stripping voltammetry.

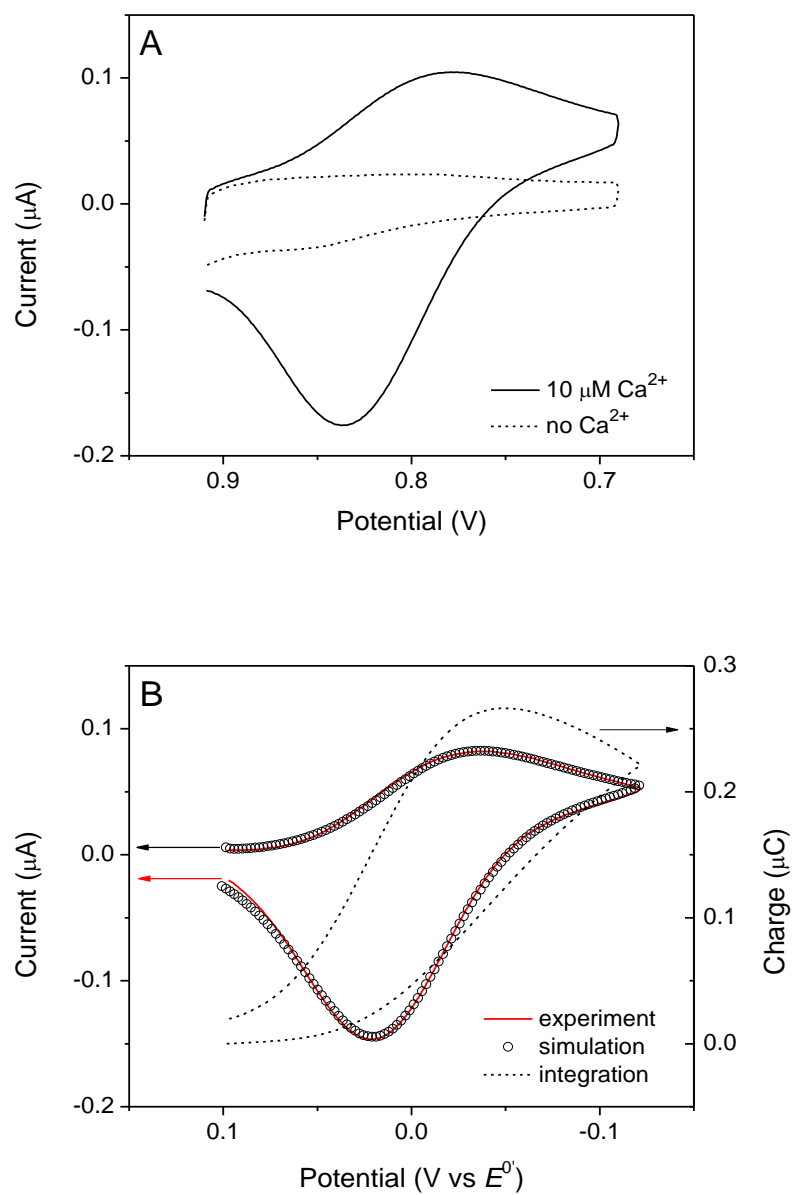


Figure 3-1. (A) CVs of 0 and 10 μM Ca^{2+} (cell 1) at a PEDOT- C_{14} -modified gold electrode spin-coated with an *o*NPOE-plasticized PVC membrane containing ETH 129. Potential sweep rate, 0.05 V/s. (B) Corresponding background-subtracted CV, simulated CV, and the integration of the background-subtracted CV.

The experimental CV was analyzed more quantitatively by fitting with the theoretical CV based on the finite element simulation.²² A background-subtracted CV (red line in Figure 3-1B) was obtained from the CVs of 0 and 10 μM Ca^{2+} (dashed and solid lines in Figure 3-1A, respectively). The characteristically high reverse peak was fitted with a theoretical one with a membrane thickness of 1.3 μm (circles), which is thin enough to exhaustively strip Ca^{2+} from the membrane to the aqueous solution. In addition, the CV was integrated to ensure that charges due to transferred Ca^{2+} return to nearly zero at the end of a potential cycle (dashed line), which corresponds to the exhaustive stripping of Ca^{2+} from the thin membrane. Moreover, the best fit was obtained when the facilitated Ca^{2+} transfer was quasi-reversible with a standard ion-transfer rate constant, k^0 , of 7.7×10^{-3} cm/s. This value is slightly higher than a k^0 value of 3.8×10^{-3} cm/s as obtained by using a thick PVC membrane drop-cast on the PEDOT- C_{14} -modified electrode.²⁷ The CV is nearly reversible so that the peak current of the forward wave is nearly equal to the value expected for reversible ion transfer as given by²⁸

$$i_p = 0.4463 \left(\frac{F^3}{RT} \right)^{1/2} z^{3/2} A v^{1/2} D_w^{1/2} c_w \quad (4)$$

where A is the area of the membrane/sample interface, v is the sweep rate of the phase boundary potential across the interface, and D_w is the diffusion coefficient of Ca^{2+} in the aqueous phase. Noticeably, the v value is smaller than an actual sweep rate of 0.05 V/s for the potential applied to the underlying gold electrode, E . Because the applied potential is used to drive not only Ca^{2+} transfer at the PVC membrane/water interface, but also the redox reaction of the PEDOT- C_{14} film.

Empirically, the phase boundary potential at the membrane/water interface is related to the applied potential as given by¹⁷

$$D_w^m f - D_w^m f_{iL_n}^{\theta'} = (E - E^{0'}) \frac{\partial D_w^m f}{\partial E} \quad (5)$$

where $E = E^{0'}$ when $D_w^m f = D_w^m f_{iL_n}^{\theta'}$ (see Supporting Information). The best fit was obtained by assuming that 55% of the change in the applied potential was used to change the phase boundary potential at the membrane/water interface, i.e., $\partial D_w^m f / \partial E = 0.55$, thereby broadening the resultant CV and also enhancing its electrochemical reversibility. In the following, eq 5 was also used to calibrate the applied potential against $E^{0'}$ for all voltammograms by measuring the CV of facilitated Ca^{2+} transfer for each electrode.

3.3.2 Rotating-Electrode Voltammetry.

A PVC/PEDOT- C_{14} -modified gold electrode was rotated to hydrodynamically accelerate the mass transport of Ca^{2+} between the aqueous solution and the membrane/water interface during stripping voltammetry. The resultant steady-state condition also simplifies the theoretical treatment of the preconcentration step.²² Importantly, the rotating-electrode system was setup in the polyethylene bag filled with Ar (Figure 3-6)²² to prevent the contamination of a sample solution with airborne Ca^{2+} . In addition, Ca^{2+} contamination was caused by the brushes that contacted the rotating shaft for electrical connection. Thus, a Teflon dish was attached to the rotating shaft to capture Ca^{2+} contaminants falling from the brushes. Subsequently, the additional weight from the

dish limited the rotation speed to 3000 rpm for short-time CV measurement. At this rotation speed or higher, the rotator made some noise so that 2000 rpm was employed for stripping voltammetry, which required long-time preconcentration.

Rotating-electrode CVs of 2 μM Ca^{2+} were measured to quantitatively confirm that the resultant limiting current agrees with the Levich equation as given by²⁹

$$i_l = 0.62zFAD_w^{2/3}\omega^{1/2}\nu^{-1/6}c_w \quad (6)$$

where ω is the rotation speed and ν is the viscosity of the aqueous electrolyte solution. Background-subtracted rotating-electrode CVs (Figure 3-2A) demonstrate that limiting current was obtained at sufficiently negative potentials and became higher at a higher rotation speed. A plot of the background-subtracted limiting current versus the square root of rotation speed (radian per second) was linear with a slope of $(6.1 \pm 0.1) \times 10^{-8}$ (Figure 3-2B), which agrees with a slope of 6.2×10^{-8} as expected from eq 6 with $A = 0.196 \text{ cm}^2$, $D_w = 1.5 \times 10^{-5} \text{ cm}^2/\text{s}$, and $\nu = 0.010 \text{ cm}^2/\text{s}$. Noticeably, the reverse peak current based on exhaustive stripping of preconcentrated Ca^{2+} also increased at a higher rotation speed, where Ca^{2+} was more effectively preconcentrated owing to a higher mass transport condition at the aqueous side of the membrane/water interface. Higher stripping current at a higher rotation speed is not relevant to the mass transport of Ca^{2+} -ionophore complex in the viscous PVC membrane, which is not affected by electrode rotation.

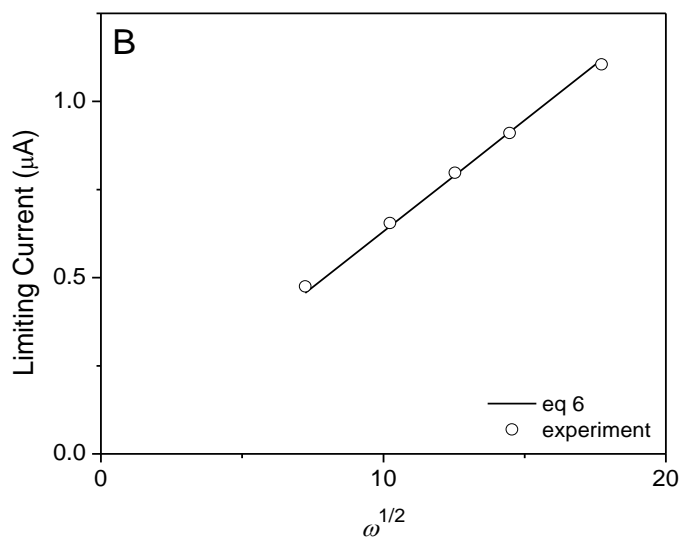
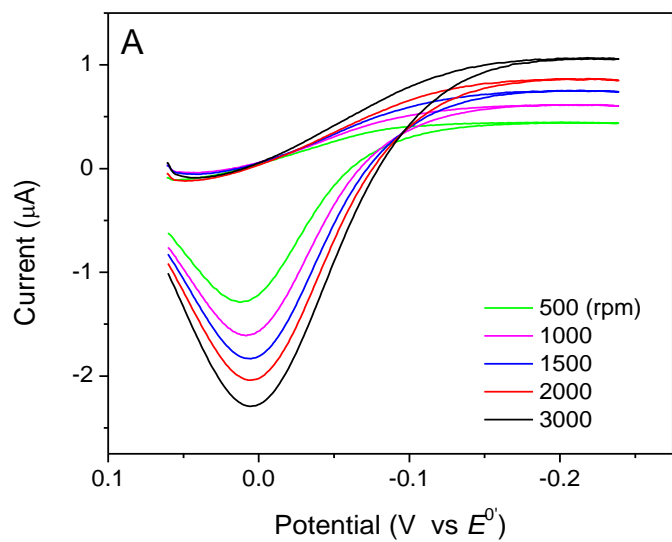


Figure 3-2. (A) Background-subtracted rotating-electrode CVs of $2 \mu\text{M Ca}^{2+}$ at a PEDOT-C₁₄-modified gold electrode spin-coated with an *o*NPOE-plasticized PVC membrane containing ETH 129 (cell 2). Potential sweep rate, 0.05 V/s. (B) A plot of the corresponding limiting current versus

the square root of rotation speed (radian per second). The solid line is the best fit with the Levich equation.

3.3.3 No Membrane Saturation with Ca²⁺.

Stripping voltammograms of 10 nM Ca²⁺ were measured with different preconcentration times, t_p , at 2000 rpm to confirm no saturation of the ionophore-doped membrane with Ca²⁺ for up to 1 hour preconcentration. Clearly, the stripping current response to Ca²⁺ varies with preconcentration time (Figure 3-3A). More quantitatively, the stripping voltammograms were integrated to demonstrate that the resultant charge, $Q(t_p)$, linearly increased with preconcentration time, t_p (Figure 3-3B). In general, $Q(t_p)$ is the sum of charge due to stripping of Ca²⁺ preconcentrated in the membrane and charge due to background processes during the stripping step, Q_{bg} , which is mainly charging of the membrane/water interface. Overall, $Q(t_p)$ is given by²²

$$Q(t_p) = Q_{eq} \left[1 - \exp\left(-\frac{i_l t_p}{Q_{eq}}\right) \right] + Q_{bg} \quad (7)$$

with

$$Q_{eq} = zFV_m c_m \quad (8)$$

where Q_{eq} is equilibrium charge due to the exhaustive stripping of Ca^{2+} preconcentrated in a saturated membrane. The linear t_p -dependence of $Q(t_p)$ is expected when $i_1 t_p \ll Q_{\text{eq}}$ in eq 7, thereby yielding

$$Q_{\text{total}}(t_p) = i_1 t_p + Q_{\text{bg}} \quad (9)$$

Importantly, there is no contribution of Q_{eq} in eq 9, where the preconcentration of Ca^{2+} is controlled solely by its mass transport at the aqueous side of the PVC membrane/water interface. The best fit of eq 9 with the experimental plot in Figure 3-3B gives $i_1 = 4.8 \text{ nA}$ and $Q_{\text{bg}} = 3.88 \text{ } \mu\text{C}$. This limiting current is immeasurably small by CV and is equivalent to a low concentration of 10.8 nM aqueous Ca^{2+} in eq 6. This concentration agrees with the concentration of spiked Ca^{2+} (10 nM). Moreover, a membrane concentration of Ca^{2+} -ionophore complex, $c_m(t_p)$, can be obtained from this i_1 value as

$$c_m(t_p) = \frac{i_1 t_p}{z F V_m} \quad (10)$$

Specifically, eq 10 with $t_p = 60 \text{ min}$ and $V_m = 2.6 \times 10^{-8} \text{ L}$ for a 1.3 μm -thick and 5 mm-diameter membrane yields $c_m(t_p) = 3.5 \text{ mM}$, which is 3.5×10^5 times higher than the spiked aqueous concentration of Ca^{2+} . Noticeably, the formation of 3.5 mM complexes requires an ionophore concentration of 10.5 mM, which corresponds to ~18% of ionophore in the membrane (originally ~58 mM as calculated by assuming a density of the PVC membrane to be ~1 g/mL).

This significant change in ionophore concentration during the preconcentration step resulted in a shift of the peak potential during the stripping step (Figure 3-3A).

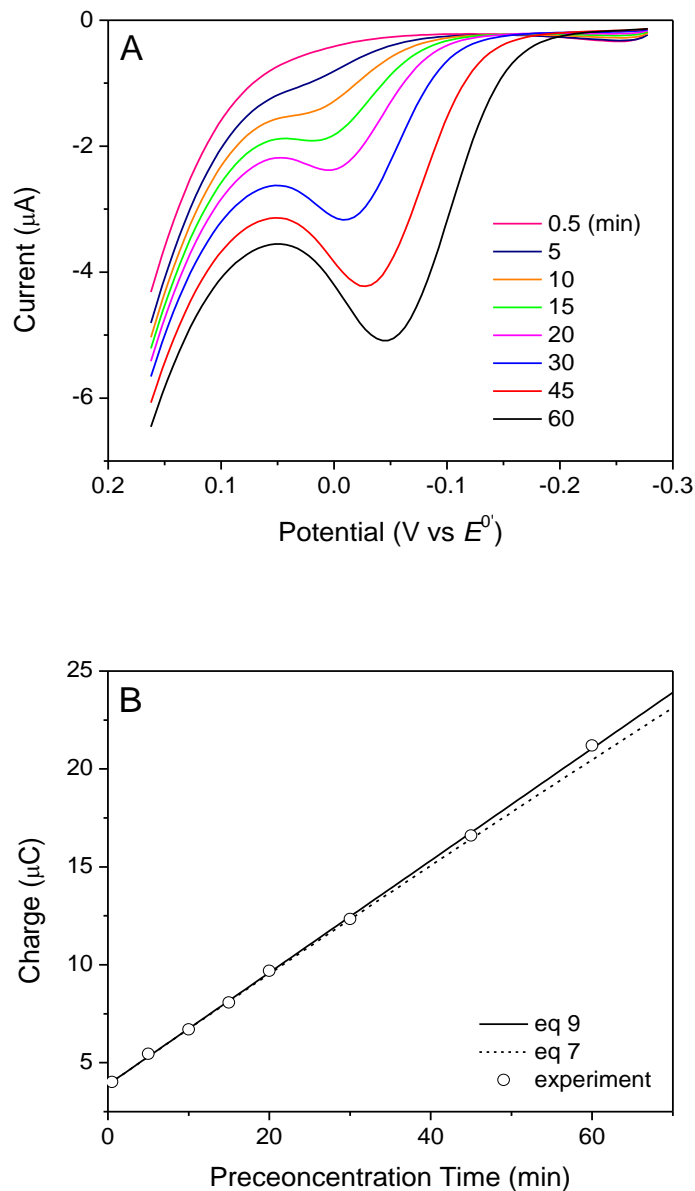


Figure 3-3. (A) Stripping voltammograms of 10 nM Ca²⁺ in Milli-Q water (cell 2) with different preconcentration times. Potential sweep rate, 0.05 V/s. (B) Charge under the stripping voltammograms (circles) and the best fits with eqs 7 and 9 (dotted and solid lines, respectively).

No saturation of the thin membrane with Ca^{2+} for 1 hour preconcentration is remarkable because membrane saturation was observed for all ions investigated in our previous studies of monovalent ions.^{17,19,22} The high Ca^{2+} capacity is ascribed to its divalent charge as supported by the quantitative analysis of the experimental plot in Figure 3-3B with eq 7. When the i_l and Q_{bg} values determined by using eq 9 are employed, the experimental plot deviates from eq 7 with $Q_{eq} = 250 \mu\text{C}$ (dashed line) or lower. This Q_{eq} value can be used as a minimum value to estimate parameters relevant to equilibrium preconcentration, which are otherwise unobtainable. Specifically, $Q_{eq} = 250 \mu\text{C}$ in eq 8 corresponds to $c_m = 51 \text{ mM}$, which is much higher than a c_w value of 10 nM . The corresponding preconcentration factor, Y , of 5.1×10^6 is ~ 15 times higher than the $c_m(t_p)/c_w$ value reached after 60 minute preconcentration. Remarkably, this extraordinarily large preconcentration factor is due to the divalent charge of Ca^{2+} and is corresponding to a moderate value of $D_w^m f - D_w^m f_{\text{CaL}}^{\theta'} = -0.20 \text{ V}$ in eq 1 for facilitated ion transfer. In fact, a much smaller preconcentration factor of 3.7×10^3 was obtained for K^+ with a similar $D_w^m f - D_w^m f_{\text{KL}}^{\theta'}$ value of -0.21 V by using a valinomycin-doped membrane, which was saturated with K^+ complexes within 5 minutes.²²

Overall, a $D_w^m f - D_w^m f_{\text{CaL}}^{\theta'}$ value of -0.20 V (see above) is large enough to prevent membrane saturation for 1 hour preconcentration, thereby yielding a sub-nanomolar detection limit (see below). The sufficiently large overpotential was obtained by employing TMA^+ as a supporting electrolyte with sufficiently high purity ($\text{Ca} \leq 2 \mu\text{g/kg}$) although this relatively hydrophobic cation narrows the negative limit of the potential window. Remarkably, the sub-nanomolar detection limit was achieved in the presence of 10 mM TMA^+ , i.e., an eight orders of magnitude higher

background concentration. High Ca^{2+} selectivity of ETH 129 ensures an even wider potential window with such interfering cations as Na^+ , K^+ , and Mg^{2+} , which are not commercially available as salts with negligible Ca^{2+} contamination. Specifically, potentiometric Ca^{2+} -selective electrodes based on ETH 129 give excellent selectivity coefficients of 2.0×10^{-8} , 1.3×10^{-10} , and 2.0×10^{-9} against Na^+ , K^+ , and Mg^{2+} , respectively.³⁰ These selectivity coefficients, K_{ij}^{pot} , are relevant to a difference in the formal potentials of facilitated ion transfer as given by³¹

$$D_w^m f_{jL_n}^{\theta'} - D_w^m f_{iL_n}^{\theta'} = \frac{RT}{z_i F} \ln K_{ij}^{\text{pot}} \quad (11)$$

where i is a target ion with charge, z_i , and j is an interfering ion. Eq 11 with these potentiometric selectivity coefficients against $j = \text{Na}^+$, K^+ , and Mg^{2+} gives $D_w^m f_{jL_n}^{\theta'} - D_w^m f_{\text{Ca}L_n}^{\theta'} = -0.246, -0.299,$ and -0.275 V, respectively. These values are much more negative than a value of -0.20 V as limited by TMA^+ . On the other hand, the positive side of the potential window was limited by chloride or acetate, which were obtained as high purity acids ($\text{Ca} \leq 10$ and $20 \mu\text{g}/\text{kg}$, respectively). The simple transfer of these extremely hydrophilic anions partially overlaps with Ca^{2+} transfer, which is strongly facilitated by ETH 129.

3.3.4 Sub-Nanomolar Detection Limit.

Stripping voltammetric responses to sub-nanomolar Ca^{2+} were measured after 30 minute preconcentration (Figure 3-4A). No clear response to Ca^{2+} was observed by using the background electrolyte solution prepared from Milli-Q water. By contrast, a peak-shaped response was clearly

observed for a range of 0.1–1 nM Ca²⁺, which is clearer after background subtraction (see the inset). The peak currents of background-subtracted stripping voltammograms were linear to the Ca²⁺ concentrations (Figure 3-4B). The slope of the calibration plot was assessed quantitatively to reveal the effect of analyte charge on peak current as predicted by eq 3. Specifically, eq 3 was combined with eqs 6 and 10 to yield

$$i_p = \frac{0.62z^2F^2Av_t D_w^{2/3}W^{1/2}\eta^{-1/6}}{4RT} c_w \quad (12)$$

As discussed for eq 5, the potential sweep rate in eq 12 corresponds to a change in the phase boundary potential at the membrane/water interface, which is slower than the actual potential sweep rate of 0.05 V/s by a factor of $\partial D_w^m f / \partial E$ (= 0.55; see Supporting Information). With this correction, eq 12 gives a slope of 4.3×10^2 (ampere/molar) for a plot of i_p versus c_w for Ca²⁺. This slope is consistent with a value of $(3.9 \pm 0.3) \times 10^2$ as determined from three calibration plots including the plot in Figure 3-4B. By contrast, a lower theoretical slope of 1.1×10^2 is expected for a monovalent ion using the otherwise same parameters in eq 12, thereby confirming the enhanced sensitivity to a more highly charged ion. Advantageously, current sensitivity depends on analyte charge more strongly in stripping voltammetry (eq 12) than in transient and steady-state CV (eqs 4 and 6, respectively).

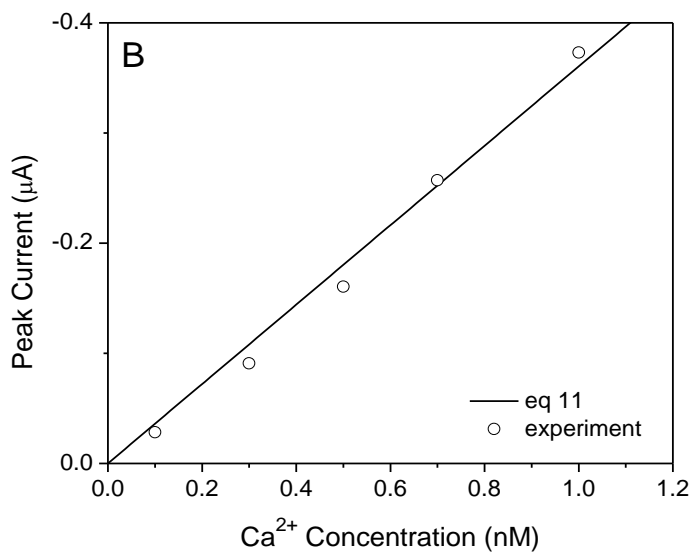
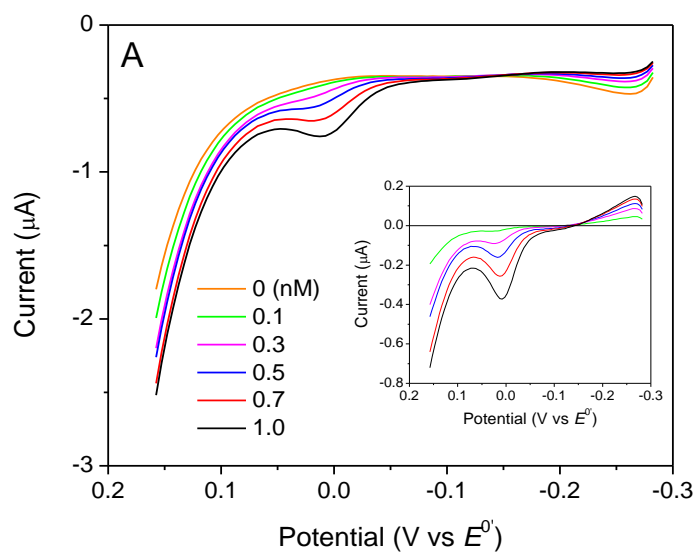


Figure 3-4. (A) Stripping voltammograms of 0–1 nM Ca^{2+} in Milli-Q water (cell 2) after 30 minute preconcentration. Potential sweep rate, 0.05 V/s. The inset shows the corresponding background-subtracted voltammograms. (B) A plot of background-subtracted peak current versus Ca^{2+} concentration (circles) and best fit with eq 11 (solid line).

Importantly, extra care was needed to prevent Ca^{2+} contamination of the background electrolyte solution prepared from Milli-Q water. Eventually, no Ca^{2+} peak was detectable in the stripping voltammogram of a background solution with 30 minute preconcentration (pink curve in Figure 3-4A), which nearly perfectly overlaps with the stripping voltammogram of the same background solution with 5 minute preconcentration (see Figure 3-7 for this comparison). This result confirms that Milli-Q water and aqueous supporting electrolytes are intrinsically free from Ca^{2+} contamination. To obtain the “ Ca^{2+} -free” background solution, origins of airborne Ca^{2+} contamination were identified by using stripping voltammetry and eliminated. A PVC/PEDOT- C_{14} -modified electrode was seriously contaminated with airborne Ca^{2+} during its preparation. Low-nanomolar Ca^{2+} contamination in the background aqueous solution made upon the first immersion of a newly prepared electrode was readily detected by stripping voltammetry with 5 minute preconcentration (Figure 3-8). No Ca^{2+} peak was detectable after the electrode was washed in two or three background solutions during stripping voltammetry with 5 minute preconcentration. Sub-nanomolar Ca^{2+} contamination, however, was still detectable after 30 minute preconcentration when Milli-Q water was collected from the dispenser in air. The airborne Ca^{2+} contamination of Milli-Q water was prevented by placing the dispenser in a class-100 laminar flow hood (see Figure 3-6). In addition, an operator wore a cleanroom mask and worked alone in the laboratory to reproducibly eliminate sub-nanomolar Ca^{2+} contamination. These results indicate that ultrapure water was contaminated at sub-nanomolar level by the Ca^{2+} -containing aerosol produced from those who are in the laboratory. Noticeably, background Ca^{2+} contamination was masked by using a Ca^{2+} buffer in the previous study of potentiometric Ca^{2+} -selective electrodes to achieve sub-nanomolar detection limits.¹⁵ By contrast, low-nanomolar^{7-9,32,33} and sub-nanomolar^{10,34,35}

detection limits were somehow obtained in recent potentiometric studies, where no elimination or masking of Ca^{2+} contamination was reported.

3.3.5 Ca^{2+} Contamination in Commercial Ultrapure Water.

We carried out stripping voltammetry at different preconcentration times to determine sub-nanomolar Ca^{2+} contamination in commercial ultrapure water. In our previous study, this water was used as “ K^+ -free” water because its K^+ concentration was undetectably low ($<0.02 \mu\text{g}/\text{kg}$, i.e., $<0.5 \text{ nM}$) by stripping voltammetry with valinomycin-doped K^+ -selective electrodes.²² In this study, the sub-nanomolar detection limit of the stripping voltammetric Ca^{2+} -selective electrode revealed the sub-nanomolar Ca^{2+} contamination of the commercial ultrapure water. Figure 3-5A shows the effect of preconcentration time on stripping voltammograms of a background supporting electrolyte solution prepared with the commercial ultrapure water. A Ca^{2+} peak grew at a longer preconcentration time, which contrasts to no Ca^{2+} peak in the background electrolyte solution of Milli-Q water (Figure 3-7). Each voltammogram was integrated in a range between -0.12 V and 0.12 V (Figure 3-5A) to obtain charge under the voltammogram. The resultant plot of the charge against the preconcentration time (Figure 3-5B) fitted well with eq 9 to yield $i_l = 0.189 \text{ nA}$ and $Q_{\text{bg}} = 2.05 \mu\text{C}$. This low i_l value is directly immeasurable and corresponds to 0.43 nM Ca^{2+} in eq 6. This result confirms the sub-nanomolar detection limit of the Ca^{2+} -selective electrode. The stripping voltammetric measurement was repeated using three different electrodes for the commercial ultrapure water from the same bottle to obtain a Ca^{2+} concentration of $0.3 \pm 0.1 \text{ nM}$. Importantly, this Ca^{2+} contamination was not caused by us because the bottle of fresh ultrapure water was opened and used for sample preparation in the Ar-filled polyethylene bag, which did

not cause any Ca^{2+} contamination of the Milli-Q water. The sub-nanomolar Ca^{2+} concentration is within a range of the Ca^{2+} concentration ($<0.2 \mu\text{g}/\text{kg}$, i.e., $<5 \text{ nM}$) as given by the provider of the commercial ultrapure water. A relatively high residual concentration is expected for Ca^{2+} , which is hard to remove and is the most abundant ionic impurity in laboratory ultrapure water.³⁶ Moreover, the presence of sub-nanomolar Ca^{2+} in ultrapure water is undetectable by measuring its resistivity ($18.2 \text{ M}\Omega\cdot\text{cm}$ at $25 \text{ }^\circ\text{C}$), which is determined by 10^{-7} M of H^+ and OH^- . In addition, the detection of trace Ca^{2+} by ICP-MS is challenging owing to ^{40}Ar interference.³⁷

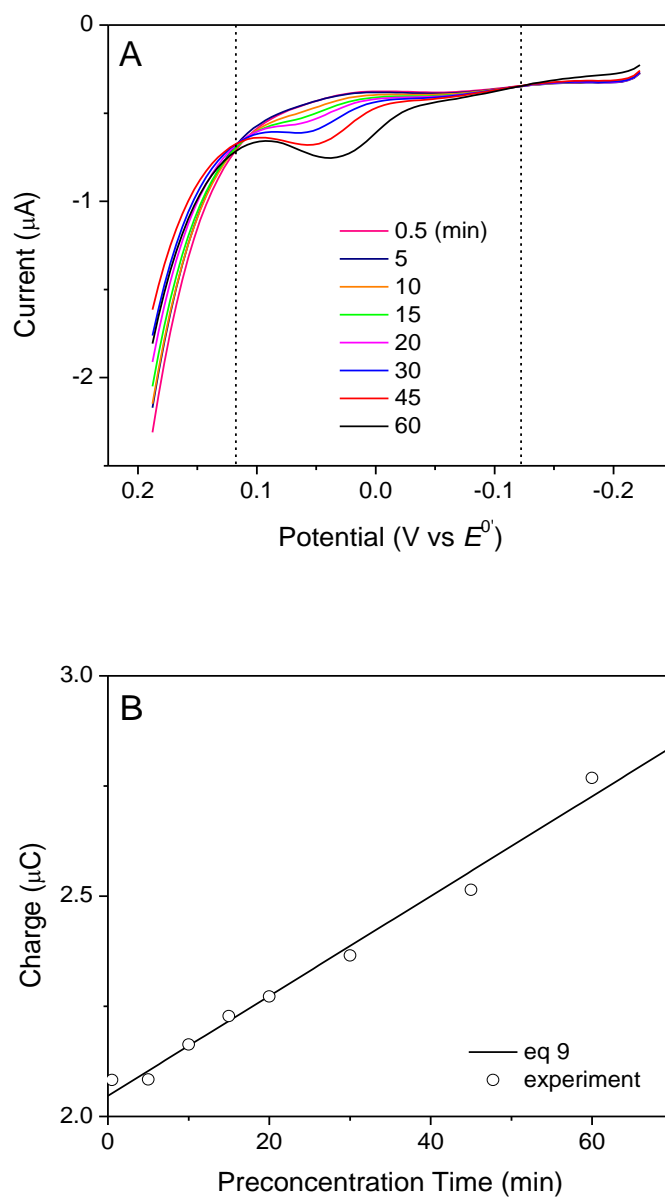


Figure 3-5. (A) Stripping voltammograms of commercial ultrapure water (cell 2) with different preconcentration times. Potential sweep rate, 0.05 V/s. (B) Charge under the stripping voltammograms (circles) as obtained by integrating current between potentials indicated by dotted lines and the best fit with eq 9 (solid line).

3.4 CONCLUSIONS

In this work, we demonstrated two advantageous effects of higher analyte charge on the enhanced sensitivity of the stripping voltammetric Ca^{2+} -selective electrode based on a thin ionophore-doped membrane. The resultant sub-nanomolar detection limit is significantly superior to the low-nanomolar detection limit of the valinomycin-based K^{+} -selective electrode developed in our previous study.²² The voltammetric responses of the Ca^{2+} -selective electrode were quantitatively analyzed to confirm the theoretical prediction that an analyte ion with a higher charge can be not only accumulated at an exponentially higher concentration in the thin membrane with the same overpotential during the preconcentration step (eq 1), but also exclusively stripped from the thin membrane to yield the current response that varies with the square of the charge (eq 3). The charge-dependent sensitivity of stripping voltammetric ISEs based on a thin membrane is attractive for the ultrasensitive detection of heavy metal ions, e.g., Pb^{2+} ,²⁷ and also for polyionic drugs, e.g., protamines and heparins, which are extractable into non-polar organic phases when appropriate ionophores are used.^{38,39} Some other biological macromolecules, e.g., α -chymotrypsin⁴⁰ and cytochrome c,^{41,42} can be also voltammetrically extracted into non-polar organic solutions.

Finally, this study demonstrates the importance of ultrapure water for trace ion analysis, which is well recognized for ICP-MS applications.⁴³ Sufficiently high purity for the detection of sub-nanomolar Ca^{2+} was achievable by using commercial water purification systems but was

readily compromised without the protection of ultrapure water from airborne contamination. Advantageously, stripping voltammetry enables the identification and quantitation of background contaminants, which was helpful for eliminating contamination sources. By contrast, not enough attention was paid to Ca^{2+} contamination in the recent potentiometric studies of ultrasensitive Ca^{2+} -selective electrodes. In these studies, low-nanomolar detection limits^{7-9,32,33} may be due to Ca^{2+} contamination while the effectiveness of the approaches developed for sub-nanomolar detection limits^{10,34,35} must be carefully reassessed.

ACKNOWLEDGEMENTS

This work was supported by the National Science Foundation (CHE-1213452).

3.5 SUPPORTING INFORMATION

3.5.1 Finite Element Analysis of CV of Facilitated Ca^{2+} Transfer.

Experimental CV in Figure 3-1B was fitted with the CV simulated using the finite element method as reported elsewhere.^{S-1} Table 3-1 lists the mass transport and kinetic parameters for facilitated Ca^{2+} transfer^{S-2} used for the finite element simulation. To obtain the best fit, we assumed that the potential applied to the gold electrode, E , was distributed to the PVC membrane/water interface to drive facilitated ion transfer and also to the PVC/PEDOT- C_{14} /gold junction to mediate ion-to-electron transduction, thereby yielding^{S-3}

$$E = D_m^{\text{Au}} f + D_w^{\text{m}} f - E_{\text{ref}} \quad (\text{S-1})$$

where $D_m^{\text{Au}} f$ is the potential drop across the PVC/ PEDOT-C₁₄/gold junction, and E_{ref} is the reference electrode potential. Empirically, $D_w^{\text{m}} f$ and $D_m^{\text{Au}} f$ varied linearly with E during a potential sweep to yield a constant $\partial D_w^{\text{m}} f / \partial E$ value in eq 5.

Table 3-1. Parameters Employed for the Finite Element Analysis of Facilitated Ca²⁺ Transfer.

D_w (cm ² /s) ^a	D_m^b (cm ² /s) ^a	k^0 (cm/s)	α^c	$\partial D_w^{\text{m}} f / \partial E$	l^d (μm)
1.5×10^{-5}	5.8×10^{-8}	7.7×10^{-3}	0.5	0.55	1.3

^a From ref. S-2. ^b Diffusion coefficient of Ca²⁺ complexes in the membrane. ^c Transfer coefficient. ^d Membrane thickness.

3.5.2 Rotating-Electrode Setup.

Figure 3-6 shows a rotating electrode system in an Ar-filled polyethylene bag. The bag was accommodated in a laminar flow hood to prevent airborne contamination. A double-polymer electrode was attached to the rotating shaft with a Teflon dish and immersed in an electrolyte

solution filled in a polytetrafluoroethylene beaker. The laminar flow hood was also used to collect ultrapure water from the Milli-Q system.



Figure 3-6. Image of electrode rotator in a Ar-filled polyethylene glove bag. The bag was accommodated in a class 100 laminar flow hood.

3.5.3 No Detectable Ca^{2+} Contamination in Background Electrolyte Solution.

We did not detect any Ca^{2+} contamination of electrolyte solutions prepared from Milli-Q water when it was collected from the dispenser in a laminar flow hood. Figure 3-7 shows the stripping voltammograms of a Milli-Q-based electrolyte solution (cell 2) with 5 and 30 minute preconcentration. The stripping voltammograms nearly perfectly overlap, thereby yield no Ca^{2+} peak after the former voltammogram was subtracted from the latter voltammogram (blue line).

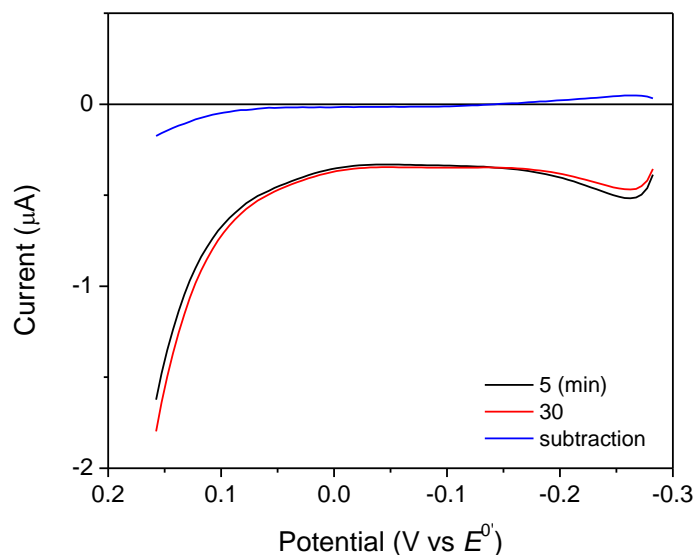


Figure 3-7. Stripping voltammograms of a background electrolyte solution prepared from Milli-Q water (cell 2) after 5 and 30 minutes pre-concentration. Potential sweep rate, 0.05 V/s. The blue line represents the subtraction of the 5 minutes voltammogram from the 30 minute voltammogram.

3.5.4 Ca²⁺ contamination of background solutions.

We were able to prevent the contamination of background solutions with low- and sub-nanomolar Ca²⁺. Low-nanomolar Ca²⁺ contamination was caused by immersing an as-prepared electrode in a background solution as detected by stripping voltammetry with 5 minute pre-concentration (black line in Figure 3-8A). The electrode was cleaned in two more background solutions to, eventually, observe no Ca²⁺ peak after 5 minute pre-concentration (red and blue lines).

By contrast, sub-nanomolar Ca^{2+} contamination was caused by airborne Ca^{2+} when Milli-Q water was collected from the dispenser in air although the background solutions were prepared in the Ar-filled polyethylene bag in the laminar flow hood. The stripping voltammograms of the background electrolyte solution gave higher Ca^{2+} peak when preconcentration time increased from 5 minutes to 30 minutes (Figure 3-8B). Charges under these stripping voltammograms were analyzed by using eq 9 to yield a Ca^{2+} concentration of 0.42 nM.

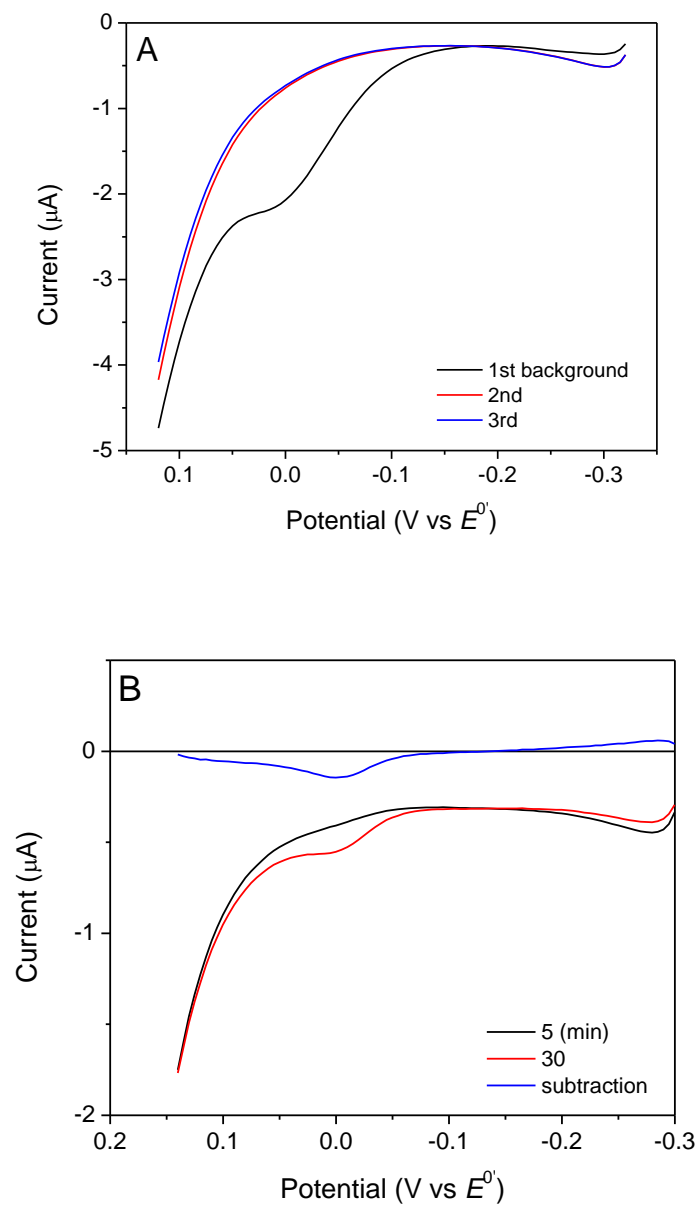


Figure 3-8. Stripping voltammograms of (A) three background solutions after 5 minutes preconcentration and (B) a background electrolyte solution after 5 and 30 minutes preconcentration (cell 2). In part (B), the blue line represents the subtraction of the 5 minutes voltammogram from the 30 minutes voltammogram. Potential sweep rate, 0.05 V/s.

3.5.5 REFERENCES

- (S-1) Kabagambe, B.; Izadyar, A.; Amemiya, S. *Anal. Chem.* **2012**, *84*, 7979.
- (S-2) Ishimatsu, R.; Izadyar, A.; Kabagambe, B.; Kim, Y.; Kim, J.; Amemiya, S. *J. Am. Chem. Soc.* **2011**, *133*, 16300.
- (S-3) Kim, Y.; Amemiya, S. *Anal. Chem.* **2008**, *80*, 6056.

3.6 REFERENCES

- (1) Bakker, E.; Pretsch, E. Advances in Potentiometry. In *Electroanalytical Chemistry*; Bard, A. J., Zoski, C. G., Eds.; Taylor & Francis: Boca Raton, FL, 2012; Vol. 24, p 1.
- (2) Bakker, E.; Pretsch, E. *Anal. Chem.* **2002**, *74*, 420A.
- (3) Horváth, V.; Horvai, G.; Pungor, E. *Microchim. Acta* **1990**, *100*, 217.
- (4) Senda, M.; Katano, H.; Kubota, Y. *Collect. Czech. Chem. Commun.* **2001**, *66*, 445.
- (5) Szigeti, Z.; Vigassy, T.; Bakker, E.; Pretsch, E. *Electroanalysis* **2006**, *18*, 1254.
- (6) Sokalski, T.; Ceresa, A.; Zwickl, T.; Pretsch, E. *J. Am. Chem. Soc.* **1997**, *119*, 11347.
- (7) Qin, W.; Zwickl, T.; Pretsch, E. *Anal. Chem.* **2000**, *72*, 3236.
- (8) Ceresa, A.; Sokalski, T.; Pretsch, E. *J. Electroanal. Chem.* **2001**, *501*, 70.
- (9) Vigassy, T.; Huber, C. G.; Wintringer, R.; Pretsch, E. *Anal. Chem.* **2005**, *77*, 3966.
- (10) Vigassy, T.; Gyurcsányi, R. E.; Pretsch, E. *Electroanalysis* **2003**, *15*, 375.
- (11) Vigassy, T.; Gyurcsányi, R. E.; Pretsch, E. *Electroanalysis* **2003**, *15*, 1270.
- (12) Pergel, E.; Gyurcsányi, R. E.; Toth, K.; Lindner, E. *Anal. Chem.* **2001**, *73*, 4249.
- (13) Sutter, J.; Lindner, E.; Gyurcsányi, R.; Pretsch, E. *Anal. Bioanal. Chem.* **2004**, *380*, 7.
- (14) Sutter, J.; Radu, A.; Peper, S.; Bakker, E.; Pretsch, E. *Anal. Chim. Acta* **2004**, *523*, 53.
- (15) Schefer, U.; Ammann, D.; Pretsch, E.; Oesch, U.; Simon, W. *Anal. Chem.* **1986**, *58*, 2282.
- (16) Amemiya, S.; Kim, J.; Izadyar, A.; Kabagambe, B.; Shen, M.; Ishimatsu, R. *Electrochim. Acta* **2013**, *110*, 836.
- (17) Kim, Y.; Amemiya, S. *Anal. Chem.* **2008**, *80*, 6056.
- (18) Izadyar, A.; Kim, Y.; Ward, M. M.; Amemiya, S. *J. Chem. Edu.* **2012**, *89*, 1323.
- (19) Kim, Y.; Rodgers, P. J.; Ishimatsu, R.; Amemiya, S. *Anal. Chem.* **2009**, *81*, 7262.

- (20) Katano, H.; Senda, M. *Anal. Sci.* **1998**, *14*, 63.
- (21) Guo, J.; Amemiya, S. *Anal. Chem.* **2006**, *78*, 6893.
- (22) Kabagambe, B.; Izadyar, A.; Amemiya, S. *Anal. Chem.* **2012**, *84*, 7979.
- (23) Bard, A. J.; Faulkner, L. R. *Electrochemical Methods: Fundamentals and Applications*; 2nd ed.; John Wiley & Sons: New York, 2001, p 455.
- (24) Darbouret, D.; Kano, I.; Castillo, E.; Stewart, B. In *The R&D Notebook*; Millipore: 1999, p 1.
- (25) Bühlmann, P.; Pretsch, E.; Bakker, E. *Chem. Rev.* **1998**, *98*, 1593.
- (26) Qin, Y.; Mi, Y.; Bakker, E. *Anal. Chim. Acta* **2000**, *421*, 207.
- (27) Ishimatsu, R.; Izadyar, A.; Kabagambe, B.; Kim, Y.; Kim, J.; Amemiya, S. *J. Am. Chem. Soc.* **2011**, *133*, 16300.
- (28) Bard, A. J.; Faulkner, L. R. *Electrochemical Methods: Fundamentals and Applications*; 2nd ed.; John Wiley & Sons: New York, 2001, p 231.
- (29) Bard, A. J.; Faulkner, L. R. *Electrochemical Methods: Fundamentals and Applications*; 2nd ed.; John Wiley & Sons: New York, 2001, p 339.
- (30) Bakker, E. *Anal. Chem.* **1997**, *69*, 1061.
- (31) Amemiya, S. Potentiometric Ion-Selective Electrodes, In *Handbook of Electrochemistry*; Zoski, C. G., Ed.; Elsevier: New York, 2007, p 261.
- (32) Sokalski, T.; Ceresa, A.; Fibbioli, M.; Zwickl, T.; Bakker, E.; Pretsch, E. *Anal. Chem.* **1999**, *71*, 1210.
- (33) Chumbimuni-Torres, K. Y.; Rubinova, N.; Radu, A.; Kubota, L. T.; Bakker, E. *Anal. Chem.* **2006**, *78*, 1318.

- (34) Bedlechowicz, I.; Maj-Żurawska, M.; Sokalski, T.; Hulanicki, A. *J. Electroanal. Chem.* **2002**, 537, 111.
- (35) Konopka, A.; Sokalski, T.; Michalska, A.; Lewenstam, A.; Maj-Zurawska, M. *Anal. Chem.* **2004**, 76, 6410.
- (36) Kano, I.; Castillo, E.; Darbouret, D.; Mabic, S. *J. Chromatogr. A* **2004**, 1039, 27.
- (37) Darbouret, D.; Kano, I. *Acta Physica Polonica A* **2009**, 116, S203.
- (38) Yuan, Y.; Amemiya, S. *Anal. Chem.* **2004**, 76, 6877.
- (39) Jing, P.; Kim, Y.; Amemiya, S. *Langmuir* **2009**, 25, 13653.
- (40) Vagin, M. Y.; Trashin, S. A.; Karpachova, G. P.; Klyachko, N. L.; Karyakin, A. A. *J. Electroanal. Chem.* **2008**, 623, 68.
- (41) Shinshi, M.; Sugihara, T.; Osakai, T.; Goto, M. *Langmuir* **2006**, 22, 5937.
- (42) Osakai, T.; Yuguchi, Y.; Gohara, E.; Katano, H. *Langmuir* **2010**, 26, 11530.
- (43) Darbouret, D.; Kano, I. *Ultrapure Water* **1998**, 15, 53.
- .

4.0 ION-TRANSFER VOLTAMMETRY OF PERFLUOROALKYL SULFONATES AND CARBOXYLATES: PICOMOLAR DETECTION LIMIT AND HIGH LIPOPHILICITY

This work has been published as Mohammed B. Garada, Benjamin Kabagambe, Yushin Kim, and Shigeru Amemiya, *Anal. Chem.* **2014**, *86*, 11230–11237. The thesis author contributed in conducting stripping voltammetry experiments to determine picomolar detection limit for perfluoroalkyl sulfonates.

4.1 INTRODUCTION

Here we report on ion-transfer voltammetry of perfluoroalkyl sulfonates and carboxylates at the interface between a plasticized polymer membrane and water to enable the ultrasensitive detection of these persistent environmental contaminants with adverse health effects. The ion-transfer cyclic voltammograms of the perfluoroalkyl oxoanions are obtained by using the ~1 μm -thick poly(vinyl chloride) membrane plasticized with 2-nitrophenyl octyl ether. The cyclic voltammograms are numerically analyzed to determine formal ion-transfer potentials as a measure of ion lipophilicity. The fragmental analysis of the formal potentials reveals that the 10^4 times higher lipophilicity of a perfluoroalkyl sulfonate in comparison to the alkyl sulfonate with the same chain length is due to the inductive effect of perfluorination on lowering the electron density of the adjacent sulfonate group, thereby weakening its hydration. The fragmental analysis also

demonstrates that the lipophilicity of perfluoroalkyl and alkyl groups with the same length is nearly identical and varies with the length. Advantageously, the high lipophilicity of perfluorooctane sulfonate allows for its stripping voltammetric detection at 50 pM in the presence of 1 mM aqueous supporting electrolytes, a $\sim 10^7$ times higher concentration. Significantly, this detection limit for perfluorooctane sulfonate is unprecedentedly low for electrochemical sensors and is lower than its minimum reporting level in drinking water set by the US Environmental Protection Agency. In comparison, the voltammetric detection of perfluoroalkyl carboxylates is compromised not only by the lower lipophilicity of the carboxylate group but also by its oxidative decarboxylation at the underlying poly(3-octyl thiophene)-modified gold electrode during voltammetric ion-to-electron transduction.

Significant attention has been given to the electrochemical studies of perfluoroalkyl sulfonates and carboxylates, which need to be monitored¹ and remediated² owing to environmental persistence³ and public health effects.⁴ The oxidation of these perfluoroalkyl oxoanions has been demonstrated for remediation by generating hydroxyl radicals at the electrodes based on boron-doped diamond,⁵⁻⁸ SnO₂,⁹ and PbO₂.¹⁰ By contrast, the perfluoroalkyl oxoanions are less amenable to direct electrode reactions than their non-fluorinated analogues,² thereby hampering electrochemical detection. The oxidation of the anionic head groups is slowed down by the inductive effect of perfluorination on their electron density, thereby limiting the Kolbe-type decarboxylation of perfluoroalkyl carboxylates.¹¹ Oxidative defluorination is even more difficult because of the high electronegativity of fluorine atoms. Reductive defluorination is also sluggish at platinum and carbon electrodes.¹² Alternatively, an electrochemical biosensor based on the inhibition of glutamic dehydrogenase by perfluorooctane sulfonate (PFOS⁻) was developed to achieve a low detection limit of 1.6 nM, i.e., 0.80 µg/L.¹³ The US Environmental Protection

Agency (EPA), however, set even lower concentrations as the minimum reporting levels for the assessment monitoring of PFOS⁻ (0.04 µg/L), perfluorooctanoate (PFO⁻; 0.02 µg/L), and 4 homologous compounds (0.01–0.09 µg/L) in drinking water.¹⁴ Presently, this challenging analytical task requires LC/MS/MS coupled with solid phase extraction.¹⁵

Recently, we applied ion-transfer micropipet voltammetry^{16,17} at the interface between 1-octanol and water to find that perfluoroalkyl oxoanions are ~10² times more lipophilic than their alkyl counterparts.¹⁸ Significantly, this finding supports the hypothesis that the bioaccumulation and toxicity of the perfluoroalkyl oxoanions originate from their lipophilic nature.¹⁹ The higher lipophilicity of the perfluoroalkyl oxoanions is due to the strong electron-withdrawing effect of the perfluoroalkyl group on the adjacent oxoanion group, which is weakly hydrated to decrease its hydrophilicity. By contrast, perfluoroalkyl and alkyl chains with the same length are similarly hydrophobic. These conclusions were made separately by conducting the fragmental analysis²⁰ of the formal partition coefficient, P_i^{0c} , of a target ion, i , as a measure of ion lipophilicity. A formal partition coefficient was determined from a formal potential, $D_w^m f_i^{0'}$, as given by²¹

$$\log P_i^{0c} = \frac{z_i F D_w^m f_i^{0'}}{2.303RT} \quad (1)$$

where z_i is the charge of the target ion. Experimentally, the formal potential as well as all kinetic and mass-transport parameters were obtainable²² by ion-transfer cyclic voltammetry at micropipet-supported 1-octanol/water interfaces. The thermodynamically favorable and fast transfer of the perfluoroalkyl oxoanions is advantageous for their selective electrochemical detection without the

need of their electrolysis. However, neither fragile micropipet electrode nor fluidic 1-octanol is suitable.

In this work, we take advantage of the high lipophilicity of perfluoroalkyl oxoanions to enable ion-transfer voltammetric detection at a picomolar level. Importantly, ion-transfer stripping voltammetry with the thin double-polymer membrane coated on a solid electrode²³ (Figure 4-1) gives a lower detection limit for a more lipophilic ion.²⁴ We characterize the lipophilicity of a homologous series of PFOS⁻ and PFO⁻ voltammetrically by employing the ~1 μm-thick poly(vinyl chloride) (PVC) membrane plasticized with 2-nitrophenyl octyl ether (*o*NPOE) as a robust ion-selective membrane. In contrast to our recent studies of hydrophilic potassium²⁵ and calcium²⁶ ions, no ionophore is needed to transfer the lipophilic anions into the lipophilic membrane. The *o*NPOE/PVC membrane is supported by the gold electrode modified with a poly(3-octylthiophene) (POT) film as a voltammetric ion-to-electron transducer.^{27,28}

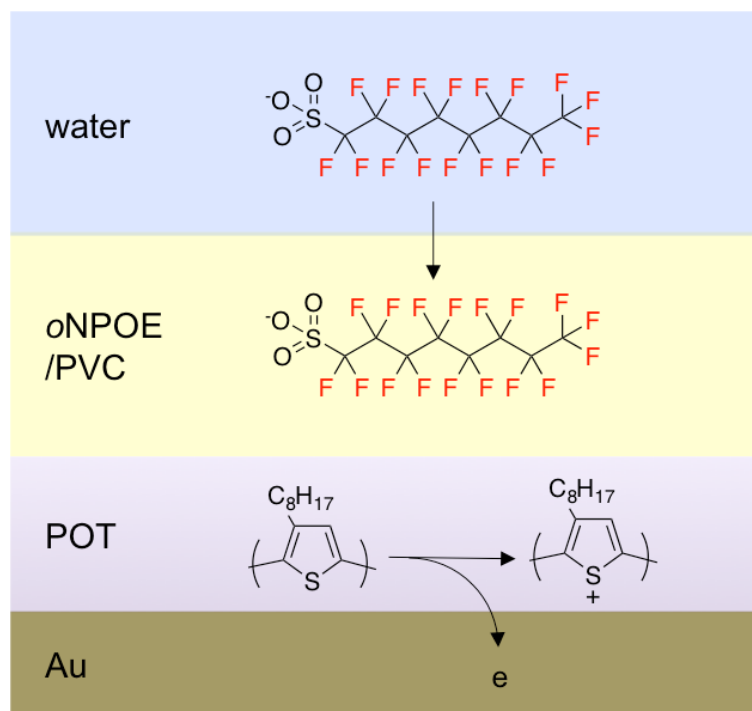


Figure 4-1. Scheme of the voltammetric transfer of PFOS^- from water into the *o*NPOE/PVC membrane coated on a POT-modified Au electrode at positive potentials. Charge transfer between the POT film and the *o*NPOE/PVC membrane is mediated by organic electrolytes in the membrane.

Specifically, we demonstrate that PFOS^- is most lipophilic among the six perfluoroalkyl oxoanions monitored by the US EPA¹⁴ and is detectable by ion-transfer stripping voltammetry at a remarkably low concentration of 50 pM (0.025 $\mu\text{g/L}$) in the presence of 1 mM aqueous supporting electrolytes, i.e., a seven orders of magnitude higher concentration. Significantly, this detection limit is below the minimum reporting level of PFOS^- set by the US EPA¹⁴ and is lower than achieved by any electrochemical sensor for perfluoroalkyl oxoanions including potentiometry with a fluorous membrane, i.e., 0.86 nM PFOS^- and 0.17 nM PFO^- .²⁹ In comparison,

perfluoroalkyl carboxylates are less lipophilic and more oxidizable at the POT-modified gold electrode, which not only compromises their voltammetric detection but also manifests the limitation of the POT film as a voltammetric ion-to-electron transducer. In addition, we reveal that the fluorophilicity of perfluoroalkyl oxoanions^{29,30} is higher than their lipophilicity, which renders the fluoruous membrane attractive for ultrasensitive ion-transfer voltammetry of the multiple perfluoroalkyl oxoanions.

4.2 EXPERIMENTAL SECTION

4.2.1 Chemicals.

The sodium salt of PFO⁻ was obtained from Strem Chemicals (Newburyport, MA). The potassium salt of PFOS⁻ was obtained from Synquest Laboratories (Alachua, FL). The potassium salts of the other perfluoroalkyl sulfonates, the sodium salts of alkyl sulfonates, perfluoroalkyl carboxylic acids, tetradodecylammonium (TDDA) bromide, PVC (high molecular weight), *o*NPOE (≥99.0 %), 3-octyl thiophene, potassium chloride (≥99.9995 %), Li₂SO₄ (≥99.99 %), and LiClO₄ were purchased from Aldrich (Milwaukee, WI). The perfluoroalkyl carboxylic acids were dissolved in a sample solution and converted to sodium forms by adding a solution of sodium hydroxide. Sodium tetradecanoate was obtained from TCI America (Portland, OR). Potassium tetrakis(pentafluorophenyl)borate (TFAB, Boulder Scientific Company, Mead, CO) was used to prepare TDDATFAB as organic supporting electrolytes.²⁷ All reagents were used as received.

All sample solutions were prepared by using water (18.2 M Ω ·cm and TOC of 3 ppb) from the Milli-Q Advantage A10 system equipped with Q-Gard T2 Pak and Quantum TIX or TEX cartridge (EMD Millipore Corporation, Billerica, MA).²⁶ The sample solutions were prepared by using polypropylene volumetric flasks (VITLAB GmbH, Grossostheim, Germany) and poured into polypropylene beakers (VITLAB GmbH) for electrochemical measurement. We used polypropylene flasks and beakers, which PFOS⁻ and PFO⁻ do not adsorb to in contrast to glass.²⁹ To prevent airborne contamination during storage, the flasks were filled with Milli-Q water and the beakers were immersed in Milli-Q water filled in polypropylene wide-mouth jars (Thermo Scientific, Marietta, OH).

4.2.2 Electrode Modification.

A 5 mm-diameter gold disk attached to a rotating disk electrode tip (Pine Research Instrumentation, Raleigh, NC) was modified with a POT film and then with an *o*NPOE/PVC membrane (Figure 4-1) as follows. To minimize airborne contamination, a bare gold disk was cleaned as reported elsewhere.²⁶ A POT film was electrochemically deposited on gold from an acetonitrile solution containing 0.1 M 3-octylthiophene and 0.03 M TDDATFAB by using a 13 mm-diameter graphite rod (99%, Alfa Aesar, Ward Hill, MA) as a counter electrode and a POT-modified Pt wire as a quasi-reference electrode.³¹ The potential of the gold electrode was controlled by using an electrochemical workstation (CHI 600A, CH Instruments, Austin, TX) and cycled four times at 0.1 V/s between -0.50 V and the switching potentials that yield a current of 0.65 mA for monomer oxidation. The final potential was set to -0.50 V to obtain a neutral POT film in the reduced form. The POT-modified gold electrode was soaked in acetonitrile for 30 min

and then in THF for 1 min to remove the soluble fractions of the POT film. Then, an *o*NPOE/PVC membrane was spin-coated on the POT-modified gold electrode from a solution containing 4 mg PVC, 16 mg *o*NPOE, and 2.2 mg TDDATFAB in 1.0 mL THF. Specifically, a 30 μ L aliquot of the THF solution was dropped from a 50 μ L syringe onto the gold disk rotating at 1500 rpm in a spin-coating device (model SCS-G3-8, Cookson Electronics, Providence, RI). The modified gold disk was removed from the spin coater and dried in air for at least 20 min.

4.2.3 Electrochemical Measurement.

An electrochemical workstation (CHI 900A or CHI 600A, CH Instruments) was used for voltammetric measurement. A Pt-wire counter electrode was employed in the following three-electrode cells

Ag | AgCl | 3 M KCl || 1 mM Li₂SO₄ | *x* M the potassium or sodium salts of perfluoroalkyl or alkyl oxoanions in 1 mM Li₂SO₄ | *o*NPOE/PVC | POT | Au (cell 1)

Ag | AgCl | *y* M the potassium salt of PFOS⁻ in 1 mM Li₂SO₄ and 0.1 mM KCl | *o*NPOE/PVC | POT | Au (cell 2)

The concentrations of each oxoanion are given in the Results and Discussion section. The current carried by an anion from the aqueous phase to the membrane was defined to be negative. All electrochemical experiments were performed at 22 ± 3 °C.

Noticeably, additional setups and procedures were used for different voltammetric measurements. A piece of Teflon tube²⁷ was put on a PVC/POT-modified gold electrode for cyclic voltammetry to define a disk-shaped membrane/water interface with a diameter of 1.5 mm. A PVC/POT-modified gold electrode was rotated during stripping voltammetry by using a modulated speed rotator (Pine Research Instrumentation). For stripping voltammetry of picomolar PFOS⁻, the electrochemical cell and rotator were placed in an Ar-filled polyethylene glove bag (AtmosBag, Aldrich), which was protected from airborne contaminants inside a class 100 vertical laminar flow hood (model AC632LFC, AirClean Systems, Raleigh, NC).²⁶ Inside the bag, Milli-Q water was collected and sample solutions were prepared. An as-prepared electrode was contaminated during preparation and was cleaned in the background Milli-Q water solution of supporting electrolytes (cell 2) by repeating stripping voltammetric measurements until no contaminant response was detected.

4.3 RESULTS AND DISCUSSIONS

4.3.1 Cyclic Voltammetry of Perfluoroalkyl Sulfonates.

The transfer of perfluoroalkyl sulfonates across the interface between water and the *o*NPOE/PVC membrane was studied by cyclic voltammetry (CV) to demonstrate their high lipophilicity in comparison with their alkyl counterparts. Specifically, PFOS⁻, perfluorohexane sulfonate (PFHS⁻), and perfluorobutane sulfonate (PFBS⁻) were studied as the perfluoroalkyl

sulfonates monitored by the US EPA¹⁴ and were compared with octane sulfonate (OS⁻). Their voltammograms were observed at different potentials in the order of PFOS⁻ < PFHS⁻ < PFBS⁻ < OS⁻ (Figure 4-2), where the potentials were calibrated against the formal potential of ClO₄⁻.²⁶ This order corresponds to the reversed order of lipophilicity, thereby confirming that a perfluoroalkyl sulfonate with a longer chain is more lipophilic. In addition, a comparison of PFOS⁻ with OS⁻ indicates that a perfluoroalkyl sulfonate is much more lipophilic than the alkyl sulfonate with the same chain length. This result is ascribed to the electron-withdrawing effect of a perfluoroalkyl group, which reduces the electron density of the adjacent sulfonate group to be more weakly hydrated.¹⁸ By contrast, the shape of CVs for the different sulfonates was very similar. A peak-shaped wave on anodic potential sweep showed a diffusional tail, which corresponds to the planar diffusion of a sulfonate from the bulk aqueous solution to the membrane/water interface. A diffusional tail was not seen for the reverse wave, where current quickly dropped to zero because the sulfonate was exhaustively stripped from the thin membrane into the aqueous phase. In addition, the background-subtracted CVs were integrated to ensure that charges due to transferred sulfonates return to nearly zero at the end of a potential cycle (data not shown). This exhaustive stripping is advantageous for the ultrasensitive voltammetric detection of picomolar PFOS⁻ (see below).

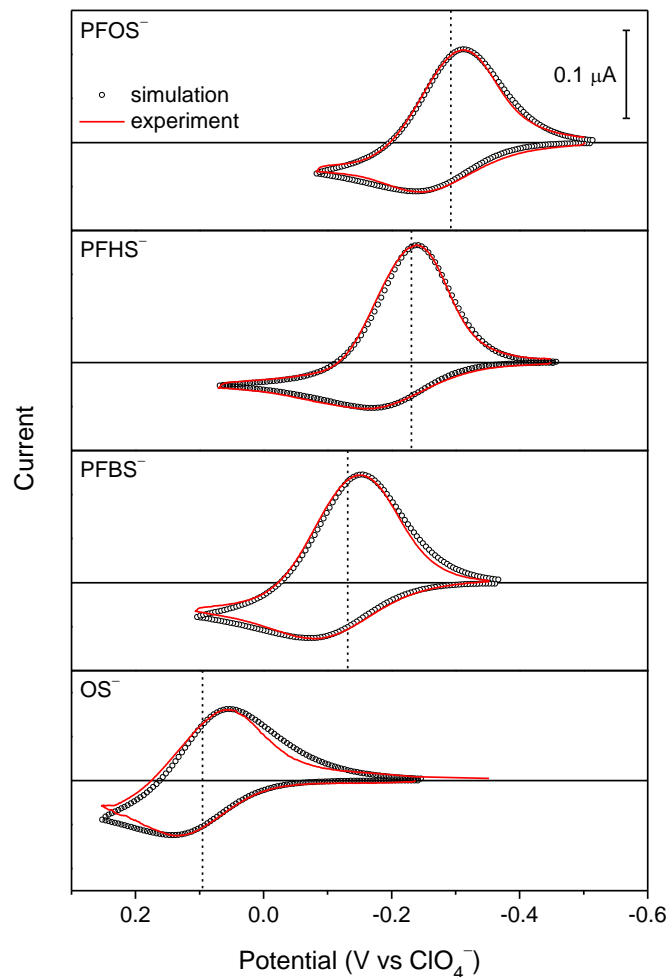


Figure 4-2. Background-subtracted CVs (red lines) of 20 μM perfluorooctane sulfonate, perfluorohexane sulfonate, perfluorobutane sulfonate, and octane sulfonate (from the top) in cell 1. The potential was applied to the gold electrode, swept at 0.1 V/s, and defined against the formal potential of perchlorate. Circles represent the CVs simulated by using the parameters listed in Table 4-1 (Supporting Information). Dotted lines correspond to the formal potentials of the sulfonates.

The experimental CVs were analyzed quantitatively to determine formal ion-transfer potentials, which are related to formal partition coefficients as a measure of ion lipophilicity (eq 1). Finite element analysis was required to simulate ion diffusion in the thin layer membrane.²⁸ Good fits were obtained for all experimental CVs with the CVs simulated for the reversible transfer of the sulfonates, which is fast and controlled by their diffusion. A characteristically high reverse peak current was fitted by considering a membrane thickness of ~1 μm (Table 4-1, Supporting Information), which is thin enough for the exhaustive stripping of membranous sulfonates. Noticeably, the good fits of the experimental CVs with the simulated CVs required the correction of the potential at the gold electrode because the applied potential polarized not only the PVC membrane/water interface but also the PVC/POT/gold junction for voltammetric ion-to-electron transduction.²⁷ Empirically, the phase boundary potential at the PVC membrane/water interface, $D_w^m f$, is related to the applied potential, E , as given by²⁸ (see Supporting Information)

$$D_w^m f - D_w^m f_{\text{ClO}_4}^{\theta'} = (E - E_{\text{ClO}_4}^{0'}) \frac{\partial D_w^m f}{\partial E} \quad (2)$$

where the applied potential was calibrated against the formal potential of ClO_4^- transfer so that $D_w^m f = D_w^m f_{\text{ClO}_4}^{\theta'}$ when $E = E_{\text{ClO}_4}^{0'}$.²⁶ The best fits were obtained by assuming that 60–69% of a change in the applied potential was used to change the phase boundary potential across the membrane/water interface, i.e., $\partial D_w^m f / \partial E = 0.60 - 0.69$ (Table 4-1, Supporting Information), thereby broadening the resultant CVs and also enhancing their electrochemical reversibility.

4.3.2 Lipophilicity of Perfluoroalkyl Sulfonates: Fragmental Analysis.

The formal potentials of perfluoroalkyl and alkyl sulfonates were quantitatively compared by employing fragmental analysis²⁰ to demonstrate that the 10^4 times higher lipophilicity of perfluoroalkyl sulfonates is exclusively ascribed to the higher lipophilicity of their sulfonate groups. Specifically, the formal potential of a sulfonate, i , against that of perchlorate, $D_w^m f_i^{\theta'} - D_w^m f_{ClO_4}^{\theta'}$, was obtained by using eq 2 with the parameters determined from the numerical analysis of CVs for perfluoroalkyl and alkyl sulfonates and OS^- (for the CVs of decane and dodecane sulfonates, DS^- and DDS^- , respectively, see Figure 4-7, Supporting Information). Figure 4-3 shows plots of $D_w^m f_i^{\theta'} - D_w^m f_{ClO_4}^{\theta'}$ values against the number of the carbon atoms of the sulfonates, n , for the *o*NPOE/PVC membrane. Good linear relationships were obtained for the perfluoroalkyl and alkyl sulfonates to yield

$$D_w^m f_i^{\theta'} - D_w^m f_{ClO_4}^{\theta'} = (n - 1)f(CX_2) + f(CX_3) + f(SO_3^-) \quad (3)$$

where f is a fragmental contribution of each unit and $X = H$ or F . Similar $f(CF_2)$ and $f(CH_2)$ values of -0.029 V and -0.027 V, respectively, were obtained as slopes, thereby indicating that the lipophilicity of a CF_2 group is similar to that of a CH_2 group. By contrast, remarkably different $f(CX_3) + f(SO_3^-)$ values of 0.00 V and 0.24 V were determined for perfluoroalkyl and alkyl sulfonates, respectively, from eq 3 with $n = 1$. This difference of 0.24 V in $D_w^m f_i^{\theta'} - D_w^m f_{ClO_4}^{\theta'}$ values corresponds to a difference in P_i^{0c} values by 4 orders of magnitude in eq 1. The 10^4 times higher

lipophilicity of perfluoroalkyl sulfonates is ascribed to a difference in $f(\text{SO}_3^-)$ values because similar $f(\text{CF}_3)$ and $f(\text{CH}_3)$ values are expected from similar $f(\text{CF}_2)$ and $f(\text{CH}_2)$ values.

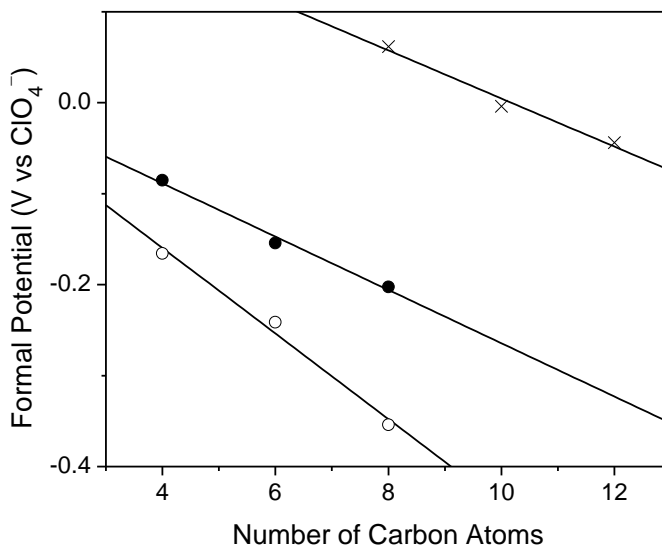


Figure 4-3. Plots of formal potentials versus the number of the carbon atoms of perfluoroalkyl (closed circles) and alkyl (crosses) sulfonates for the *o*NPOE/PVC membrane. The formal potentials of the perfluoroalkyl sulfonates for the fluoruous membrane (open circles) were calculated from selectivity coefficients against perchlorate²⁹ by using eq 4. Solid lines are the best fits with eq 3.

The 10^4 times different lipophilicity of the sulfonate groups adjacent to perfluoroalkyl and alkyl groups is related to the solvation energies of the sulfonate groups not only in water but also in the *o*NPOE/PVC membrane. On one hand, the inductive effect of a perfluoroalkyl group on the electron density of the adjacent sulfonate group raises its hydration energy to enhance its lipophilicity. On the other hand, a lack of a specific interaction of a sulfonate group with *o*NPOE

and PVC results in a relatively small change in the resultant solvation energy of a sulfonate group upon perfluorination. Overall, the difference in the hydration energies of the sulfonate groups dominates a difference in their lipophilicity for the *o*NPOE/PVC membrane. Noticeably, this is not the case for 1-octanol, which can form a hydrogen bond with the oxygen atom of a sulfonate group. The sulfonate group adjacent to a perfluoroalkyl group is less charged and is a weaker hydrogen-bonding acceptor owing to the electron-withdrawing effect to be less favorably solvated in 1-octanol. Subsequently, PFOS⁻ is only 7.1×10 times more lipophilic than OS⁻ in 1-octanol.¹⁸ By contrast, the $f(\text{CF}_2)$ and $f(\text{CH}_2)$ values with the *o*NPOE/PVC membrane are relatively similar to those of -0.036 V with 1-octanol.¹⁸

4.3.3 Lipophilicity and Fluorophilicity of Perfluoroalkyl Sulfonates.

We employed fragmental analysis to find that the lipophilicity of perfluoroalkyl sulfonates is lower than their fluorophilicity. The fluorophilicity was evaluated by using the potentiometric selectivity coefficient determined by Bühlmann and co-workers.^{29,30} With this potentiometric approach, a perfluoroalkyl sulfonate was selectively partitioned between the aqueous phase and the fluorous membrane to obtain a Nernstian response based on a change in the phase boundary potential. Logarithmic potentiometric selectivity coefficients for PFOS⁻, PFHS⁻, and PFBS⁻ against perchlorate, $\log K_{i,\text{ClO}_4}^{\text{pot}}$, were -6.0 , -4.1 , and -2.8 , respectively, when perfluorooligoether, α -(heptafluoropropyl)- ω -(pentafluoroethoxy)-poly[oxy(1,1,2,2,3,3-hexafluoro-1,3-propanediyl)], was used as the fluorous membrane doped with a fluorous anion exchanger.²⁹ We converted the selectivity coefficients to differences between formal potentials as given by³²

$$D_w^m f_i^{\theta'} - D_w^m f_{\text{ClO}_4}^{\theta'} = -\frac{2.303RT}{z_1 F} \log K_{i,\text{ClO}_4}^{\text{pot}} \quad (4)$$

The resultant $D_w^m f_i^{\theta'} - D_w^m f_{\text{ClO}_4}^{\theta'}$ values were used as a measure of fluorophilicity to yield a linear relationship against the number of carbon atoms as expected from eq 3 (Figure 4-3). Importantly, the fluorophilicity of a perfluoroalkyl sulfonate is higher than its lipophilicity for the *o*-NPOE/PVC membrane. More quantitatively, fragmental analysis with eq 3 reveals that this difference originates from a difference in $f(\text{CF}_2)$ values of -0.047 V and -0.029 V for the fluorous and *o*-NPOE/PVC membranes, respectively. This result indicates that a CF_2 group is more favorably solvated in the fluorophilic membrane than in the lipophilic *o*NPOE/PVC membrane. By contrast, both membranes gave an identical $f(\text{CF}_3) + f(\text{SO}_3^-)$ value of -0.029 V. The $f(\text{CF}_3)$ value for the fluorous membrane should be more negative than that for the *o*NPOE/PVC membrane as expected from the more negative $f(\text{CF}_2)$ value for the fluorous membrane. Therefore, the $f(\text{SO}_3^-)$ value for the *o*NPOE/PVC membrane is more negative, thereby indicating that a sulfonate group is more stabilized in the *o*NPOE/PVC membrane although a sulfonate group would be strongly ion-paired with an anion exchanger in the fluorous membrane.³³

4.3.4 Stripping Voltammetry of PFOS⁻.

The remarkably high lipophilicity of PFOS⁻ is highly advantageous for its ultrasensitive detection by stripping voltammetry because a more lipophilic ion can be preconcentrated at a higher concentration in the thin double-polymer membrane on the gold electrode to yield a lower detection limit.²⁴ In fact, this study shows that PFOS⁻ is most lipophilic among the perfluoroalkyl

sulfonates and carboxylates monitored by the US EPA¹⁴ (see below for the lipophilicity of the carboxylates). In the preconcentration step, an aqueous analyte ion is potentiostatically transferred into the confined volume of the solid-supported membrane, which is eventually saturated with the analyte ion.²⁸ The resultant equilibrium concentration of the analyte ion in the membrane, c_m , is given by the Nernst equation as

$$Y = \frac{c_m}{c_w} = \exp \left[- \frac{z_i F (D_w^m f_p - D_w^m f_i^{\theta'})}{RT} \right] \quad (5)$$

where Y is a preconcentration factor, c_w is the bulk aqueous concentration of the analyte ion, and $D_w^m f_p$ is the phase boundary potential during preconcentration. Eq 5 predicts that, with a given $D_w^m f_p$ value, a preconcentration factor is higher for a more lipophilic anion with a more negative $D_w^m f_i^{\theta'}$ value.

We performed stripping voltammetry of 10 nM PFOS⁻ at preconcentration times of 0.5–40 minutes (Figure 4-4A) to determine a high preconcentration factor, Y , of 2.2×10^5 . The electrode was rotated at 2000 rpm to achieve steady states, which facilitate data analysis. The voltammetric peak grew at a longer preconcentration time, which increased the concentration of PFOS⁻ in the membrane. More quantitatively, a stripping voltammogram was integrated to obtain a charge, $Q(t_p)$, at a preconcentration time, t_p . This total charge is a sum of the charge due to the stripping of PFOS⁻ preconcentrated in the membrane and the charge due to background processes during the stripping step, Q_{bg} , which is mainly charging of the membrane/water interface. In theory, $Q(t_p)$ is given by²⁸

$$Q(t_p) = Q_{\text{eq}} \left[1 - \exp\left(-\frac{i_l t_p}{Q_{\text{eq}}}\right) \right] + Q_{\text{bg}} \quad (6)$$

where Q_{eq} is the equilibrium charge due to the exhaustive stripping of PFOS⁻ from a saturated membrane and i_l is the limiting current during the preconcentration step under the rotating-electrode condition. The best fit of eq 6 with the experimental plot (Figure 4-4B) gives $i_l = 1.7$ nA, $Q_{\text{eq}} = 4.1$ μC , and $Q_{\text{bg}} = 1.7$ μC . This limiting current is immeasurably small by CV and is given by the Levich equation as³⁴

$$i_l = 0.62z_i F A D_w^{2/3} \omega^{1/2} \nu^{-1/6} c_w \quad (7)$$

where D_w is the diffusion coefficient of a target ion in the aqueous phase, ω is the rotation speed and ν is the viscosity of the aqueous electrolyte solution. Eq 7 with $A = 0.196$ cm^2 , $D_w = 5.7 \times 10^{-6}$ cm^2/s (Table 4-1, Supporting Information), and $\nu = 0.010$ cm^2/s gives $c_w = 10.8$ nM, which agrees with the spiked PFOS⁻ concentration of 10 nM. In addition, a preconcentration factor, Y , can be calculated from a Q_{eq} value as given by²⁸

$$Q_{\text{eq}} = z_i F Y V_m c_w \quad (8)$$

where V_m is the membrane volume. A Y value of 2.2×10^5 is obtained from the Q_{eq} value by using eq 8 with $V_m = 2.0 \times 10^{-8}$ L for a 1 μm -thick and 5 mm-diameter membrane. This large

preconcentration factor corresponds to a large overpotential, $D_w^m f_p - D_w^m f_{PFOS}^{\theta'}$, of 0.32 V in eq 5.

This large overpotential can be applied without the limitation of the potential window because of

the high lipophilicity of $PFOS^-$, i.e., very negative $D_w^m f_{PFOS}^{\theta'}$.

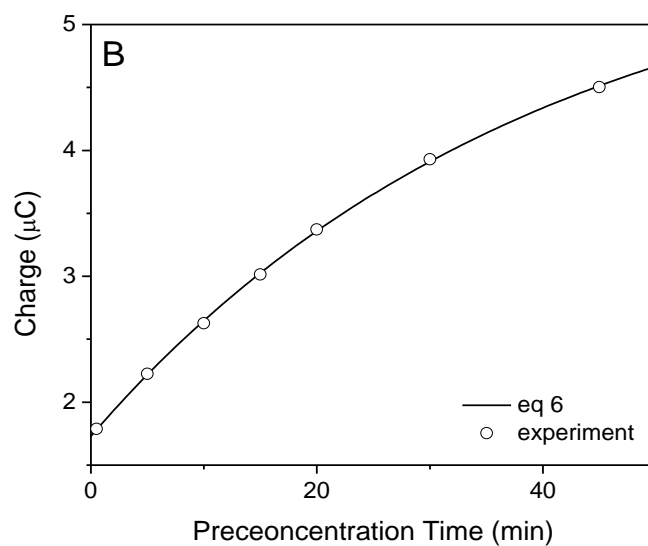
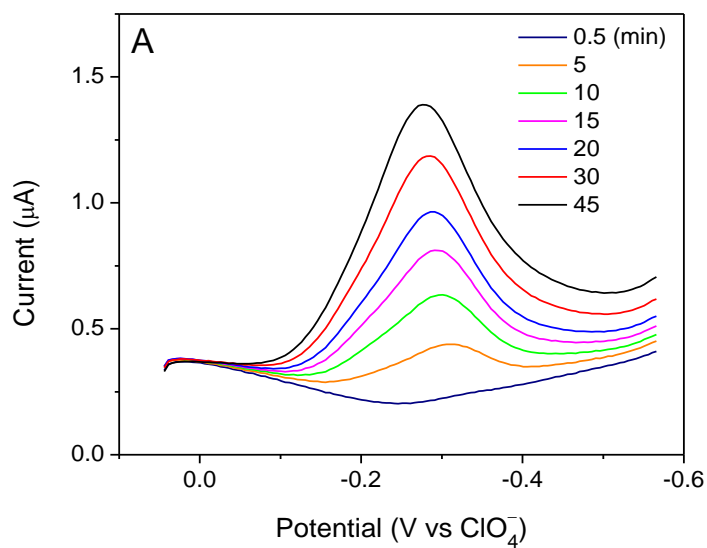


Figure 4-4. (A) Stripping voltammograms of 10 nM PFOS⁻ (cell 2) at different preconcentration times. The potential was applied to the gold electrode, swept at 0.1 V/s, and defined against the formal potential of perchlorate. (B) Charge under the stripping voltammograms (circles) and the best fit with eq 6 (solid line).

4.3.5 Picomolar Detection Limit for PFOS⁻.

Stripping voltammetric responses to PFOS⁻ were measured after 30 min preconcentration to yield a detection limit of 50 pM (Figure 4-5A). The electrode was rotated at 2000 rpm to enhance the mass transport of PFOS⁻ from water to the membrane/water interface. The background-subtracted stripping voltammograms (Figure 4-8, Supporting Information) show the clearer peak currents that linearly vary with the PFOS⁻ concentration in a range of 0–1 nM (Figure 4-5B). Remarkably, a detection limit of 50 pM (0.025 µg/L) for PFOS⁻ is much lower than that of 0.86 nM by potentiometry with the fluorinated membrane²⁹ and is lower than the minimum reporting level of 0.04 µg/L in drinking water set by the US EPA.¹⁴ Moreover, the slope of the calibration plot was assessed quantitatively to find its consistency with theory. A peak current response, i_p , based on the exhaustive and reversible transfer of an analyte ion from a thin double-polymer membrane is given by³⁵

$$i_p = \frac{z_i^2 F^2 \nu V_m c_m(t_p)}{4RT} \quad (9)$$

with

$$Y(t_p) = \frac{c_m(t_p)}{c_w} = Y \left[1 - \exp\left(-\frac{i_l}{Q_{eq}} t_p\right) \right] \quad (10)$$

where ν is the potential sweep rate during the stripping process, $c_m(t_p)$ and $Y(t_p)$ are the membrane ion concentration and preconcentration factor at the preconcentration time of t_p , and i_l/Q_{eq} is independent of c_w (see eqs 7 and 8) and is given by the aforementioned i_l and Q_{eq} values. Noticeably, the potential sweep rate in eq 9 corresponds to a change in the phase boundary potential across the membrane/water interface, which is slower than the actual potential sweep rate of 0.1 V/s by a factor of $\partial D_w^m f / \partial E$ (≈ -0.65 ; Table 4-1, Supporting Information). Subsequently, eq 9 gives a slope of 1.26×10^2 (ampere/M) for a plot of i_p versus c_w for PFOS⁻. This slope is close to a value of $(1.01 \pm 0.08) \times 10^2$ (ampere/M) as determined from three calibration plots including the plot in Figure 4-5B.

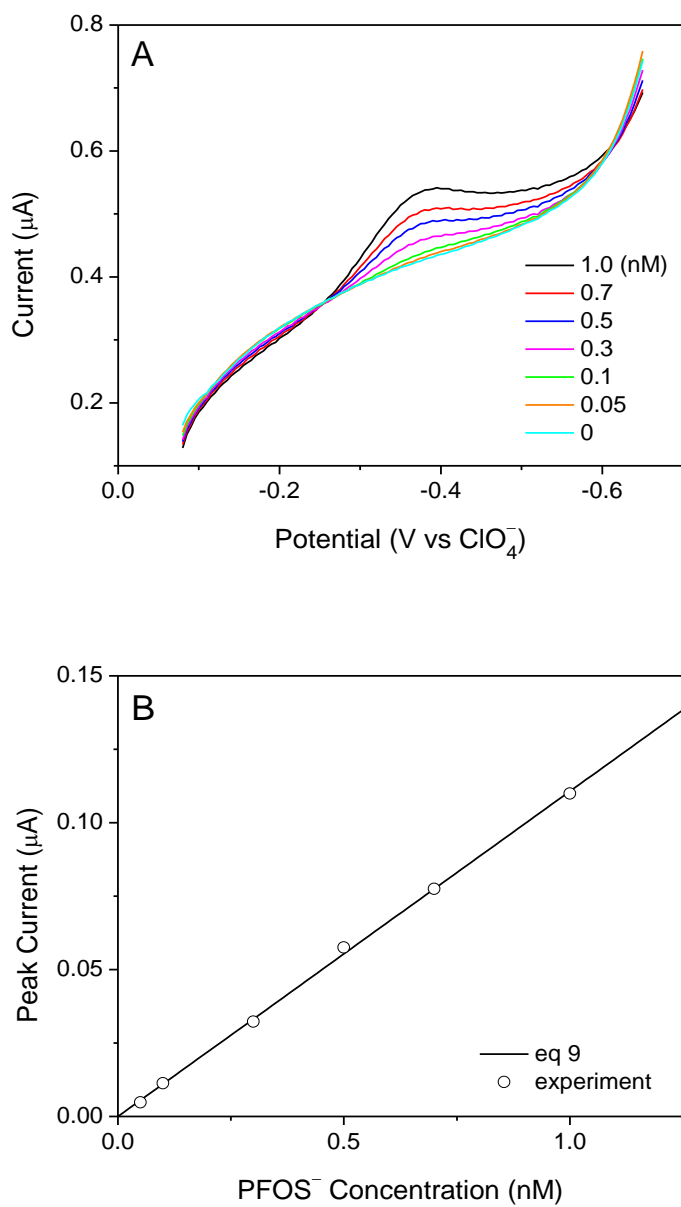


Figure 4-5. (A) Stripping voltammograms of 0–1 nM PFOS^- (cell 2) after 30 min pre-concentration. The potential was applied to the gold electrode, swept at 0.1 V/s, and defined against the formal potential of perchlorate. (B) A plot of background-subtracted peak current versus PFOS^- concentration (circles) and best fit with eq 9 (solid line).

Importantly, the contamination of background electrolyte solutions with a lipophilic anion had to be prevented to enable the detection of picomolar PFOS⁻ by stripping voltammetry. The peak potential of the contaminant anion was more positive than that of PFOS⁻ only by ~0.1 V (Figure 4-9, Supporting Information), thereby indicating the relatively high lipophilicity of the contaminant anion. Moreover, the contaminant responses were much higher than the responses to 0.1–1 nM PFOS⁻, which were seriously distorted. The contaminant responses are not due to the transfer of a cation from the membrane to water because these responses were not seen when extra care was taken to protect sample solutions from airborne contaminants (Figure 4-5A). Specifically, the electrochemical cell was placed in the Ar-filled polyethylene glove bag, which was accommodated in the class 100 vertical laminar flow hood as reported elsewhere.^{25,26} In addition, we extensively cleaned PVC/POT-modified electrodes, which were seriously contaminated during their preparation. A contaminant response was readily detected by stripping voltammetry upon the first immersion of a newly prepared electrode in the background aqueous solution. Eventually, no contaminant response was detectable (Figure 4-5A) after the electrode was washed in two background solutions during stripping voltammetry with 5 minute preconcentration.

4.3.6 Cyclic Voltammetry of Perfluoroalkyl Carboxylates.

The transfer of perfluoroalkyl carboxylates at the *o*NPOE/PVC membrane was studied by CV (Figure 4-6) to demonstrate their low lipophilicity and high oxidizability in comparison with perfluoroalkyl sulfonates. Initially, we investigated PFO⁻, perfluorohexanoate (PFH⁻), and perfluorobutanoate (PFB⁻), which have the same number of carbon atoms as the perfluoroalkyl

sulfonates studied in this work (see above). A perfluoroalkyl carboxylate with a longer chain is expected to be more lipophilic and was indeed transferred at less positive potentials, thereby yielding the order of lipophilicity as $\text{PFO}^- > \text{PFH}^- > \text{PFB}^-$. These perfluoroalkyl carboxylates, however, are much less lipophilic than the perfluoroalkyl sulfonates with the same number of carbon atoms, which possess much less positive formal potentials (dotted lines in Figure 4-6). Remarkably, PFOS^- is even more lipophilic than perfluorodecanoate (PFD^-) and perfluorododecanoate (PFDD^-) (Figure 4-9, Supporting Information). This result indicates that PFOS^- is more lipophilic than any perfluoroalkyl carboxylate monitored by the US EPA (i.e., PFO^- , perfluoroheptanoate, and perfluorononanoate).¹⁴ The lower lipophilicity of perfluoroalkyl carboxylates is due to the intrinsically stronger hydration of a carboxylate group,³⁶ which is smaller and more basic than a sulfonate group. Nevertheless, the least lipophilic perfluoroalkyl carboxylate, PFB^- , is as lipophilic as tetradecanoate (TD^-) as shown in Figure 4-6, where both carboxylates were transferred at similar potentials. The similar lipophilicity is due to the inductive effect of the perfluoroalkyl group on reducing the electron density of the adjacent carboxylate group. Noticeably, a lack of reverse peak for TD^- is due to its oxidative consumption at the POT-modified gold electrode as discussed in the following paragraph.

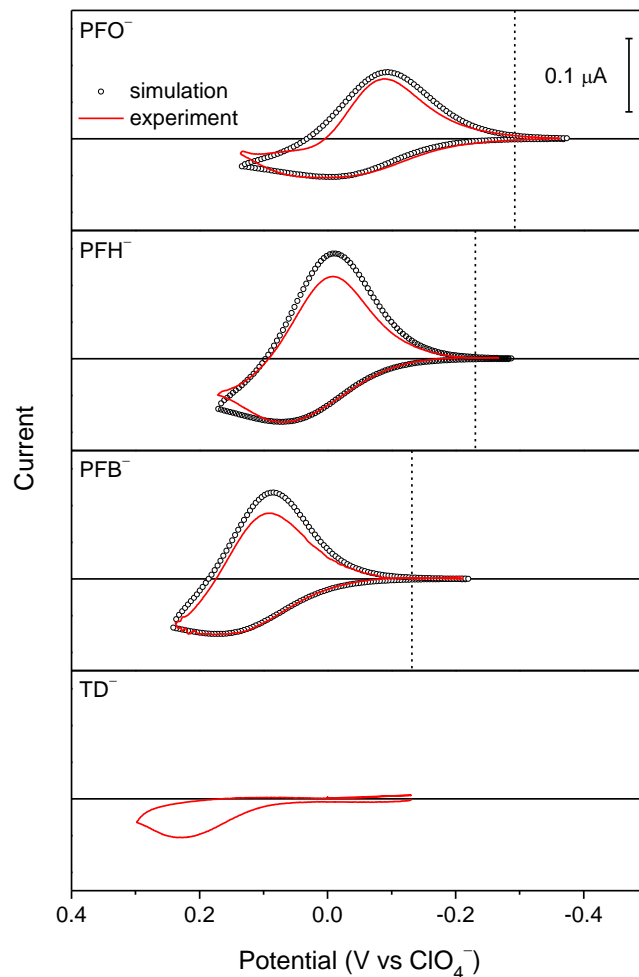


Figure 4-6. Background-subtracted CVs (red lines) of 20 μM perfluorooctanoate, perfluorohexanoate, perfluorobutanoate, and 10 μM tetradecanoate (from the top) in cell 1. The potential was applied to the gold electrode, swept at 0.1 V/s, and defined against the formal potential of perchlorate. Circles represent the CVs simulated by using the parameters listed in Table 4-1 (Supporting Information). Dotted lines correspond to the formal potentials of the sulfonates with the same number of carbon atoms.

Unfortunately, the lipophilicity of the perfluoroalkyl carboxylates can not be determined quantitatively owing to their oxidative loss at the POT-modified gold electrode, which is seen as the lower cathodic peaks of the experimental CVs than those of the simulated CVs (Figure 4-6). Accordingly, the charge under the experimental CVs does not return to zero upon the completion of a potential cycle (data not shown) although the reverse peak does not have a diffusional tail. This result confirms that the perfluoroalkyl carboxylates are not exhaustively stripped from the membrane during the reverse potential sweep. We propose that the loss of the perfluoroalkyl carboxylates in the *o*NPOE/PVC membrane is due to their oxidative decarboxylation based on the Kolbe reaction³⁷ at the POT-modified gold electrode as given by



This reaction not only consumes the carboxylates but also does not generate any anionic product, thereby decreasing the cathodic response during the reverse potential sweep. We confirmed the oxidation of PFO at the PVC/POT/gold junction by cyclic voltammetry with non-polarizable PVC/water interface (see Figure 4-11). Moreover a reverse peak was not seen for TD⁻ (Figure 4-6), which is more readily oxidizable. The lower oxidizability of perfluoroalkyl carboxylates is ascribed to the inductive effect and is supported further by the fact that similarly positive potentials were applied to the gold electrode for PFB⁻ and TD⁻ to observe a reverse peak only for the former. Noticeably, the oxidation of perfluoroalkyl carboxylates will be preventable by employing the conducting polymer film that is oxidized at less positive potentials than the POT film for voltammetric ion-to-electron transduction.

4.3.7 Voltammetry versus Potentiometry with the *o*NPOE/PVC Membrane.

Interestingly, this study revealed that the voltammetric responses based on the interfacial transfer of PFOS⁻ and PFO⁻ can be obtained by using the *o*NPOE/PVC membrane, which gave no potentiometric response to either species.³⁰ This voltammetric result strongly suggests that no potentiometric response of the *o*NPOE/PVC membrane to highly lipophilic PFO⁻ and PFOS⁻ is due to the insufficient solubility of these fluorophilic anions in the lipophilic membrane doped with 5% (w/w) tridodecylmethylammonium chloride. Detrimentally, all chloride ions must be replaced with PFO⁻ or PFOS⁻, i.e., conditioning,²⁹ to obtain a Nernstian potentiometric response to the analyte ion. Advantageously, ion-transfer voltammetry needs no conditioning and required a much lower PFOS⁻ concentration of <2.2 mM ($=c_m$ from eq 5 with $Y = 2.2 \times 10^5$ and $c_w = 10$ nM) in the membrane even when the highest current response of ~1.5 μ A in this study was obtained (Figure 4-4A). On the other hand, no extraction of PFDD⁻ into the *o*NPOE/PVC membrane was observed voltammetrically (Figure 4-10, Supporting Information), thereby indicating that this extremely fluorophilic anion was not detectably soluble in the lipophilic membrane. Importantly, the CV of PFDD⁻ showed its interfacial adsorption, which would not be detectable by potentiometry. This result exemplifies the power of voltammetry in diagnostic strength to understand ion-transfer mechanism.³⁸ In fact, adsorption was also observed for PFO⁻ (around 0.1 V in Figure 4-6) while both extraction and adsorption were observed for PFD⁻ (Figure 4-10, Supporting Information) in addition to DS⁻ and DDS⁻ (Figure 4-7, Supporting Information). As expected,³⁹ the adsorption peak currents were proportional to potential sweep rates (data not shown).

4.4 CONCLUSIONS

In this work, we demonstrated the ultrasensitive voltammetric detection of highly lipophilic perfluoroalkyl oxoanions at a picomolar level by using the thin *o*NPOE/PVC membrane supported by the POT-modified gold electrode. Specifically, ion-transfer stripping voltammetry enabled the detection of down to 50 pM PFOS⁻, which is most lipophilic among the six perfluoroalkyl oxoanions monitored by the US EPA.¹⁴ This detection limit is lower than the minimum reporting level of PFOS⁻ in drinking water set by the US EPA¹⁴ and is the lowest achieved electrochemically for any perfluoroalkyl oxoanion so far.^{13,29} The high lipophilicity of PFOS⁻ contributed not only to the unprecedentedly low detection limit but also to its highly selective detection in the presence of 1 mM aqueous electrolytes.

This work also indicates that the fluoruous membrane^{29,30} is highly attractive for the ultrasensitive voltammetry of the multiple perfluoroalkyl oxoanions monitored by the US EPA¹⁴ because of the high fluorophilicity of a perfluoroalkyl group in comparison to its lipophilicity as discovered in this study. Our theory (eq 5) predicts that stripping voltammetry with the fluoruous membrane will give a lower detection limit for a perfluoroalkyl oxoanion, which can be potentiostatically accumulated at a higher concentration in the fluoruous membrane. Moreover, the multiple perfluoroalkyl oxoanions will be simultaneously detectable by using the single voltammetric electrode based on the fluoruous membrane owing to larger differences in formal potentials among the oxoanions with different chain lengths. On the other hand, the high resistivity of the fluoruous membrane due to the strong ion pairing of supporting electrolytes³³ must be lowered for its voltammetric applications to avoid a significant ohmic potential drop across the membrane.

ACKNOWLEDGEMENT

This work was supported by the National Science Foundation (CHE-1213452).

4.5 SUPPORTING INFORMATION

4.5.1 Finite Element Simulation.

This supporting information contains finite element simulation for CVs, experimental CVs of alkyl sulfonates, stripping voltammograms of PFOS⁻, experimental CVs of perfluoroalkyl carboxylates, and CV of PFO⁻ oxidation.

Experimental CVs in Figures 4-2 and 4-6 were fitted with the CVs simulated by using the finite element method as reported elsewhere.^{S-1} In this simulation, we assumed that the potential applied to the gold electrode, E , was distributed to the PVC membrane/water interface to drive facilitated ion transfer and also to the PVC/POT/gold junction to mediate voltammetric ion-to-electron transduction, thereby yielding^{S-1}

$$E = D_w^m f + D_m^{Au} f - E_{ref} \quad (S-1)$$

where $D_m^{Au} f$ is the potential drop across the PVC/POT/gold junction, and E_{ref} is the reference electrode potential. Empirically, $D_w^m f$ and $D_m^{Au} f$ varied linearly with E during a potential sweep to yield a constant $\partial D_w^m f / \partial E$ value in eq 2. The parameters used for simulated CVs in Figures 4-

2 and 4-6 are listed in Table 4-1, where l is the membrane thickness. The $E_i^{0c} - E_{\text{ClO}_4}^{0c}$ and $\partial D_w^m f / \partial E$ values were used to calculate $D f_i^{\theta'} - D f_{\text{ClO}_4}^{\theta'}$ values from eq 2 with $E = E_i^{0c}$ and $D_w^m f = D_w^m f_i^{\theta'}$.

Table 4-1. Parameters Used for Simulated CVs in Figures 4-2 and 4-6.

ion i	$E_i^{0c} - E_{\text{ClO}_4}^{0c} / \text{V}$	$\partial D_w^m f / \partial E / \text{V}$	$l / \mu\text{m}$	$D_w / 10^{-5} \text{ cm}^2/\text{s}$
PFOS ⁻	-0.292	0.65	0.85	0.57
PFHS ⁻	-0.231	0.69	0.61	0.48
PFBS ⁻	-0.132	0.60	1.0	0.80
OS ⁻	0.095	0.65	1.8	1.1
PFO ⁻	-0.071	0.55	1.0	0.93
PFH ⁻	0.003	0.59	0.97	1.2
PFB ⁻	0.086	0.56	0.67	1.1

4.5.2 Cyclic Voltammetry of Alkyl Sulfonates.

Dodecyl and decyl sulfonates (DDS⁻ and DS⁻, respectively) were studied by CV (Figure 4-7) to determine their formal potentials. The extraction of the sulfonates into the membrane gave the first anodic wave, which was paired with the larger cathodic peak based on their exhaustive stripping. The numerical analysis of the extraction waves, however, was complicated by a pair of the surface waves based on the adsorption of the sulfonates at the *o*NPOE/PVC membrane as observed around

0.15 V. Therefore, a formal potential was estimated from a reverse peak potential by assuming that their difference is identical to that of OS^- (Figure 4-2).

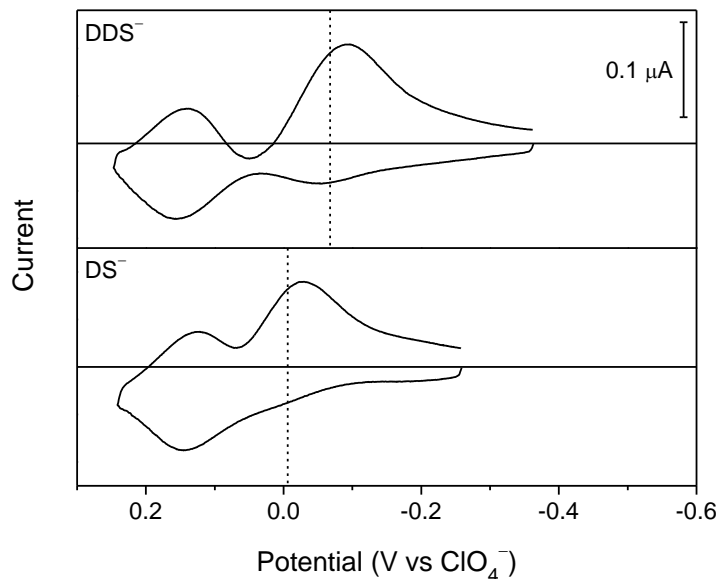


Figure 4-7. Background-subtracted CVs (red lines) of 20 μM dodecyl and decyl sulfonates (from the top) in cell 1. The potential was applied to the gold electrode, swept at 0.1 V/s, and defined against the formal potential of perchlorate. Dotted lines correspond to the formal potentials of the sulfonates.

4.5.3 Background-Subtracted Stripping Voltammograms of Picomolar PFOS⁻.

Peak-shaped responses to 0.05–1 nM PFOS⁻ were more clearly seen after background subtraction (Figure 4-8). The peak currents of the background-subtracted stripping voltammograms were linear to the PFOS⁻ concentrations (Figure 4-5B).

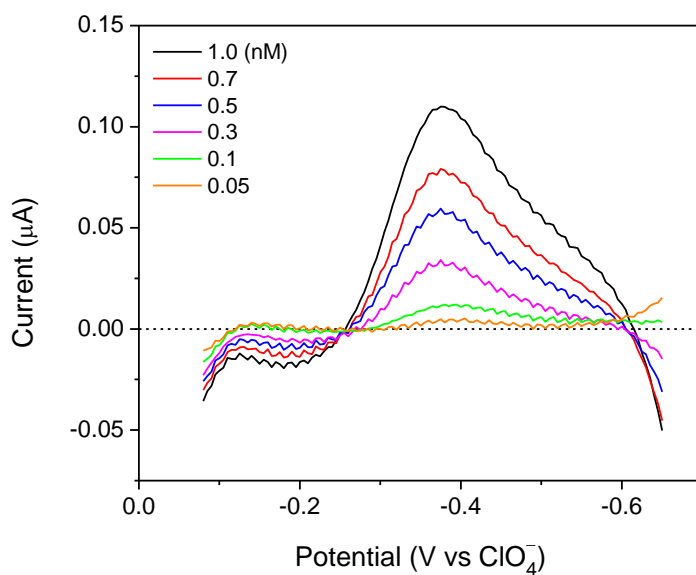


Figure 4-8. Background-subtracted stripping voltammograms of 0.05–1 nM PFOS⁻ (cell 2) after 30 min preconcentration. The potential was applied to the gold electrode, swept at 0.1 V/s, and defined against the formal potential of perchlorate. The dotted line represents zero current.

4.5.4 Stripping Voltammetric Responses to a Contaminant Anion.

Significant stripping voltammetric responses to a contaminant anion were observed near PFOS⁻ responses (Figure 4-9) when the electrochemical cell (cell 2) was exposed to air during the measurements. The contaminant responses were not seen when the electrochemical cell was placed in the Ar-filled bag (Figure 4-5A) and the electrode was sufficiently cleaned.

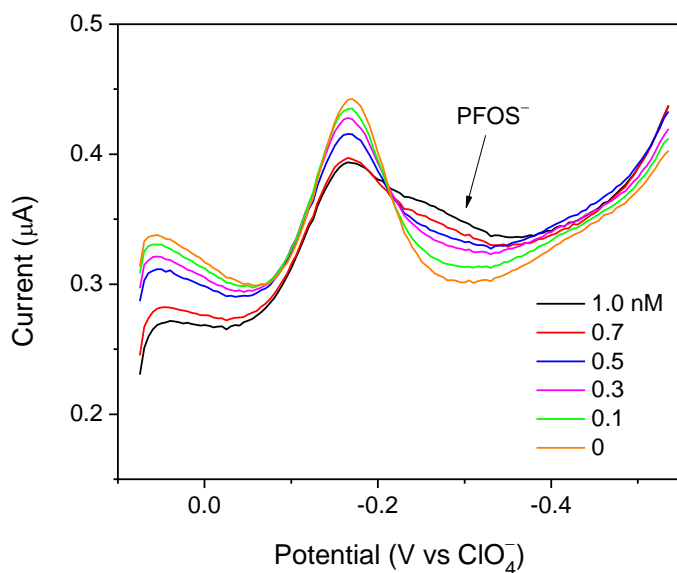


Figure 4-9. Stripping voltammograms of 0–1 nM PFOS⁻ (cell 2) after 30 min preconcentration in the presence of a contaminant anion in the sample solutions. The potential was applied to the gold electrode, swept at 0.1 V/s, and defined against the formal potential of perchlorate.

4.5.5 Lipophilicity of Perfluoroalkyl Carboxylates.

The interfacial behaviors of perfluorododecanoate (PFDD⁻) and perfluorodecanoate (PFD⁻) were studied by CV to compare their lipophilicity with the lipophilicity of PFOS⁻ (Figure 4-10). All peak potentials of PFDD⁻ and PFD⁻ are more positive than the formal potential of PFOS⁻ (dotted line), which is more lipophilic. Interestingly, PFDD⁻ gave two pairs of surface waves based on adsorption and desorption at the membrane/water interface, thereby indicating that PFDD⁻ can not be extracted into the oNPOE/PVC membrane. By contrast, the extraction of PFD⁻ into the membrane gave the anodic wave paired with the much higher cathodic wave based on exhaustive stripping while a pair of surface waves was observed around 0.05 V.

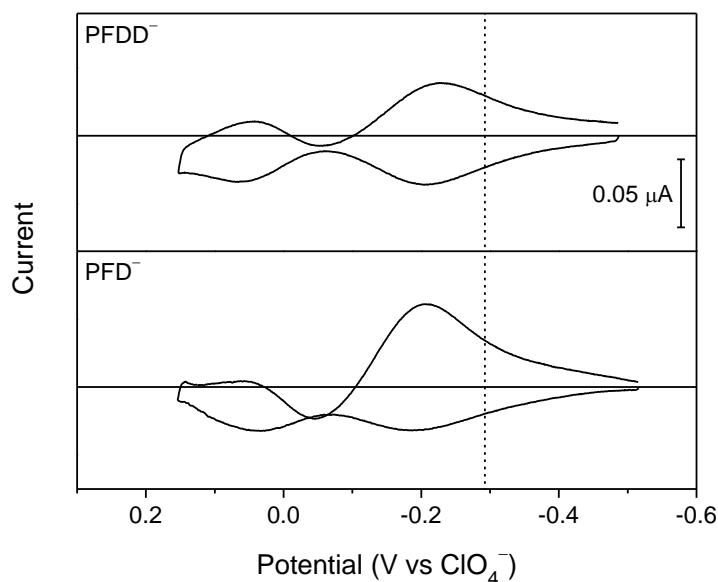


Figure 4-10. Background-subtracted CVs (red lines) of 20 μM perfluorododecanoate and perfluorodecanoate (from the top) in cell 1. The potential was applied to the gold electrode, swept

at 0.1 V/s, and defined against the formal potential of perchlorate. The dotted line corresponds to the formal potential of PFO⁻.

4.5.6 Oxidation of PFO⁻ at the PVC/POT/Gold Junction.

We employed non-polarizable PVC/water interfaces^{S-2} to voltammetrically study the oxidation of PFO⁻ at the PVC/POT/gold junction. In this experiment, an *o*NPOE/PVC/POT-modified electrode was immersed in the solution of 8 mM tetrabutylammonium (TBA⁺) perchlorate, which is partitioned into the PVC membrane to fix the phase boundary potential across the membrane/water interface as given by^{S-3}

$$D_w^m f = \frac{D_w^m f_{\text{PFO}}^{\theta'} + D_w^m f_{\text{TBA}}^{\theta'}}{2} \quad (\text{S-2})$$

By contrast, the PVC/POT/gold junction can be polarizable externally to yield a CV controlled by the oxidation and reduction of the POT film (black line Figure 4-11). This well-defined CV resembles that of the POT film in acetonitrile.^{S-2} By contrast, a distorted CV (red line) was obtained when 1 mM TBA⁺ and PFO⁻ were added to the TBAClO₄ solution as chloride and sodium salts, respectively, to partition TBAPFO into the PVC membrane. The distorted CV indicates the oxidation of PFO⁻ at the PVC/POT/gold junction.

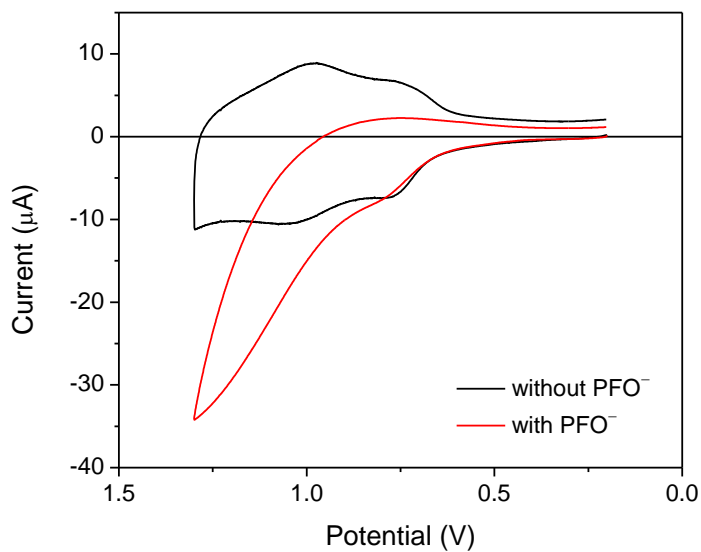


Figure 4-11. CVs of a POT film with a PVC membrane/water interface non-polarized by partitioning of TBAClO₄. The potential was applied to the gold electrode against a Ag/AgCl reference electrode in 3 M KCl. Potential sweep rate, 0.1 V/s.

4.5.7 REFERENCES

- (S-1) Kim, Y.; Amemiya, S. *Anal. Chem.* **2008**, *80*, 6056.
- (S-2) Guo, J.; Amemiya, S. *Anal. Chem.* **2006**, *78*, 6893.
- (S-3) Samec, Z. *Pure Appl. Chem.* **2004**, *76*, 2147

4.6 REFERENCES

- (1) Houde, M.; De Silva, A. O.; Muir, D. C. G.; Letcher, R. J. *Environ. Sci. Technol.* **2011**, *45*, 7962.
- (2) Vecitis, C. D.; Park, H.; Cheng, J.; Mader, B. T.; Hoffmann, M. R. *Front. Environ. Sci. China* **2009**, *3*, 129.
- (3) Zareitalabad, P.; Siemens, J.; Hamer, M.; Amelung, W. *Chemosphere* **2013**, *91*, 725.
- (4) Chang, E. T.; Adami, H. O.; Boffetta, P.; Cole, P.; Starr, T. B.; Mandel, J. S. *Crit. Rev. Toxicol.* **2014**, *44*, 1.
- (5) Carter, K. E.; Farrell, J. *Environ. Sci. Technol.* **2008**, *42*, 6111.
- (6) Ochiai, T.; Iizuka, Y.; Nakata, K.; Murakami, T.; Tryk, D. A.; Fujishima, A.; Koide, Y.; Morito, Y. *Diamond Relat. Mater.* **2011**, *20*, 64.
- (7) Xiao, H.; Lv, B.; Zhao, G.; Wang, Y.; Li, M; Li, D. *J. Phys. Chem. A* **2011**, *115*, 13836.
- (8) Zhuo, Q. F.; Deng, S; Yang, B.; Huang, J.; Wang, B.; Zhang, T.; Yu, G. *Electrochim. Acta* **2012**, *77*, 17.
- (9) Zhuo, Q; Deng, S.; Yang, B.; Huang, J.; Yu, G. *Environ. Sci. Technol.* **2011**, *45*, 2973.
- (10) Niu, J.; Lin, H.; Xu, J.; Wu, H.; Li, Y. *Environ. Sci. Technol.* **2012**, *46*, 10191.
- (11) Niu, J.; Lin, H.; Gong, C.; Sun, X. *Environ. Sci. Technol.* **2013**, *47*, 14341.
- (12) Manivel, A.; Velayutham, D.; Noel, M. *Ionics* **2010**, *16*, 153.
- (13) Zhang, T.; Zhao, H.; Lei, A.; Quan, X. *Electrochemistry* **2014**, *82*, 94.
- (14) Methods and Contaminants for the Unregulated Contaminant Monitoring Rule 3 (UCMR 3). UCMR 3 Contaminants and Corresponding Analytical Methods. Assessment Monitoring (List 1 Contaminants).

<http://water.epa.gov/lawsregs/rulesregs/sdwa/ucmr/ucmr3/methods.cfm#assessment>

(accessed July 2014).

- (15) Shoemaker, J. A.; Grimmett, P. E.; Boutin, B. K. *Method 537. Determination of Selected Perfluorinated Alkyl Acids in Drinking Water by Solid Phase Extraction and Liquid Chromatography/Tandem Mass Spectrometry (LC/MS/MS)*; EPA/600/R-08/092; U. S. Environmental Protection Agency: Cincinnati, OH, 2009; Version 1.1.
- (16) Arrigan, D. W. M.; Herzog, G.; Scanlon, M. D.; Strutwolf, J. Bioanalytical Applications of Electrochemistry at Liquid-Liquid Micro-Interfaces. In *Electroanalytical Chemistry*; Bard, A. J., Zoski, C. G., Eds.; Taylor & Francis: Boca Raton, FL, 2013; Vol. 25, p 105.
- (17) Amemiya, S.; Wang, Y.; Mirkin, M. V. Nanoelectrochemistry at the Liquid/Liquid Interfaces. In *Specialist Periodical Reports in Electrochemistry*; Compton, R. G., Wadhawan, J. D., Eds.; RSC: Cambridge, UK, 2013; Vol. 12, p 1.
- (18) Jing, P.; Rodgers, P. J.; Amemiya, S. *J. Am. Chem. Soc.* **2009**, *131*, 2290.
- (19) Kelly, B. C.; Ikonomou, M. G.; Blair, J. D.; Morin, A. E.; Gobas, F. *Science* **2007**, *317*, 236.
- (20) Sangster, J. *Octanol–Water Partition Coefficients: Fundamentals and Physical Chemistry*; John Wiley & Sons: New York, 1997; Vol. 2.
- (21) Reymond, F.; Steyaert, G.; Carrupt, P. A.; Testa, B.; Girault, H. H. *J. Am. Chem. Soc.* **1996**, *118*, 11951.
- (22) Rodgers, P. J.; Amemiya, S. *Anal. Chem.* **2007**, *79*, 9276.
- (23) Amemiya, S.; Kim, J.; Izadyar, A.; Kabagambe, B.; Shen, M.; Ishimatsu, R. *Electrochim. Acta* **2013**, *110*, 836.
- (24) Kim, Y.; Rodgers, P. J.; Ishimatsu, R.; Amemiya, S. *Anal. Chem.* **2009**, *81*, 7262.

- (25) Kabagambe, B.; Izadyar, A.; Amemiya, S. *Anal. Chem.* **2012**, *84*, 7979.
- (26) Kabagambe, B.; Garada, M. B.; Ishimatsu, R.; Amemiya, S. *Anal. Chem.* **2014**, *86*, 7939.
- (27) Guo, J.; Amemiya, S. *Anal. Chem.* **2006**, *78*, 6893.
- (28) Kim, Y.; Amemiya, S. *Anal. Chem.* **2008**, *80*, 6056.
- (29) Chen, L. D.; Lai, C.-Z.; Granda, L. P.; Fierke, M. A.; Mandal, D.; Stein, A.; Gladysz, J. A.; Bühlmann, P. *Anal. Chem.* **2013**, *85*, 7471.
- (30) Boswell, P. G.; Anfang, A. C.; Buhlmann, P. *J. Fluorine Chem.* **2008**, *129*, 961.
- (31) Izadyar, A.; Kim, Y.; Ward, M. M.; Amemiya, S. *J. Chem. Edu.* **2012**, *89*, 1323.
- (32) Amemiya, S. Potentiometric Ion-Selective Electrodes. In *Handbook of Electrochemistry*; Zoski, C. G., Ed.; Elsevier: New York, 2007, p 261.
- (33) Boswell, P. G.; Buhlmann, P. *J. Am. Chem. Soc.* **2005**, *127*, 8958.
- (34) Bard, A. J.; Faulkner, L. R. *Electrochemical Methods: Fundamentals and Applications*; 2nd ed.; John Wiley & Sons: New York, 2001, p 339.
- (35) Bard, A. J.; Faulkner, L. R. *Electrochemical Methods: Fundamentals and Applications*; 2nd ed.; John Wiley & Sons: New York, 2001, p 455.
- (36) Kihara, S.; Suzuki, M.; Sugiyama, M.; Matsui, M. *J. Electroanal. Chem.* **1988**, *249*, 109.
- (37) Vijh, A. K.; Conway, B. E. *Chem. Rev.* **1967**, *67*, 623.
- (38) Ishimatsu, R.; Izadyar, A.; Kabagambe, B.; Kim, Y.; Kim, J.; Amemiya, S. *J. Am. Chem. Soc.* **2011**, *133*, 16300.
- (39) Bard, A. J.; Faulkner, L. R. *Electrochemical Methods: Fundamentals and Applications*; 2nd ed.; John Wiley & Sons: New York, 2001, p 591.